

Mechanisms of *Chlamydia* Manipulation of Host Cell Biology Revealed Through Genetic Approaches

by

Marcela Kokes

Department of Molecular Genetics and Microbiology
Program in Cell and Molecular Biology
Duke University

Date: _____

Approved:

Raphael H. Valdivia, Supervisor

Daniel J. Lew

Jörn Coers

Patrick C. Seed

Dissertation submitted in partial fulfillment of
the requirements for the degree of Doctor of Philosophy
in the Department of Molecular Genetics and
Microbiology in the Graduate School
of Duke University

2015

ABSTRACT

Mechanisms of *Chlamydia* Manipulation of Host Cell Biology Revealed Through Genetic Approaches

by

Marcela Kokes

Department of Molecular Genetics and Microbiology
Program in Cell and Molecular Biology
Duke University

Date: _____

Approved:

Raphael H. Valdivia, Supervisor

Daniel J. Lew

Jörn Coers

Patrick C. Seed

An abstract of a dissertation submitted in partial fulfillment of the requirements for the degree of Doctor of Philosophy in the Department of Molecular Genetics and Microbiology in the Graduate School of Duke University

2015

Copyright by
Marcela Kokes
2015

Abstract

Chlamydia trachomatis is the most common sexually transmitted bacterial pathogen and is the leading cause of preventable blindness worldwide. *Chlamydia* is particularly intriguing from the perspective of cell biology because it is an obligate intracellular pathogen that manipulates host cellular pathways to ensure its proliferation and survival. This is achieved through a significant remodeling of the host cell's internal architecture from within a membrane-bound vacuole, termed the inclusion. However, given a previous lack of tools to perform genetic analysis, the mechanisms by which *Chlamydia* induces host cellular changes remained unclear. Here I present genetic and molecular mechanisms of chlamydial manipulation of the host cytoskeleton and organelles. Using a forward genetics screen, InaC was identified as a necessary factor for the assembly of an F-actin structure surrounding the inclusion. InaC associated with the vacuolar membrane where it recruited Golgi-specific ARF-family GTPases. Actin dynamics and ARF GTPases regulate Golgi morphology and positioning within cells, and InaC acted to redistribute the Golgi to surround the *Chlamydia* inclusion. These findings suggest that *Chlamydia* places InaC at the inclusion-cytosolic interface to recruit host ARF GTPases and F-actin to form a platform for rearranging intracellular organelles around the inclusion. The inclusion is also surrounded by the intermediate filament vimentin and the chlamydial protease CPAF cleaves vimentin *in vitro*. CPAF-dependent remodeling of vimentin occurred selectively in late stages of the infection. In living cells, this cleavage occurred only after a loss of inclusion membrane integrity, suggesting that CPAF cleaves intermediate filaments specifically during chlamydial exit of host cells. In summary, I have implemented recent forward and reverse genetic approaches in *Chlamydia* to

reveal how it employs effector proteins to manipulate the internal organization of cells in novel ways.

Contents

Abstract	iv
List of Tables	xi
List of Figures	xii
Acknowledgements	xiv
1. Cell Biology of the <i>Chlamydia</i> Inclusion	1
1.1 Introduction	1
1.2 Chlamydia heavily interacts with host trafficking machinery	4
1.2.1 The nascent inclusion is rapidly segregated from classical early endocytic pathways	4
1.2.2 Inclusion membrane proteins mediate inclusion interactions	5
1.2.3 The nascent inclusion migrates to the host centrosome	9
1.2.4 The inclusion membrane recruits critical mediators of membrane traffic	10
1.2.5 Chlamydia acquires host lipids	13
1.2.6 Chlamydia acquires host lipids partly via Golgi-dependent vesicular trafficking mechanisms	14
1.2.7 Chlamydia acquires host lipids via non-vesicular pathways	16
1.3 The inclusion interacts with and redistributes host organelles	19
1.3.1 Chlamydia induces Golgi fragmentation	19
1.3.2 Chlamydia interactions with multivesicular bodies	21
1.3.3 Chlamydia targets lipid droplets and peroxisomes	22
1.3.4 Recycling endosomes and lysosomes closely appose the inclusion	24
1.3.5 Chlamydia species interact with mitochondria	25
1.4 Manipulation of the host cytoskeleton during mid to late stages of infection	26

1.4.1 F-actin and intermediate filaments surround the inclusion	26
1.4.2 Septins are enriched in proximity to the inclusion	28
1.4.3 Microtubules near the inclusion are post-translational modified.....	29
1.4.4 Chlamydia can exit host cells by actin-dependent extrusion.....	30
1.5 Conclusions and future perspectives	32
2. F-actin assembly at the <i>C. trachomatis</i> inclusion	34
2.1 Introduction.....	34
2.2 Genetic approach to investigate F-actin assembly	35
2.2.1 Forward genetic screen for bacterial effectors involved in F-actin rearrangements at the <i>C. trachomatis</i> inclusion	35
2.2.2 F-actin assembly around the inclusion is enhanced by a S314F mutation in the uncharacterized Chlamydia predicted ORF CTL0496	37
2.2.2.1 Primary sequence analysis of CTL0496	38
2.2.3 The inclusion membrane protein InaC is necessary for F-actin assembly at the inclusion periphery	38
2.2.3.1 Expression of full-length InaC in M407 rescues F-actin assembly	40
2.2.3.2 Primary sequence analysis of InaC	42
2.3 Mechanisms of F-actin assembly at the inclusion	43
2.3.1 Filamins and α -actinin co-assemble with F-actin at inclusions.....	43
2.3.2 InaC recruits ARF and 14-3-3 proteins to the inclusion	47
2.3.2.1 InaC selectively recruits a GTP-locked ARF1 variant to the inclusion.....	51
2.3.2.2 Different aspects of InaC mediate interactions with ARF and 14-3-3 proteins.....	53
2.4 Functions of F-actin assembly at the inclusion	56
2.4.1 Golgi redistribution around the inclusion requires InaC and F-actin.....	56

2.4.2 InaC-mediated Golgi redistribution is dispensable for <i>Chlamydia</i> sphingolipid acquisition and growth	58
2.4.2.1 Mutant 338 is defective in the generation of infectious progeny but forms wild-type-sized inclusions.....	61
2.4.3 InaC may affect the distribution of various organelles	63
2.4.3.1 InaC affects recycling endosome accumulation at the inclusion	66
2.4.3.2 InaC alters STING translocation kinetics	66
2.4.4 InaC is dispensable for maintenance of gross inclusion integrity and morphology	69
2.4.5 InaC does not globally affect IFN transcriptional responses during <i>C. trachomatis</i> infection	70
2.5 Discussion	75
2.5.1 Insights into mechanisms of F-actin assembly at the inclusion	75
2.5.2 Impact of F-actin assembly at the <i>C. trachomatis</i> inclusion on subcellular architecture and function.....	79
2.6 Materials and Methods.....	82
2.6.1 Cell lines, <i>Chlamydia</i> strains, growth conditions, and antibodies.....	82
2.6.2 Forward genetics screen for F-actin recruitment altered mutants	83
2.6.3 Identification of lesions in CTL0184 and CTL0496 as causal	84
2.6.4 Complementation of M407 with wild type and variants of InaC.....	84
2.6.5 Visual and quantitative analysis of F-actin assembly at inclusions	85
2.6.6 Identification of host proteins that interact with InaC or RhoA(G17A)	86
2.6.7 Assessing ARF, 14-3-3, recycling endosome markers, and RhoA-interacting protein recruitment to inclusions.....	87
2.6.8 Visual and quantitative analysis of Golgi redistribution around inclusions.....	88
2.6.9 Inclusion forming units (IFU) and inclusion size analysis	89

2.6.10 Visual and quantitative analysis of sphingolipid trafficking to inclusions	90
2.6.11 Screen of InaC-dependent changes to organelle distribution	91
2.6.12 Quantitative measurement of RNA transcript abundance	91
3. Reassessing the role of the secreted protease CPAF in <i>Chlamydia trachomatis</i> infection through genetic approaches	93
3.1 Introduction	94
3.2 A <i>Chlamydia</i> mutant defective for Type II secretion accumulates unprocessed CPAF zymogen	97
3.3 Identification of <i>Chlamydia</i> strains with loss-of-function mutations in CPAF	100
3.4 HeLa cells infected with CPAF-deficient <i>Chlamydia</i> mutants display normal Golgi fragmentation.....	101
3.5 CPAF mediates cleavage of intermediate filaments late in infection.....	102
3.6 CPAF-dependent modification of vimentin filaments occurs after inclusion rupture	106
3.7 CPAF-dependent processing of LAP1 occurs after inclusion rupture	109
3.8 Discussion	111
3.9 Materials and Methods.....	113
3.9.1 Reagents	113
3.9.2 Cell Culture and <i>Chlamydia</i> Infections	114
3.9.3 Identification and whole genome sequencing of CPAF-deficient LGV-L2 strains.....	115
3.9.4 Western blot analyses.....	116
3.9.5 <i>In Vitro</i> CPAF cleavage assays.....	117
3.9.6 Immunofluorescence.....	118
3.9.7 Golgi Fragmentation Analysis	119
3.9.8 Detergent Extraction Assays	120

3.9.9 EGFP-Vimentin and LAP1-EGFP transfection and live cell microscopy	121
4. The rising tide - Impacts of recent genetic tools on our understanding of <i>Chlamydia</i> infections and outlook.....	122
5. Appendix I. Differential translocation of host cellular materials into the <i>Chlamydia trachomatis</i> inclusion lumen during chemical fixation.....	126
5.1 Introduction.....	127
5.2 A subset of inclusion-proximal subcellular organelles localize to the lumen of inclusions.....	129
5.3 ER components appear as large structures inside the inclusion of fixed but not living cells	132
5.4 Chemical fixation induces ER internalization into the inclusion lumen.....	134
5.5 Chemical fixation influences the degree to which organelles are observed within the inclusion.....	135
5.6 ER material is internalized into the vacuole of another intracellular pathogen ..	138
5.7 Discussion	139
5.8 Materials and Methods.....	143
5.8.1 Cell culture, <i>Chlamydia</i> infections, transfection, antibodies and plasmids ...	143
5.8.2 Imaging of subcellular organelles and quantitation of intraluminal structures in fixed inclusions	144
5.8.3 Comparison of intraluminal structures in living and fixed cells	145
5.8.4 Time-lapse imaging of ER-RFP translocation during chemical fixation	145
5.8.5 Quantitation of ER-RFP intraluminal structures in inclusions after various fixation and permeabilization conditions.....	146
5.8.6 Imaging and quantitation of ER-RFP structures within fixed <i>Coxiella burnettii</i> pathogenic vacuoles	147
Works Cited.....	147
Biography	167

List of Tables

Table 1. Proteins that co-IP with GFP-InaC as identified by LC-MS/MS	51
Table 2. Organelle markers assessed for InaC-dependent effects on inclusion association.	64
Table 3. Coding transcripts with InaC-dependent change in abundance at FDR<0.05...	72

List of Figures

Figure 1. Diagram of the life cycle of <i>Chlamydia trachomatis</i>	2
Figure 2. <i>Chlamydia</i> significantly alters the internal architecture of host cells.	19
Figure 3. <i>C. trachomatis</i> strains M407 and M338 display altered F-actin assembly at inclusions..	36
Figure 4. Enhanced F-actin assembly at M338 inclusions maps to a nonsense mutation in <i>CTL0496</i>	37
Figure 5. Loss of F-actin assembly at M407 inclusions maps to a nonsense mutation in <i>CTL0184</i>	39
Figure 6. The inclusion membrane protein InaC (<i>CTL0184</i>) is required for F-actin assembly at the inclusion.....	41
Figure 7. Schematic of InaC protein.	43
Figure 8. RhoA is active during <i>Chlamydia</i> infection and interacts with a subset of cytoskeletal proteins specifically during infection.....	44
Figure 9. Host cytoskeletal proteins that co-IP with EGFP-RhoA(G17A) during infection colocalize with F-actin at inclusions.....	47
Figure 10. InaC recruits 14-3-3 and Golgi-specific ARF proteins to the inclusion.....	50
Figure 11. InaC recruits GTP-locked ARF1(Q70L)-GFP to inclusions.....	53
Figure 12. InaC domains and residues are differentially involved in interactions with ARF and 14-3-3 proteins.	54
Figure 13. F-actin and InaC mediate Golgi redistribution around the inclusion.....	57
Figure 14. InaC is dispensable for sphingolipid traffic to the <i>C. trachomatis</i> inclusion, bacterial growth, and inclusion expansion.	60
Figure 15. M338 has a reduced replication potential but WT-sized inclusions.	62
Figure 16. Recycling endosomes and lysosome localization around inclusions is altered by InaC.....	65
Figure 17. STING translocation is enhanced in the absence of InaC.....	68
Figure 18. InaC does not grossly affect inclusion membrane integrity.....	70

Figure 19. Assessment of IFN-related transcript abundance..	74
Figure 20. Identification of <i>C. trachomatis</i> strains deficient in CPAF secretion or expression.	99
Figure 21. <i>C. trachomatis</i> -induced Golgi fragmentation occurs in a z-WEHD-fmk-dependent manner in the absence of CPAF.	102
Figure 22. Evidence for CPAF mediated processing of vimentin in intact cells.	104
Figure 23. The solubility of vimentin filaments are altered in a CPAF-dependent manner at late stages of infection.	105
Figure 24. Cleavage of vimentin in live infected cells occurs after inclusion rupture and is dependent on CPAF and T2S.	108
Figure 25. Cleavage of LAP1 in live infected cells occurs after inclusion rupture and is dependent on CPAF and T2S.	110
Figure 26. Mitochondria, ER, and inclusion membranes are found within the lumen of <i>C. trachomatis</i> inclusions.	131
Figure 27. ER markers reveal expansive structures within the inclusion lumen of fixed but not living cells.	133
Figure 28. ER-RFP translocates into the inclusion lumen during chemical fixation.	135
Figure 29. ER structures are detected via immunofluorescence microscopy within inclusions after both formaldehyde and alcohol-based chemical fixation.	136
Figure 30. Fixation-induced intraluminal ER-RFP structures within inclusions persist through many post-fixation manipulations.	137
Figure 31. ER-RFP within the pathogenic vacuole of <i>Coxiella burnettii</i> .	139

Acknowledgements

I would like to thank my advisor, Raphael Valdivia for his continuous support and for granting me independence and breadth in what I chose to pursue. I thank the Duke Light Microscopy Core Facility, the Duke Center for Genomic and Computational Biology (DCGCB) Genome Sequencing and Analysis Core Resource, DCGCB Integrative Genomic Analysis Shared Resource, the Functional Genomics Shared Resource, and the Duke Proteomics and Metabolomics Shared Resource Core. I thank Sean Peterson and current and former members of the Valdivia lab for valuable discussions. Other contributions are as follows: Raphael Valdivia contributed to data analysis and manuscript preparation, Emily Snively performed experiments for and compiled data for Figure 20C-E, Figure 22B-C, and Figure 23B, and compiled images for Figure 22B, Dora Posfai constructed GFP-InaC vectors, and Joe Dan Dunn performed experiments and compiled data Figure 22A, and prepared DNA libraries of M407 and M338 to submit for next-gen sequencing.

1. Cell Biology of the *Chlamydia* Inclusion¹

1.1 Introduction

The obligate, intracellular bacterial pathogen *Chlamydia trachomatis* primarily infects epithelial cells of the urogenital tract and the conjunctiva, leading to sexually transmitted diseases and conjunctivitis (Belland et al., 2004). Disease is often associated with immune damage resulting from chronic inflammation due to repeated and recurring infections. In women, genital tract infections can result in severe sequelae such as pelvic inflammatory disease, ectopic pregnancies and infertility (Darville and Hiltke, 2010). Similarly, recurrent and untreated *C. trachomatis* conjunctival infections can lead to trachoma, a prominent cause of blindness worldwide (Hu et al., 2010).

C. trachomatis infection (Figure 1) begins with the attachment and entry of elementary bodies (EB), the infectious form of *Chlamydia*, into epithelial cells. Upon entry, the EB form transitions into the replicative reticulate body (RB) form, and establishes a pathogenic vacuole termed an inclusion (Belland et al., 2004). At mid to late stages of infection, RBs transition back to the EB form and by the end of the cycle, bacteria within the inclusion are released to infect neighboring cells (Hybiske and Stephens, 2007). Since *Chlamydiae* must be within cells to differentiate to the replicative RB, they are obligate intracellular pathogens. All aspects of *Chlamydia* survival are intimately linked to the cell biology of its host. The inclusion must avoid degradation by lysosomal compartments and limit detection by innate immune surveillance systems that

¹ Parts of Chapter 1 are reused and edited with permission of the following published book chapter of which I am first author: Kokes M, and Valdivia RH (2012). Cell Biology of the Chlamydial Inclusion. In Intracellular Pathogens I: Chlamydiales, Tan M, and Bavoil PM, eds. (Washington, DC: ASM Press), pp. 170–191.

may activate cell autonomous defense mechanisms or recruit immune cells with potent antimicrobial functions. At the same time, *Chlamydia* must ensure the acquisition of nutrients to support robust bacterial replication and prepare it for eventual exit and dissemination.

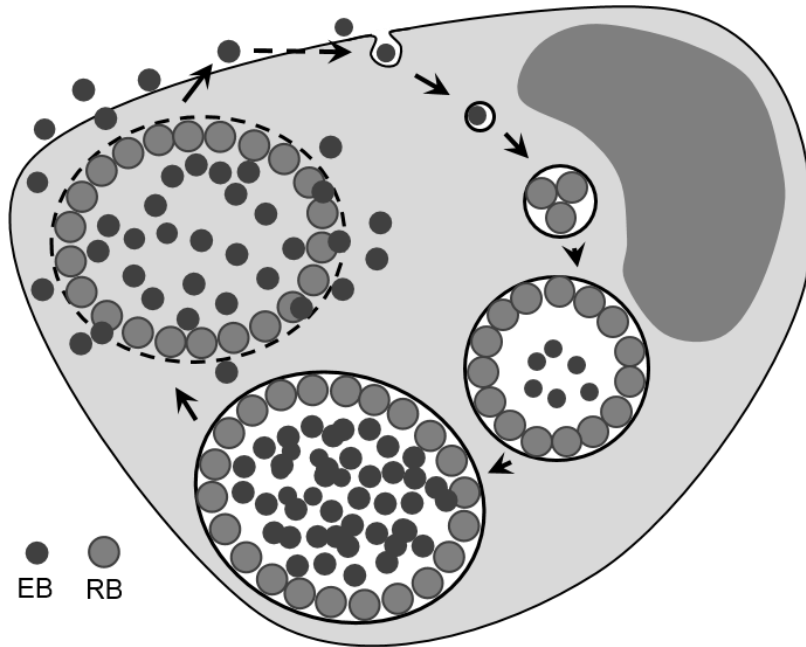


Figure 1. Diagram of the life cycle of *Chlamydia trachomatis*.

Not unexpectedly, *Chlamydia* is equipped with a vast arsenal of proteins to modulate cellular pathways important for invasion, inclusion remodeling, innate immune manipulation, and nutrient acquisition (Betts et al., 2009; Cocchiaro and Valdivia, 2009). Despite a previous lack of genetic tools to identify these *Chlamydia* factors by bacterial mutational analysis, significant progress has been made to link chlamydial proteins to unique events during the infectious cycle. Effector proteins translocated early in infection have been defined as central to cytoskeletal re-arrangements that mediate bacterial invasion (Clifton et al., 2004; Jewett et al., 2006; Lane et al., 2008). Similarly, inclusion membrane proteins expressed early after entry have been associated with the

recruitment of Rab GTPases during inclusion biogenesis (Cortes et al., 2007; Rzomp et al., 2006).

Advances in cell biological techniques and new tools to perform loss of function experiments in mammalian cells have accelerated our understanding of the extent to which *Chlamydia* manipulates the host. For instance, new markers of functionally distinct subcellular compartments and fluorescent reporter proteins permit the tracking of cellular events in real time in live cells. These tools have revealed an underappreciated complexity of the interactions between *Chlamydia* and its host cell. Similarly, RNAi-mediated silencing of mammalian gene expression and the application of unbiased genome-wide screens for host factors required for chlamydial replication have revealed new pathways that this pathogen must modulate for efficient replication (Derré et al., 2007; Elwell et al., 2008; Gurumurthy et al., 2010). On the bacterial side, the availability of genome sequences allowed the implementation of genome-wide functional approaches to identify proteins likely involved in the co-option of its host. These include targeted screens for chlamydial type III secreted proteins based on their ability to be recognized by type III secretion systems of enteric bacteria (Ho and Starnbach, 2005; Subtil et al., 2005), screens for chlamydial proteins that disrupt basic eukaryotic cellular processes upon ectopic expression (Sisko et al., 2006), or the generation of comprehensive libraries of antibodies to chlamydial proteins that can be screened to identify proteins translocated into the host cell at different stages in infection (Li et al., 2008). Overall, these approaches suggest that ~10% of *Chlamydia* ORFs encode proteins with the potential to access the host cytoplasm or inclusion membranes (Valdivia, 2008). Achieving a molecular understanding of the functions of these proteins, their host targets and the pathways they target will be a daunting task, especially when

one considers that these proteins can be highly variable among closely related *Chlamydia* species and/or have no homology to proteins with known functions. Nonetheless, this is a fertile area of study that will not only reveal unique pathogenic strategies used by the *Chlamydiae* but also further our understanding of the basic cell biology of eukaryotic cells.

1.2 *Chlamydia* heavily interacts with host trafficking machinery

Trafficking through the mammalian endomembrane system involves multiple protein and lipid determinants. These include small GTPases that initiate vesicle formation, coat proteins, lipid-modifying enzymes, lipid subdomains, tethering factors, and membrane fusogenic proteins (reviewed in (Lippincott-Schwartz and Phair, 2010)). In particular, ARF and Rab GTPases (reviewed in (Stenmark, 2009)) function as molecular switches that alternate between a GTP-bound 'on' conformation and a GDP-bound 'off' state to recruit coat proteins, generate vesicular carriers and eventually dock these vesicles to the appropriate target membrane. In addition, phosphatidylinositol is differentially phosphorylated to define distinct subcellular membrane compartments that recruit proteins important in membrane trafficking events (reviewed in (Behnia and Munro, 2005)). In the following sections we discuss how *Chlamydia* co-opts these various determinants of cellular membrane traffic.

1.2.1 The nascent inclusion is rapidly segregated from classical early endocytic pathways

Shortly after invasion, *Chlamydia*-containing endosomes lose plasma membrane and early endocytic markers (Scidmore et al., 2003). Some of this rapid remodeling of the nascent endosome is likely mediated by the chlamydial proteins synthesized and translocated early after invasion (Scidmore et al., 1996a). In addition, physical properties

unique to the EB – or possibly its method of entry – lead to a significant delay in the fusion of EB-containing endosomes with lysosomes. For instance, heat-killed EBs fuse with endosomes at rates significantly slower than other invasive bacteria (Scidmore et al., 2003). Overall, there is a concerted effort by intracellular chlamydiae to dissociate their inclusions from endolysosomal trafficking pathways.

Rab GTPases associated with classical endolysosomal transport (Rab5, Rab7, and Rab9) are not recruited to inclusions (Rzomp et al., 2003). Similarly, the phosphoinositides PI3P and PI(4,5)P₂, which mark endosomal and the plasma membranes, respectively, are absent from inclusions (Moorhead et al., 2010). As a result, the inclusion was originally viewed as being completely dissociated from all endocytic traffic (reviewed in (Fields and Hackstadt, 2002). However, with the application of newer cell biological tools, there is a growing appreciation that the inclusion is not completely segregated from membrane transport pathways and that some proteins that normally function in Golgi-mediated transport and on recycling/sorting endosomes are recruited to inclusions (reviewed in (Cocchiario and Valdivia, 2009).

1.2.2 Inclusion membrane proteins mediate inclusion interactions

The inclusion membrane is an important interface between *Chlamydia* and the host cell. The limiting membrane of the inclusion is heavily modified with *Chlamydia*-encoded integral membrane proteins. These proteins are collectively termed Incs, for inclusion membrane proteins and typically have a bi-partite hydrophobic motif that is thought to facilitate interaction with the inclusion membrane (Rockey et al., 2002). Many Incs are variable between *Chlamydia* species, suggesting that they may be involved in differential host or tissue tropisms; however, a group of 23 core Incs are conserved between species (Lutter et al., 2012). Localization to the cytoplasmic surface of the

inclusion membrane places Incs in an ideal position to mediate interactions between the inclusion and host organelles and trafficking pathways. Some Incs have the intrinsic ability to induce membranous structures some with unique properties in host cells and could play important roles in inclusion biogenesis (Mital et al., 2013). Furthermore, a recent study using affinity purification-mass spectrometry identified significant interactions between 38 Incs and host proteins that act in many of the cellular processes that are altered during *Chlamydia* infection (Mirrashidi et al., 2015). One set of Incs is pre-packaged into EBs (Saka et al., 2011) and another set is expressed within 1h post bacterial invasion (Belland et al., 2003), suggesting that modification of the nascent inclusion by Inc proteins begins immediately after bacterial entry.

Different Incs may mediate interactions with specific host subcellular compartments. Based on tertiary structural predictions, three *C. trachomatis* Incs (IncA/CT119, CT223, and InaC/CT813) display SNARE (soluble NSF (N-ethylmaleimide-sensitive factor)-like motifs (Delevoye et al., 2008). SNAREs are integral membrane proteins that are central to vesicle-mediated membrane transport (reviewed in (Chen and Scheller, 2001; Martens and McMahon, 2008). Vesicular SNAREs (v-SNARE) pair with specific target SNAREs (t-SNAREs) on acceptor membranes to provide specificity to vesicle targeting and the energy required to fuse two membranes (Chen and Scheller, 2001). IncA interacts through its SNARE-like domain with a subset of host SNAREs which are enriched at the inclusion (Delevoye et al., 2008). These three SNAREs, Vamp3, Vamp7, and Vamp8, are often associated with membrane fusion events in the endocytic pathway. SNAREs that are not recruited to the inclusion, Vamp4 and Sec22, are associated with exocytosis and ER-to-Golgi transport (Delevoye et al., 2008).

The recruitment of these SNAREs to the inclusion, however, should not be seen as evidence that the inclusion fuses with these compartments. IncA, in reconstituted SNARE-mediated fusion reactions with purified protein and liposomes, inhibits rather than promotes membrane fusion (Paumet et al., 2009). IncA disrupts *in vitro* fusion between t-SNARE (syntaxin7/syntaxin8/Vti1b) and v-SNARE (Vamp8) in liposomes, as well as t-SNARE (syntaxin4/SNAP23) and v-SNARE-mediated membrane transport in *in vivo* cellular assays (Paumet et al., 2009). Therefore, some Incs may have evolved to mimic SNARE-like motifs that act as inhibitory SNAREs (iSNAREs) to limit fusion with host endocytic compartments (Paumet et al., 2009). Consistent with this, Vamp8 at the inclusion, as assessed by immunoelectron microscopy, is largely due to the accumulation of Vamp8-positive compartments intimately associated with the inclusion rather than on the inclusion membrane itself (Delevoye et al., 2008). Similarly, clinical strains that are deficient in the production of IncA fail to efficiently recruit Vamp8 to the inclusion membrane (Delevoye et al., 2008). Nonetheless, these strains are still viable and presumably segregated from endolysosomal transport (Suchland et al., 2000) indicating that there is an IncA-independent mechanism for *Chlamydia* avoidance of lysosomal fusion.

In contrast to a potential role in inhibiting fusion with host vesicles, IncA is required for homotypic fusion between *C. trachomatis* inclusions. Upon infection with a high dose of EBs, several non-fused inclusions will persist within an infected cell until approximately 10 hours post infection (hpi). At this stage, inclusions begin to fuse and form one larger inclusion. Blocking IncA function by microinjection with anti-IncA antibodies results in multiple inclusions (Hackstadt et al., 1999). Similarly, infections performed at lower temperature (e.g., 32°C), which limits IncA export (Fields et al.,

2002), also lead to the formation of multiple inclusions (Van Ooij et al., 1998) and clinical strains lacking IncA display fragmented inclusions (Suchland et al., 2000). Interestingly, even when cells are infected by *C. trachomatis* with a very low multiplicity of infection (MOI), microinjection of anti-IncA antibodies results in multi-lobed, fragmented inclusions (Hackstadt et al., 1999) suggesting that IncA may somehow function to prevent septation or fission of an established inclusion in addition to facilitating fusion between originally separate inclusions. Because IncA forms oligomers, it was originally thought that SNARE-like pairings would facilitate homotypic fusion of adjacent inclusions (Delevoeye et al., 2004). However, IncA cannot drive membrane fusion reactions *in vitro* (Paumet et al., 2009), suggesting that there are additional host or bacterial factors mediating IncA-dependent inclusion fusion. Homotypic fusion of *C. trachomatis* inclusions could serve to consolidate resources and reduce competition among multiple growing inclusions. However, this function is dispensable for viability in cells as bacterial replication is largely unaffected by pharmacological agents that disrupt inclusion fusion (Schramm and Wyrick, 1995), and not all *Chlamydia* species and strains display fusogenic vacuoles (Rockey et al., 1996). Nonetheless, mathematical models of RB to EB transition postulate that large, fused inclusions lead to the greatest EB yield (Wilson et al., 2006); the slow growth rates that have been observed in *Chlamydia* species with multiple or fragmented inclusions corroborates this prediction.

It is clear that Incs on early inclusions likely play important roles in remodeling the nascent inclusion to segregate from the endolysosomal pathway and maintain single inclusion morphology in fusogenic *Chlamydia* species. However, the role played by soluble effectors secreted early or even during entry should not be discounted when considering early interactions with host cell biology.

1.2.3 The nascent inclusion migrates to the host centrosome

In tissue culture cells, the nascent inclusion migrates to a perinuclear region of the cell corresponding to the microtubule-organizing center (MTOC) or centrosome (Clausen et al., 1997). Many secretory organelles reside near the MTOC, and inclusion migration to this site presumably facilitates interactions with these lipid- and nutrient-rich compartments. This migration occurs along microtubules and requires *de novo* chlamydial protein synthesis (Clausen et al., 1997; Scidmore et al., 1996a), indicating that a bacterial protein, most likely an Inc protein, coordinates transport to the MTOC.

How the inclusion gets to the MTOC is not well understood. Because inclusions intimately associate with recycling endosomes early during infection (van Ooij et al., 1997; Scidmore et al., 2003) and recycling endosomes localize pericentriolarly (Ullrich et al., 1996), *Chlamydia* could potentially use this association to migrate to the MTOC. Consistent with this, two Rab GTPases (Rab4 and Rab11) present on recycling endosomes are also recruited to the inclusion membrane early in infection (Rzomp et al., 2003, 2006). Rabs interact with molecular motors via adaptor proteins to regulate vesicular trafficking (Stenmark, 2009) and thus could influence inclusion migration to the MTOC. Rab4 and its effector FIP2 localize to the inclusion and are important for the generation of infectious progeny (Leiva et al., 2013). Rab6 and its effector BICD1, which interacts with the microtubule-dependent motor dynein (Matanis et al., 2002), localize to the inclusion and may mediate dynein-mediated inclusion migration (Moorhead et al., 2007). Consistent with this, inclusion migration is dependent on host microtubules and dynein, both of which are recruited to early inclusions (Clausen et al., 1997; Grieshaber et al., 2003). In addition, the p150^(Glued) component of the dynactin protein complex which links vesicular cargo to the dynein motor, is required for nascent inclusion migration.

Unexpectedly, the cargo recruitment component p50 dynamitin is not necessary (Grieshaber et al., 2003), indicating that its function is performed by an unknown host cargo receptor adaptor or a *Chlamydia* protein on the inclusion membrane.

Additional observations support the notion that Inc proteins may participate in dynein recruitment to the inclusion and inclusion migration to the centrosome. Host centrosomes intimately associate with the inclusion in a dynein-dependent dynactin-independent manner (Grieshaber et al., 2006). Four Incs (IncB/CT232, CT101, CT222 and CT850) localize to patches on the inclusion surface that associate with host centrosomes (Mital et al., 2010). CT222 and CT850 stably interact with each other, and ectopically expressed CT850 localizes to host centrosomes (Mital et al., 2010). IncB and CT850 are expressed by 2hpi (Belland et al., 2003; Shaw et al., 2000), and are thus good candidates for mediating early interactions with dynein and facilitating inclusion migration (Mital et al., 2010). Indeed, CT850 interacts with the dynein light chain DYNLT1 in a yeast 2-hybrid assay (Mital et al., 2015).

1.2.4 The inclusion membrane recruits critical mediators of membrane traffic

In addition to Rab4 and Rab11, *Chlamydia* recruits Rab1 in many species, Rab6 and Rab10 in select species, and Rab14 in at least one species to inclusion membranes (Capmany and Damiani, 2010; Rzomp et al., 2003). This recruitment of Rabs is independent of microtubules or the Golgi apparatus indicating that these proteins do not traffic through membrane intermediates en route to the inclusion. Rab association with the inclusion may occur via a direct binding to Inc proteins or indirectly by Rab effectors and regulators that associate with the inclusion. For instance, the Inc protein CT229 interacts with Rab4 *in vitro*, and EGFP-Rab4 expressed in chlamydia-infected cells

colocalizes with endogenous CT229 around the inclusion *in vivo* (Rzomp et al., 2006). Interestingly, CT229 only interacts with Rab4-GTP, suggesting that CT229 may mimic Rab4 effectors by binding Rab4-GTP and recruiting it to the inclusion (Rzomp et al., 2006). Similarly, the *Chlamydia pneumoniae* Inc protein Cpn0585 interacts with several Rabs in a GTP-dependent manner (Cortes et al., 2007). In contrast, the Rab6 effector BICD1 localizes to the inclusion even in the presence of a dominant-negative version of Rab6, suggesting that BICD1 is recruited to the inclusion independently of Rab6 (Moorhead et al., 2007). Overall, current evidence predominantly supports a model where Inc proteins directly recruit active Rab proteins and their bound effectors to the inclusion.

Rab proteins mediate vesicular traffic between specific subcellular compartments, and thus it is perhaps not surprising that *Chlamydia* would co-opt these proteins to gain access to essential factors within vesicular carriers. Indeed, RNAi-based depletion and dominant-negative expression experiments indicate that Rab1, Rab6, Rab11, Rab14, and Rab4/Rab11 play important roles in *Chlamydia* replication within host cells (Capmany and Damiani, 2010; Derré et al., 2007; Elwell et al., 2008; Ouellette and Carabeo, 2010; Rejman Lipinski et al., 2009).

Normal Rab functions provide clues as to how Rab recruitment to the inclusion may influence interactions with the host. Rabs specify organelle identity by regulating the recruitment of lipid kinases and phosphatases that control the levels of phosphoinositides on membranes (Behnia and Munro, 2005). OCRL1 (oculocerebrorenal syndrome of Lowe protein 1) is a PI(4,5)P₂ 5-phosphatase, binds to Rab1, Rab6, and Rab14, and is recruited to the inclusion (Moorhead et al., 2010). The PI-OH(4)-kinase PI4KII α also localizes to the inclusion, suggesting that host enzymes

are in place at the inclusion to generate phosphatidylinositol 4-phosphate (PI4P).

Consistent with these observations, the pleckstrin homology (PH) domains of OSBP and GPBP, which specifically bind to PI4P, prominently decorate the inclusion membrane (Moorhead et al., 2010). Similarly, ARF1, a small GTPase that can recruit PI-OH(4)-kinases and PI4P-binding proteins, also localizes to the inclusion and may enhance the recruitment of these PI4P-generating enzymes. siRNA-mediated depletion of OCRL, PI4KII α , or ARF1 reduces infectivity and inclusion formation, indicating that the generation of PI4P pools at the inclusion membrane plays an important role in bacterial replication and survival (Moorhead et al., 2010).

In addition to small GTPases which modulate cellular trafficking, other critical mediators of traffic are recruited to the inclusion. Components of the retromer complex, BAR-SNX proteins, which function to induce membrane tubulation and recruit factors for vesicle scission in receptor sorting during retrograde traffic from endosomes to the *trans*-Golgi, are recruited to the inclusion (Aeberhard et al., 2015; Mirrashidi et al., 2015). *C. trachomatis* inclusion membranes form remarkable long tubules extending into the cytosol, and their formation requires, and is dramatically enhanced upon overexpression of the SNX-BAR recruiting effector IncE (Mirrashidi et al., 2015). While the entire retromer complex is not recruited to the inclusion, retromer-dependent trafficking of host receptors is, suggesting that in addition to promoting inclusion tubulation, IncE disrupts distal trafficking processes by sequestering SNX-BAR proteins from their standard site of action (Mirrashidi et al., 2015). Manipulating these pathways on the host side either enhances *Chlamydia* progeny formation upon depletion of SNX-BAR (Aeberhard et al., 2015; Mirrashidi et al., 2015), or restricts it upon pharmacological retromer disruption

(Aeberhard et al., 2015), leaving the precise significance of IncE on *Chlamydia* survival unclear.

1.2.5 *Chlamydia* acquires host lipids

Even though *Chlamydia* has the capacity to synthesize its own lipids, it will preferentially acquire host-derived lipids. As a result, the lipid composition of *C. trachomatis*, which includes cholesterol, sphingolipids (SLs), and glycerophospholipids, mimics that of its host cell (Hatch and McClarty, 1998a; Wylie et al., 1997).

Glycerophospholipids are acquired as lysophospholipid precursors, through a process that may involve a host calcium-dependent cytosolic phospholipase A₂ (cPLA₂) (Su et al., 2004). The lysophospholipids are re-acylated with a *Chlamydia*-derived branched fatty acid prior to their incorporation into bacterial membranes (Wylie et al., 1997).

SLs are composed of sphingosine with both a non-polar tail of fatty acid chains and a head group of either phosphocholine (sphingomyelin) or different sugars (glycosphingolipids) (reviewed in (Lippincott-Schwartz and Phair, 2010)). SLs are synthesized in the ER as ceramide precursors, processed in the Golgi apparatus, and accumulate at the plasma membrane (reviewed in (Perry and Ridgway, 2005)). SLs are required for chlamydial replication (van Ooij et al., 2000; Robertson et al., 2009) and treatment of infected cells with myriocin, a potent inhibitor of serine palmitoyltransferase – the initial step in SL biosynthesis – leads to loss of inclusion membrane integrity, RB-to-EBs differentiation defects, and early EB release (Robertson et al., 2009).

Furthermore, homotypic fusion between inclusions and the ability to reactivate from a persistent state are inhibited (Robertson et al., 2009), indicating that SLs are important for the function of the inclusion membrane. The fatty acid chains of SLs are typically saturated and thus SLs can pack closely in lipid bilayers. The impact of SL depletion on

inclusion membrane stability could be consistent with the role of this lipid in imparting order and rigidity to membranes (Lippincott-Schwartz and Phair, 2010). The Src-family kinase Fyn is important for *C. trachomatis* sphingolipid acquisition (Mital et al., 2010), although it remains unclear if Fyn is involved in vesicular or non-vesicular acquisition pathways (described below).

1.2.6 Chlamydia acquires host lipids partly via Golgi-dependent vesicular trafficking mechanisms

Tracking of fluorescently-labeled ceramide analogues in live cells indicate that SL transport to the inclusion shares features of canonical Golgi to plasma membrane vesicular transport (Hackstadt et al., 1995; Wolf and Hackstadt, 2001). In addition, consistent with the inclusion's segregation from endocytic traffic, plasma membrane SLs are not trafficked to the inclusion (Hackstadt et al., 1996). SL-containing vesicles, seemingly in the process of fusing with the inclusion, have been observed by electron microscopy (Hackstadt et al., 1996). Of host SLs, only sphingomyelin, and not glucosylceramide, is delivered to the chlamydial inclusion (Moore et al., 2008), suggesting highly specific interactions with host lipid trafficking pathways. Furthermore, in polarized epithelial cells, *Chlamydia* preferentially intercepts basolaterally-targeted SLs (Moore et al., 2008), indicating that *Chlamydia* may interact with specific branches of exocytic pathways. Indeed, the trans-Golgi-associated SNARE syntaxin 6 (targeted via a YRGL motif (Kabeiseman et al., 2014)), required for basolaterally-directed exocytosis, and its binding partner VAMP-4, localize to the inclusion of multiple *Chlamydia* species (Kabeiseman et al., 2013; Moore et al., 2010). VAMP4 is required for syntaxin 6 recruitment to inclusions, while syntaxin 6 depletion does not significantly block SL delivery to the inclusion or inclusion development, VAMP4 depletion does

(Kabeiseman et al., 2013; Moore et al., 2010), suggesting that VAMP4 is an important mediator of SL acquisition, although it remains unclear if this is due to direct co-option of VAMP4-pathways by *Chlamydia* or rather a global defect in SL trafficking.

Experiments using the pharmacological agent brefeldin A (BFA) were important in revealing the importance of Golgi-dependent vesicular trafficking in SL acquisition by *Chlamydia* (Carabeo et al., 2003; Hackstadt et al., 1996). BFA treatment causes Golgi dispersion (Lippincott-Schwartz et al., 1989) by inhibiting guanine nucleotide exchange factors (GEFs) that activate ARF1 – a small GTPase critical in vesicle formation (reviewed in (D’Souza-Schorey and Chavrier, 2006)). These BFA-targeted GEFs are the *cis*-Golgi-localized GBF1, which is required for Golgi stack assembly and maintenance and *trans*-Golgi-localized BIG1/BIG2 which are required for *trans*-Golgi network maintenance (Claude et al., 1999; Manolea et al., 2008; Mansour et al., 1999; Yamaji et al., 2000). A recent study reveals that only GBF1 participates in SL transport to the inclusion (Elwell *et al.*, 2011). siRNA-mediated depletion of GBF1 reduced SL delivery to the inclusion by ~60% while BIG1 and/or BIG2 depletion had no effect. This decrease in SL transport did not affect the production of infectious progeny, but it did impact the integrity of the inclusion membrane with GBF1 depletion resulting in loss of inclusion integrity and bacterial release into the cytosol of the host cell (Elwell *et al.*, 2011) as has been observed with myriocin treatment (Robertson et al., 2009). These data suggest that *Chlamydia* acquire SLs via GBF1-dependent and -independent mechanisms, and blocking the former vesicular pathway is insufficient to impact *Chlamydia* replication.

As with SLs, *de novo* synthesized and extracellular cholesterol is found in EBs and the inclusion membrane (Carabeo et al., 2003). In eukaryotic cells, SLs and cholesterol are often co-transported in membrane vesicles, and cholesterol delivery to

the inclusion resembles SL vesicular delivery in that it is partially dependent on microtubules and is BFA-sensitive (Carabeo et al., 2003).

1.2.7 Chlamydia acquires host lipids via non-vesicular pathways

Early ultrastructural studies noted the presence of thin ER tubules closely apposed with *C. trachomatis* inclusion membranes (Giles and Wyrick, 2008; Peterson and de la Maza, 1988), and ER proteins (SERCA2, IP3-R, and calreticulin) are enriched at the periphery of the inclusion (Majeed et al., 1999). The significance of this association with ER tubules was unknown. There is a growing appreciation that inter-organelle lipid transport relies extensively on membrane contact sites (MCSs) between organelles, especially with the ER (reviewed in (Levine and Loewen, 2006)). For example, ceramide was originally thought to be mainly transported from the ER to the Golgi via vesicular carriers. However, it is now apparent that the cytosolic lipid transfer protein (CERT) is responsible for the bulk of this transport by transferring ceramide directly at ER-Golgi MCSs (Hanada et al., 2003; Levine and Loewen, 2006).

A pair of recent studies provide evidence that the inclusion forms MCSs with the ER where CERT transfers SL precursors from the ER to be converted to sphingomyelin by host proteins at the inclusion membrane (Derré et al., 2011; Elwell et al., 2011). Endogenous CERT associates with patches on the *C. trachomatis* inclusion where it co-localizes with VAPA or VAPB (Derré et al., 2011; Elwell et al., 2011). VAPA and VAPB are ER resident proteins that recruit FFAT-motif-containing proteins, such as CERT, to the cytoplasmic face of the ER. This binding is required for CERT to transfer ceramide from the ER to the Golgi (Kawano et al., 2006). Cryo-immunogold electron micrographs suggest that CERT localizes to the inclusion membrane at sites in close apposition to VAPB-positive ER tubules (Derré et al., 2011). Distances between membranes at these

apposition sites is ~10 nm and ultrastructurally resemble inter-organelle MCSs (Derré et al., 2011). Interestingly, STIM1, an ER calcium sensor that enriches at ER-PM membrane contact sites upon calcium depletion, localizes to ER-Inclusion membrane contact sites in a calcium-independent manner (Agaisse and Derré, 2015), suggesting that these sites are more than mere replicas of ER-Golgi membrane contact sites.

Although the PH domain of CERT binds PI4P on Golgi membranes and is necessary and sufficient for CERT binding to the inclusion (Derré et al., 2011), a mutation that disrupts PI4P binding and Golgi localization has no effect on CERT recruitment to the inclusion (Elwell et al., 2011), and CERT remains on the inclusion upon inhibition of PI4P synthesis (Derré et al., 2011). This suggests that other factors on the inclusion membrane are required for CERT recruitment. An attractive candidate for CERT recruitment is IncD (CT115), an inclusion membrane protein that interacts with the PH domain of CERT and co-localizes with CERT in patches on the inclusion membrane (Derré et al., 2011). *Chlamydia caviae* lacks IncD and does not recruit CERT to the inclusion (Derré et al., 2011). However, *C. caviae* inclusions do accumulate SLs (Rockey et al., 1996), suggesting that other pathways of SL acquisition may suffice in this species.

Depletion of CERT or VAPA and VAPB reduces inclusion size and the number of infectious progeny recovered from *C. trachomatis* infection (Derré et al., 2011; Elwell et al., 2011), and inhibition of CERT activity results in ~56% decrease in chlamydial SL acquisition (Elwell et al., 2011). Unlike vesicle-mediated pathways of SL acquisition, CERT-mediated pathways are important for progression through the normal infectious cycle. Consequently, it has been speculated that SLs obtained via CERT or GBF1-dependent mechanisms may be utilized differently by *Chlamydia* since their disruption

has different consequences on the infectious cycle (ie. decreased replication vs inclusion membrane disruption) (Elwell et al., 2011). Ceramide transported from the ER to the *trans*-Golgi via CERT is converted to sphingomyelin through the activity of sphingomyelin synthases SMS1 and SMS2 (Tafesse et al., 2007). Interestingly, SMS2 localizes to the inclusion and partially overlaps with CERT, while SMS1 remains Golgi-associated during infection (Elwell et al., 2011). Depletion of SMS1 or SMS2 results in decreased recovery of infectious progeny (Elwell et al., 2011). Together, these data suggest that SMS2 at the inclusion may convert CERT-transferred ceramide to sphingomyelin for bacterial use.

The finding that *Chlamydia* forms MCSs with the ER where ceramide is directly transferred between these membranes highlights the complexity of *Chlamydia* control of host cells and raises the critical question of whether non-vesicular communication between the inclusion and subcellular components is more widespread. As advances are made in cellular inter-organelle communication, our ability to address these questions will expand in parallel.

1.3 The inclusion interacts with and redistributes host organelles

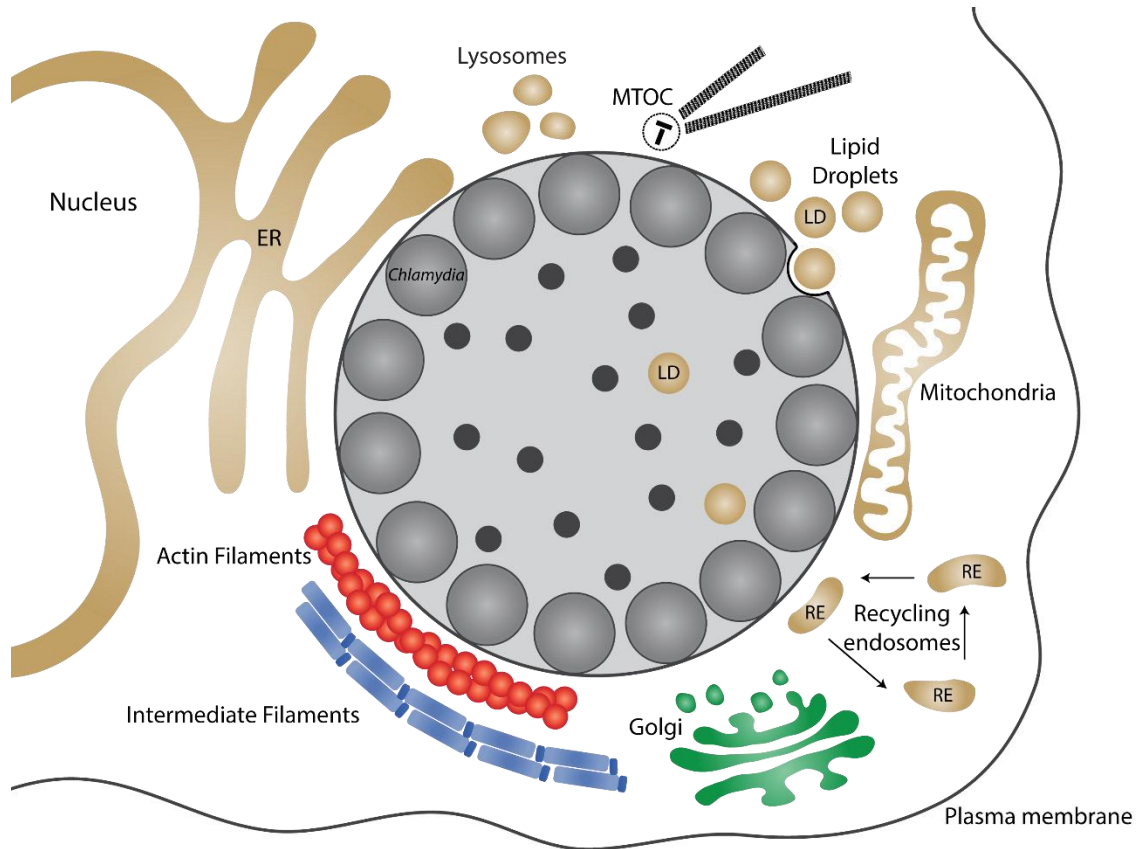


Figure 2. *Chlamydia* significantly alters the internal architecture of host cells. The ER, mitochondria, recycling endosomes, lysosomes, lipid droplets, peroxisomes (not pictured), and Golgi apparatus all associate with the periphery of the inclusion. Cytoskeletal elements including actin and intermediate filaments, microtubules (shown emanating from microtubule organizing center or MTOC), and septins (not shown) closely associate with inclusion. Golgi, actin, and intermediate filaments are displayed in color as they will be discussed to extent in Chapters 2-4.

1.3.1 *Chlamydia* induces Golgi fragmentation

The Golgi apparatus of mammalian cells consists of stacks of flattened cisternae that assemble at the MTOC and is a critical mediator of vesicular traffic (Sütterlin and Colanzi, 2010). During *Chlamydia* infection, the Golgi disperses into several distinct ministacks that envelop the inclusion (Heuer et al., 2009). Golgi fragmentation correlates

with cleavage of the matrix protein golgin-84 and pharmacological inhibitors of this cleavage inhibit Golgi fragmentation and decrease infectivity of *Chlamydia* by approximately two-fold. Although inflammatory caspases and calpains are likely responsible for golgin-84 cleavage, this does not preclude the possibility that a *Chlamydia* protease may also participate in this processing. Indeed, CPAF was been suggested to induce golgin-84 cleavage and Golgi fragmentation through the use of a caspase inhibitor (Christian et al., 2011). However, CPAF-dependent golgin-84 cleavage appears to occur post-lysis (Chen et al., 2012). Golgi fragmentation is postulated to enhance lipid delivery to the inclusion and thus *Chlamydia* replication. Consistent with this prediction, Golgi fragmentation induced by RNAi-based silencing of giantin, GPP130, or golgin-84 enhances bacterial replication (Heuer et al., 2009).

Rab6 and Rab11 modulate *Chlamydia*-induced Golgi fragmentation (Rejman Lipinski et al., 2009). Rab6 or Rab11 depletion inhibits Golgi fragmentation in infected cells and reduces infectivity, EB formation, and SL delivery to the inclusion but does not affect golgin-84 cleavage. Thus Rab6 and Rab11 appear to act downstream of golgin-84 cleavage to destabilize the Golgi. While Rab6 or Rab11 depletion blocks golgin-84-cleavage-dependent Golgi fragmentation, Golgi fragmentation induced by RNAi of the Golgi-tethering factor p115 is unaffected by Rab6 or Rab11 depletion, implying independent pathways (Rejman Lipinski et al., 2009). Significantly, Golgi fragmentation by p115 depletion rescues defects in SL transport to the inclusion in cells lacking Rab6 or Rab11, implying that Rab6 and Rab11 function can be bypassed by alternative mechanisms of Golgi fragmentation (Rejman Lipinski et al., 2009). Indeed, Golgi fragmentation itself appears to be a greater determinant of efficient SL delivery to the

Chlamydia inclusion than other functions of Rab6 and Rab11, possibly by facilitating SL delivery to the inclusion by increasing Golgi proximity and association with the inclusion.

1.3.2 Chlamydia interactions with multivesicular bodies

Multivesicular bodies (MVBs) are late endocytic compartments in which the limiting membrane of endosomes has invaginated into the lumen to form intraluminal vesicles containing membrane proteins destined for degradation (reviewed in (Piper and Katzmann, 2007)). MVBs can also fuse with the plasma membrane resulting in release of specialized intraluminal vesicles termed exosomes (reviewed in (van Niel et al., 2006)). Recent studies suggest an interaction between *Chlamydia* and MVBs as a potential intermediate in post-Golgi SL acquisition (Beatty, 2006, 2008; Robertson et al., 2009). Several markers of MVBs, including CD63, MLN64, and lysobisphosphatidic (LBPA) acid localize to the periphery and within inclusions in fixed cells (Beatty, 2006). Immunoelectron microscopy revealed CD63-positive and LBPA-positive structures adjacent to the inclusion, small CD63-positive and LBPA-positive vesicles inside the inclusion lumen, and CD63 at the inclusion membrane and within the inclusion (Beatty, 2006, 2008). Additionally, pharmacological inhibitors of MVBs disrupt inclusion growth and infectivity (Beatty, 2006). Intraluminal vesicles of MVBs are enriched in cholesterol and SLs (Piper and Katzmann, 2007) and treatment with U18666A, a cell-permeable amphiphilic amino-steroid that inhibits cholesterol transport from late endosomes, disrupts SL and cholesterol delivery to the inclusion (Beatty, 2006, 2008). However, the exact contribution of MVB function in *Chlamydia* host lipid acquisition is unclear since some of the inhibitors used to interfere with MVBs also inhibit autophagy (Al-Younes et al., 2004). Additionally, recent genome-wide RNAi screens indicated that neither MVB nor autophagy pathways are required for *C. caviae* or *C. trachomatis* replication (Derré

et al., 2007; Elwell et al., 2008), potentially due to redundant mechanisms of lipid acquisition. Other studies did not observe CD63 within the inclusion lumen or any effect of U18666A on SL acquisition in live cells (Ouellette and Carabeo, 2010). While further studies will be required to address these discrepancies, I present evidence that host cellular material can translocate into the inclusion lumen during the process of chemical fixation (Chapter 5).

1.3.3 Chlamydia targets lipid droplets and peroxisomes

Chlamydia acquires host neutral lipids presumably via interactions with lipid droplets (LDs) (Cocchiaro et al., 2008; Kumar et al., 2006). LDs are ubiquitous among eukaryotic cells with crucial roles in lipid homeostasis and energy metabolism (reviewed in (Farese Jr. and Walther, 2009; Guo et al., 2009; Walther and Farese Jr., 2009)). LDs have a unique structure comprising a hydrophobic lipid core of sterol esters and triacylglycerols encased in a single phospholipid monolayer. LD formation can be inhibited pharmacologically with the long chain acyl-coA synthase inhibitor triacsin C, which specifically blocks cholesterol ester and triacylglycerol synthesis (Igal et al., 1997). Treatment of cells with triacsin C during infection interferes with *Chlamydia* infectivity, suggesting a potential role for LDs in chlamydial pathogenesis (Kumar et al., 2006). However, caution should be exercised when considering the implications of inhibiting lipid biosynthesis since various aspects of membrane traffic may be simultaneously impaired. For example, inhibitors of acyl-CoA:cholesterol acyltransferase (ACAT), which functions in cholesterol ester synthesis, and lysophospholipid acyltransferase (LPAT) have anti-chlamydial effects (Ouellette and Carabeo, 2010). These effects have been reported to arise from the disruption of endosome recycling rather than LD formation (Ouellette and Carabeo, 2010).

LDs accumulate at the *Chlamydia* inclusion and translocate into the inclusion lumen (Cocchiari et al., 2008; Kumar et al., 2006) and have even been documented within inclusions during *in vivo* infection (Rank et al., 2011). The chlamydial protein Lda3 (CT473), which binds to LDs and to the inclusion membrane when expressed ectopically, may serve as the link between LDs and the inclusion. Within the inclusion lumen, LDs associate with RBs, allowing the possibility of direct lipid transport between the two. Alternatively, lipases present on LDs may become uncoupled from regulatory signals in the host cytoplasm upon translocation into the inclusion lumen to generate biosynthetic precursors for bacterial membrane biosynthesis (Cocchiari et al., 2008). In addition, because LDs have been implicated in vesicular trafficking, signaling, and inflammatory responses (Guo et al., 2009), it is possible that bacterial manipulation of these organelles may serve functions beyond the acquisition of nutrients. Recently, a membrane attack complex/perforin-like chlamydial protein (CT153) was reported to localize to a subpopulation of RBs, some of which may be closely apposed to intralumenal LDs (Taylor et al., 2010). CT153 lies immediately upstream of phospholipase D (PLD)-like proteins, including Lda1(CT156) which localizes to LDs when ectopically expressed (Kumar et al., 2006), raising the possibility that the functions of these proteins are related (Taylor et al., 2010).

Lipid droplets often play metabolic roles in concert with and are closely associated with another small organelle – the peroxisome. Peroxisomes are nearly ubiquitous organelles which contain enzymes that function in an array of metabolic pathways including oxidation of fatty acids and biosynthesis of ether lipids (reviewed in (Wanders and Waterham, 2006)). Peroxisomes are enriched at the inclusion periphery and can be found associated with bacteria within the inclusion lumen (Boncompain et al.,

2014). While peroxisome biogenesis is not required for chlamydial growth in a tissue culture model of infection, a host peroxisome-derived ether phospholipid not found in aerobic bacteria is present in *C. trachomatis* (Boncompain et al., 2014), suggesting that *Chlamydia* co-opts host peroxisomes to acquire nutrients.

1.3.4 Recycling endosomes and lysosomes closely appose the inclusion

Transferrin (Tf) is an iron-binding protein that delivers iron to cells through receptor-mediated endocytosis (reviewed in (Richardson and Ponka, 1997)). Tf-containing recycling endosomes associate with the inclusion (van Ooij et al., 1997; Scidmore et al., 1996a), where they are found closely juxtaposed to the inclusion membrane without evidence of fusion (Scidmore et al., 2003). Inhibitors of LPAT interfere with one of the Tf recycling pathways and decrease *Chlamydia* replication (Ouellette and Carabeo, 2010). Similarly, Rab4 and Rab11, which are required for Tf receptor recycling, are enriched at the inclusion (Rzomp et al., 2003), and their disruption results in smaller inclusions and increased retention of Tf around the inclusion (Ouellette and Carabeo, 2010). These findings are consistent with a role for recycling endosomes in promoting *Chlamydia* replication. However, removal of the Tf-containing fraction from cell serum rescues LPAT inhibitor-induced defects on bacterial replication (Ouellette and Carabeo, 2010). These data suggest that over availability of iron – an essential element for normal completion of the infectious cycle (Thompson and Carabeo, 2011) – as a result of increased retention of Tf-containing recycling endosomes around the inclusion interferes with replication (Ouellette and Carabeo, 2010).

Lysosomes are important sites of protein degradation and amino acid turnover within cells. Lysosomes are closely apposed with the inclusion over the course of the

infectious cycle and *Chlamydia* can uptake labeled amino acids or oligopeptides generated through protein degradation within lysosomes (Ouellette et al., 2011). Furthermore, pharmacological inhibition of the vacuolar ATPase that acidifies lysosomes reduces the growth potential of *Chlamydia* (Ouellette et al., 2011), suggesting that lysosomal function is important for the success of *Chlamydia*.

1.3.5 Chlamydia species interact with mitochondria

Early electron microscopy studies indicated that mitochondria closely associate with chlamydial inclusions, especially *Chlamydia psittaci* inclusions (Matsumoto et al., 1991; Peterson and de la Maza, 1988). More recently, in a genome-wide RNAi screen for host factors necessary for *C. caviae* infection, the Tim-Tom mitochondrial protein import complex was identified as important for *Chlamydia* infection (Derré et al., 2007). Recognition and import of nuclear-encoded mitochondrial proteins is disrupted upon Tim-Tom depletion and presumably results in some general mitochondrial dysfunction, although ATP levels remained comparable, indicating that energy production is not dramatically altered (Derré et al., 2007). siRNA-mediated depletion of essential Tom components resulted in smaller inclusions and decreased number of infectious progeny in cells infected with *C. caviae*. In contrast, depletion of Tom components did not affect the amount of infectious progeny recovered with *C. trachomatis* infection. These data suggest that *C. caviae* may be particularly susceptible to alterations in mitochondrial function. *C. caviae* and *C. psittaci* are closely related (reviewed in (Stephens et al., 2009) and mitochondrial interactions could be more critical in these species than other *Chlamydiae* – indeed, the same early ultrastructural studies which described mitochondria surrounding *C. psittaci* inclusions described an apparent lack of

mitochondria around both *C. trachomatis* and *C. pneumoniae* inclusions (Matsumoto et al., 1991).

Upon expression of *Chlamydia*-specific genes in eukaryotic cells, at least one phospholipase D-like protein (CT084) displayed tropism for eukaryotic mitochondria (Sisko et al., 2006), raising the possibility that one or more secreted chlamydial proteins may target host mitochondria during infection, as has been described for other bacterial effectors (Nagai et al., 2005; Papatheodorou et al., 2006). The consequence of these interactions and how they benefit the bacteria remain to be determined, although it is not difficult to envision scenarios where mitochondria may enhance acquisition of nutrients, including energy metabolites, or dampen pro-apoptotic signals. Indeed, increased rates of mitochondrial respiration are observed during the infectious cycle (Hatch and McClarty, 1998b), which may provide increased levels of ATP for replicating *Chlamydia* (Ojcius et al., 1998).

1.4 Manipulation of the host cytoskeleton during mid to late stages of infection

1.4.1 F-actin and intermediate filaments surround the inclusion

Receptors within the cytoplasm of mammalian cells constantly survey the environment for the presence of pathogens (reviewed in (Medzhitov, 2001)). By residing in a modified vacuole, *Chlamydia* can limit the availability of microbial products in the host cytoplasm and evade detection (reviewed in (Kumar and Valdivia, 2009)). As the inclusion expands, however, *Chlamydia* faces the challenge of maintaining the inclusion membrane barrier intact. A scaffold of filamentous actin (F-actin) and intermediate filaments (IF) surround the *Chlamydia* inclusion (Kumar and Valdivia, 2008a).

Perturbation of F-actin assembly in infected cells leads loss of inclusion membrane

integrity and spillage of bacteria into the host cell cytosol, which in turn leads to a hyperactive immune response, as evidenced by an increase in IL-8 activation (Kumar and Valdivia, 2008a). Rho-family GTPases, central regulators of F-actin (reviewed in (Etienne-Manneville and Hall, 2002), are required for F-actin assembly around the inclusion. The clostridial C3-transferase toxin, which inhibits RhoA-C, results in reduced F-actin assembly at the inclusion and a loss of inclusion integrity (Kumar and Valdivia, 2008a). The assembly of IFs and F-actin at the inclusion are interdependent since F-actin depolymerization disrupts the IF cage, and the F-actin cage is poorly assembled in cells lacking IFs (Kumar and Valdivia, 2008a). IFs are relatively static cytoskeletal scaffolding structures, but appear to become more flexible as a result of proteolytic processing by the *Chlamydia* protease CPAF (Dong et al., 2004a; Kumar and Valdivia, 2008a). Removal of the head domain of IFs hinders their ability to form extensive filaments, making them less rigid while still maintaining some of their structural properties. As a result, it has been speculated that F-actin and IFs collaborate to maintain structural integrity of the inclusion (Kumar and Valdivia, 2008a). These data support the model that CPAF, which accumulates in the cytoplasm through the infectious cycle, progressively modifies filaments at the inclusion periphery to facilitate enhanced flexibility and to permit expansion of the inclusion to accommodate replicating bacteria (Kumar and Valdivia, 2008a). Interestingly, treatment of infected cells with a cell-permeable CPAF-specific inhibitory peptide resulted in a loss of inclusion membrane integrity with bacteria observed directly in the cytoplasm (Jorgensen et al., 2011). Whether this collapse is due to the lack of IF modifications or interference with other CPAF functions remains to be determined.

While F-actin assembly at the inclusion is independent of myosin II (Kumar and Valdivia, 2008a), myosin II is recruited to the inclusion at early mid cycle timepoints in large patches which colocalize with active myosin light chain kinase (MLCK) and Src kinases which define a 'microdomain' on the inclusion (Lutter et al., 2013). The light chain of myosin II is phosphorylated at these patches, indicating localized myosin inactivity (Lutter et al., 2013). A subunit of myosin phosphatase, which dephosphorylates myosin allowing its activation, is recruited more ubiquitously to the inclusion and interacts with the Inc CT228 in a yeast 2-hybrid assay (Lutter et al., 2013). The significance of these myosin II-containing microdomains on mid-cycle inclusions remains to be determined particularly since the myosin pathway is not required for F-actin assembly at the inclusion.

1.4.2 Septins are enriched in proximity to the inclusion

Septins are ubiquitous GTPases that form heterocomplexes which can associate into filaments and form bundles and rings (reviewed in (Mostowy and Cossart, 2012)). They often associate with F-actin and participate in higher order structures to form scaffolds or diffusion barriers, and were first identified in the model organism *Saccharomyces cerevisiae* as critical for cell division and as a component of filamentous rings at the septating bud neck (Byers and Goetsch, 1976; Haarer and Pringle, 1987; Hartwell, 1971; Kim et al., 1991). Not surprisingly, septins also play roles during intracellular bacterial infections (Mostowy and Cossart, 2011).

Septins 2, 9, and 11 form filamentous structures at the *C. trachomatis* inclusion (Volceanov et al., 2014) which appear qualitatively distinct from the F-actin structure assembled at the inclusion previously described in (Kumar and Valdivia, 2008a). Interestingly, while septins can be observed at the inclusion periphery, they are

particularly prominent in long bundles that colocalize with F-actin underneath the inclusion in structures that appear to resemble transverse stress fibers which connect focal adhesions (adhesive structures that link extracellular substrates to the internal F-actin network) across the cell. Global F-actin depolymerization disrupts septin recruitment to the inclusion in addition to other cellular structures, and RNAi-mediated depletion of septins during infection broadly affects F-actin structures, including stress fibers (Volceanov et al., 2014), leaving the significance of these particular septin structures unclear.

1.4.3 Microtubules near the inclusion are post-translationally modified

In cells infected with *Chlamydia*, microtubules (MTs) are found throughout the host cytosol, and thus also appear in close proximity to the inclusion. Since MT pharmacological depolymerization does not affect *Chlamydia* growth in cells (Schramm and Wyrick, 1995), inclusion development (Schramm and Wyrick, 1995), or inclusion stability (Kumar and Valdivia, 2008a), for some time it was unclear whether MTs were particularly altered or co-opted during infection. More recently, it has been revealed that MTs in close proximity to the inclusion are post-translationally modified by detyrosination and acetylation, and MT detyrosination is generally upregulated during infection (Al-Zeer et al., 2014). MT modifications do not alter the inherent dynamics of MT polymers *per se*, rather MT modifications affect the recruitment of microtubule-associated proteins (MAPs), and this selective recruitment can result in altered MT dynamics (Janke and Bulinski, 2011). For instance, members of the Kinesin-13 family preferentially depolymerize tyrosinated microtubules, which can make detyrosinated MTs more stable in the presence of these MAPs. However, modification does not always result in

increased stability, and it remains unclear whether the acetylation of MTs consistently affects their stability (Janke and Bulinski, 2011). Detyrosinated MTs at the inclusion are more resistant to pharmacological depolymerization but without assessment of MT dynamics in real-time (Al-Zeer et al., 2014), it remains unclear whether modified MTs around the inclusion truly behave as a more stable subpopulation of MTs. Treatment of infected cells with sesquiterpene lactones reduces MT detyrosination and decrease *Chlamydia* growth (Al-Zeer et al., 2014). However, interpretation of these findings is confounded by the multitude of activities of sesquiterpene lactones, which have anti-inflammatory properties, inhibit NFκB, and can induce apoptosis, reactive oxygen species production, and autophagy (Whipple et al., 2013). As critical mediators of vesicular trafficking, MTs are critical for Golgi morphology, and the Golgi is dispersed upon pharmacological MT depolymerization (Wehland et al., 1983). After washout of a MT depolymerizing agent during infection, the Golgi reforms in a pattern where it is distributed along the periphery of the inclusion coincidentally with MT reappearance, and only after another few hours does MT detyrosination become evident (Al-Zeer et al., 2014), suggesting that MT detyrosination is not required for Golgi recruitment and redistribution around the inclusion. As such, the significance of MT modification around the inclusion remains unclear.

1.4.4 Chlamydia can exit host cells by actin-dependent extrusion

At the end of the infectious cycle, the exit of EBs from the infected cells involves both extrusion of the inclusion and cell lysis (Hybiske and Stephens, 2007). As assessed by live video microscopy, approximately half of exit events involve the extrusion of a portion of the intact inclusion, leaving the infected cell intact. Extrusion is a relatively slow process with the inclusion continuously encased by plasma membrane as it

protrudes out of the cell. Inhibitors of actin polymerization and myosin II function, which is important for the contractile property of actomyosin fibers, completely inhibit extrusion. RhoA-C GTPases are also required for the pinching and release of extruded inclusions, implying two sequential actomyosin-mediated steps in extrusion. F-actin at the inclusion becomes progressively more prominent at later stages of infection, extruded structures can retain an F-actin coat, and this late F-actin coat has been suggested to be involved in inclusion extrusion (Chin et al., 2012). The association of F-actin at these very late stages of the infectious cycle is dependent on myosin II which is in contrast to F-actin assembled at earlier mid cycle times (Chin et al., 2012; Kumar and Valdivia, 2008a). Septins are also required for F-actin recruitment to the inclusion very late in the infectious cycle (Chin et al., 2012), and for extrusion (Volceanov et al., 2014) and the combined involvement of Rho, myosin II, and septins suggests that the mechanism of extrusion shares similarities with formation and contraction of the cleavage furrow during cytokinesis (reviewed in (Piekny et al., 2005)). In contrast to the relatively protracted process of extrusion, the lysis exit pathway is characterized by rapid sequential rupture of the inclusion, organellar, and plasma membranes, and requires the activity of cysteine proteases (Hybiske and Stephens, 2007). This suggests a programmed set of lytic events rather than disordered rupture due to mechanical forces exerted by the inclusion (Hybiske and Stephens, 2007).

Different exit strategies could potentially be favored at different stages of infection or in response to diverse host environments. This could allow for fine control over local inflammatory responses by controlling the extent of host cell lysis – although it should be noted that these extrusion events have not yet been documented in infected animals. *C. trachomatis* serovars D and L2, and *C. caviae* all display similar lysis and

extrusion mechanisms (Hybiske and Stephens, 2007), but some differences may exist among serovars and strains since *C. trachomatis* serovar E exit is characterized by plasma membrane disruption prior to inclusion membrane permeability (Beatty, 2007). Fusion of lysosomes with the plasma membrane repairs any rupture and some bacteria remain in the cell after exit (Beatty, 2007). Whether extrusion and membrane-repaired exit of EBs enable persistent infections allowing bacteria to hide within viable cells remains to be determined.

1.5 Conclusions and future perspectives

As *Chlamydia* can only replicate within the confines of a eukaryotic cell, it is not surprising that it has evolved an intricate arsenal of effector proteins with which to manipulate its host cell. As we continue to learn about the function of these effector proteins, a few general mechanistic strategies come to light. One strategy is the modification of host factors by proteolysis and/or degradation to alter the cell cycle, inhibit apoptosis and suppress innate immune responses (Balsara et al., 2006; Chellas-Géry et al., 2007; Cocchiaro and Valdivia, 2009). In addition, protein modification by effectors like NUE (CT737), a histone methyltransferase, may silence genes involved in anti-microbial responses (Pennini et al., 2010). Conversely, removal of protein modifications by effectors like the *Chla*Dub proteins, which display de-ubiquitinating and de-neddylating activity (Misaghi et al., 2006), may assist in with silencing immune-related signaling (Le Negrate et al., 2008).

Another set of effectors appears to be restricted to the inclusion membrane. These include Inc proteins that can act to sequester host proteins to the inclusion membrane, thus interfering with innate defense processes such as apoptosis (Tse et al.,

2005; Verbeke et al., 2006). Inc proteins can also interact extensively with components of the endolysosomal system, including SNAREs and Rab proteins (Delevoeye et al., 2008; Paumet et al., 2009; Rzomp et al., 2003, 2006), presumably to avoid lysosomal degradation. Finally, Inc proteins may facilitate interactions with other organelles such as the ER to facilitate lipid acquisition (Derré et al., 2011; Elwell et al., 2011); or centrosomes for correct positioning of the inclusion within the cells (Mital et al., 2010).

There is also a growing appreciation that *Chlamydia* effectors may work cooperatively and be subjected to different levels of post-secretion regulation. For instance, CPAF cleaves a number of early effectors to regulate their activity and may play a role in niche protection by limiting superinfection of cells (Jorgensen et al., 2011). Similarly, Incs can form multi-protein complexes with other Incs to form centrosome-associated subdomains on the inclusion membrane (Mital et al., 2010). The regulation of effectors by other effectors and their ability to form multi-effector complexes may add an added level of complexity and dynamism to their functions. Indeed, our inference of how effectors affect the cell biology of the host, which is largely based on biochemical and gain-of-function approaches, may not tell the whole story. This leads to the important questions of how individual effectors contribute to the many documented alterations in the host and how do these changes influence pathogenesis. Definitive answers to these questions will require loss-of-function approaches. Reassuringly, progress in the development of genetic tools for *Chlamydia* should help address the function of effectors.

Given the long evolutionary history of *Chlamydiae* association with eukaryotic cells (Horn, 2008), these bacteria should reveal new insights into basic aspects of

eukaryotic cell biology, primordial mechanisms of cell autonomous innate immunity, and novel pathogenic strategies.

2. F-actin assembly at the *C. trachomatis* inclusion¹

2.1 Introduction

From within the inclusion, *Chlamydia* manipulates host cellular pathways to ensure its proliferation and survival, including changes to the organization of the host cell's internal architecture such as the redistribution of organelles and cytoskeletal elements around the inclusion (Chapter 1). Given the lack of robust tools for molecular genetic manipulation in *C. trachomatis*, the bacterial genes and host mechanisms underlying these cellular changes and their contribution to *Chlamydia* pathogenesis remain poorly understood.

Here, I present genetic and molecular mechanisms of chlamydial manipulation of the host cytoskeleton and potential functions. Using a forward genetics screen, I identified InaC as a necessary factor for the assembly of an F-actin structure surrounding the inclusion. InaC associated with the vacuolar membrane where it recruited 14-3-3 Golgi-specific ARF-family GTPases. Actin dynamics and ARF GTPases regulate Golgi morphology and positioning within cells, and I discovered that InaC acts to redistribute the Golgi to surround the *Chlamydia* inclusion. These findings suggest that *Chlamydia* places InaC at the inclusion-cytosolic interface to recruit host ARF

¹ Parts of Chapter 2 are reused and edited with permission of the following published article of which I am first author: Kokes, M., Dunn, J.D., Granek, J.A., Nguyen, B.D., Barker, J.R., Valdivia, R.H., and Bastidas, R.J. (2015). Integrating Chemical Mutagenesis and Whole-Genome Sequencing as a Platform for Forward and Reverse Genetic Analysis of Chlamydia. *Cell Host & Microbe* 17, 716–725.

GTPases and F-actin to form a platform for rearranging intracellular organelles around the inclusion.

Here, I present genetic and molecular mechanisms of chlamydial manipulation of the host cytoskeleton and how this may alter organelle distribution. I find that the host actin-membrane linking protein filamin and the actin bundling protein α -actinin are components of F-actin assembly at inclusions. By implementing a microscopy-based forward genetic screen of a collection of chemically mutagenized *C. trachomatis* strains, I identified two bacterial factors important for regulating cytoskeletal rearrangements at the periphery of the inclusion. InaC associated with the vacuolar membrane where it recruited 14-3-3s and Golgi-specific ARF-family GTPases. InaC mediates recycling endosome and Golgi reorganization yet is dispensable for trafficking of Golgi derived sphingolipids to the inclusion. Overall, these findings suggest that *Chlamydia* places ARF and 14-3-3-recruiting InaC at the inclusion-cytosolic interface assemble F-actin and form a platform for rearranging intracellular organelles around the inclusion.

2.2 Genetic approach to investigate F-actin assembly

2.2.1 Forward genetic screen for bacterial effectors involved in F-actin rearrangements at the *C. trachomatis* inclusion

At mid to late stages of the infectious cycle, *Chlamydia* induces a rearrangement of the host actin cytoskeleton to form a filamentous scaffold at the periphery of the inclusion which has been proposed to support inclusion integrity and maintain bacterial products sequestered from the cell cytosol thereby reducing cell-autonomous immune responses (Kumar and Valdivia, 2008a). We implemented a microscopy-based screen to identify bacterial factors modulating the rearrangement of F-actin at the periphery of the inclusion in infected cells. We screened a library of over 800 chemically mutagenized

rifampin-resistant (Rif^R) lymphogranuloma venereum (LGV) *C. trachomatis* serovar L2 (L2/434/Bu) strains (Kokes et al., 2015) for mutants with altered F-actin assembly at the inclusion. We identified two strains with contrasting phenotypes – M407 failed to promote F-actin assembly while M338 enhanced F-actin assembly at inclusions (Figure 3).

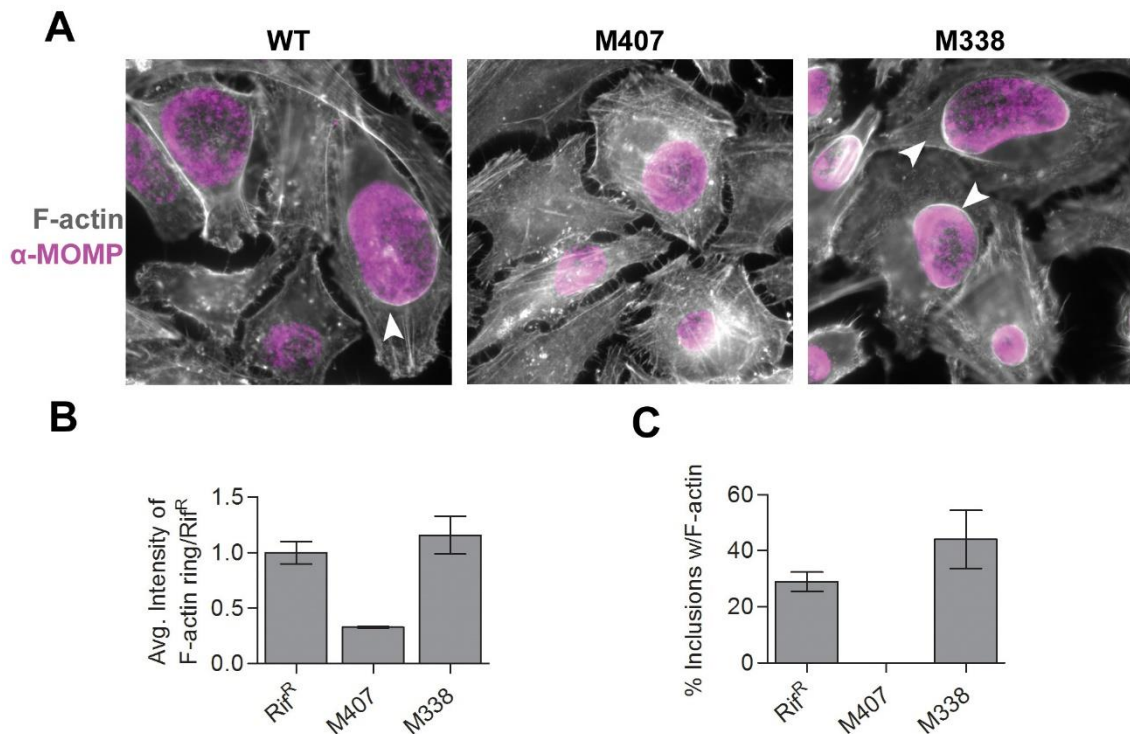


Figure 3. *C. trachomatis* strains M407 and M338 display altered F-actin assembly at inclusions. F-actin (grayscale) and *C. trachomatis* (magenta) were detected by indirect immunofluorescence at 30 hpi using rhodamine-phalloidin to label F-actin and anti-MOMP antibodies to label bacteria, respectively (A). Note the presence of distinct F-actin structures around the inclusion periphery (arrowheads) at Rif^R(WT), lacking at M407, and enhanced at M338 inclusions. M407 has decreased fluorescence of F-actin around inclusion (B) and lacks distinct F-actin structures (arrowheads, A) at an absolute frequency within the population (C). M338 has enhanced F-actin recruitment (A) and intensity (B) at a higher frequency of inclusions. Mean \pm SEM for three independent experiments is shown.

2.2.2 F-actin assembly around the inclusion is enhanced by a S314F mutation in the uncharacterized Chlamydia predicted ORF CTL0496

Since mutants within the screened library harbor on average 10 mutations, I used a combination of whole genome sequencing, strain lateral gene transfer, and linkage analysis (Nguyen and Valdivia, 2012) to identify the mutation within M338 leading to enhanced F-actin at inclusions. M338 sequencing revealed seven introduced non-synonymous mutations within open reading frames (ORFs) (labeled as single nucleotide variant (SNV) locus in Figure 4). By performing genetic crosses between M338 (which is Rif^R) and a spectinomycin resistant (Spc^R) wild type strain, assessing the phenotype of recombinants and tracking the inheritance of each parental M338 mutation, I identified a missense mutation in CTL0496 (G941A/S314F) as responsible for enhanced F-actin assembly at inclusions (Figure 4).

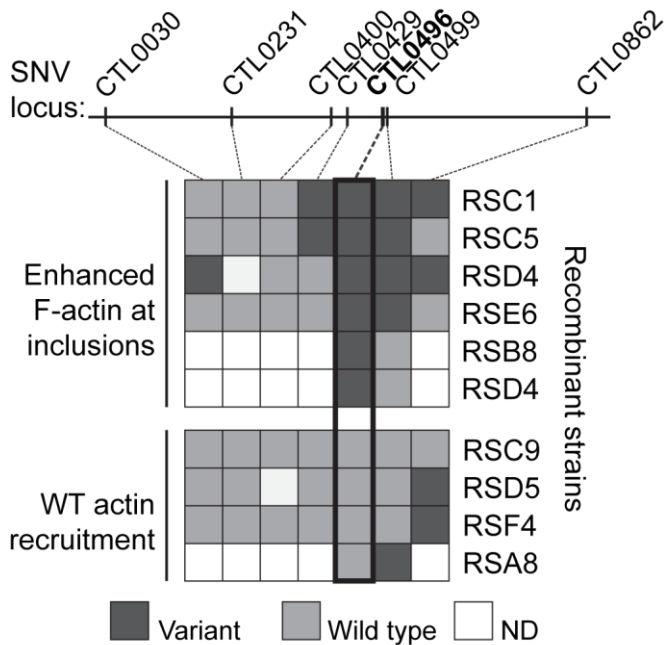


Figure 4. Enhanced F-actin assembly at M338 inclusions maps to a missense mutation in CTL0496. Mutant M338 harbors non-synonymous mutations in 7 ORFs (tick marks, CTL...). All recombinants were generated from a single co-infection between

M338 and a wild type strain. The genotype of each individual recombinant strain (row) was assessed within each indicated ORF for presence of the M338 parental (variant, dark gray boxes) or wild type (light gray boxes) allele. F-actin at inclusions was assessed for each recombinant strain (row) and grouped according to phenotype. Note that all recombinant progeny with enhanced F-actin at inclusions inherited the *CTL0496* mutant allele.

2.2.2.1 Primary sequence analysis of CTL0496

CTL0496 is a hypothetical *C. trachomatis* LGV L2 encoded protein of 398 amino acids. It is homologous to *C. trachomatis* Serovar D predicted protein CT244 at 97% identity, has a homolog in *C. muridarum* at 76% identity, has relatively poor homology at approximately 30% identity in the other more distant species of *Chlamydia*, and lacks homology to proteins outside of *Chlamydiales*. *CTL0496* is not part of an operon, and *CTL0496* is soluble but is not predicted to be secreted by any chlamydial secretion system. In other *Chlamydia* species S314 is conserved (*C. muridarum*) or occurs as a Met or Ile. Thus, the effect of the S314F mutation on *CTL0496* function is difficult to predict.

2.2.3 The inclusion membrane protein InaC is necessary for F-actin assembly at the inclusion periphery

In contrast to M338, M407 displayed a reproducible defect in the assembly of F-actin at inclusions (Figure 3). To identify the causal mutation, I first sequenced the genome of M407. M407 harbors 12 non-synonymous mutations as compared to the reference genome (SNV locus, Figure 5). By performing genetic crosses between M407 (which is Rif^R) and a spectinomycin resistant (Spc^R) wild type strain (Nguyen and Valdivia, 2012), I identified a nonsense mutation in *CTL0184* (*C307T/Q103,**), as being responsible for the failure to promote F-actin assembly at inclusions (Figure 5).

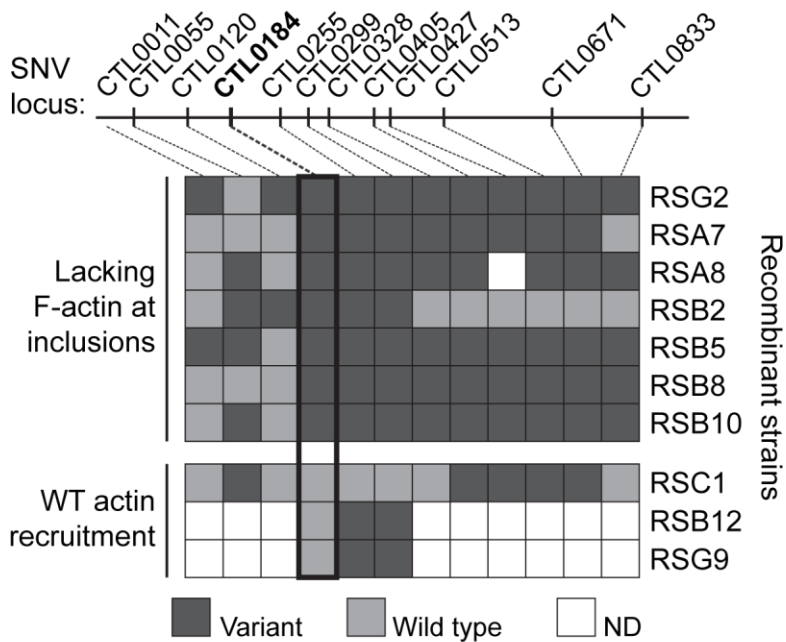


Figure 5. Loss of F-actin assembly at M407 inclusions maps to a nonsense mutation in *CTL0184*. Mutant M407 harbors 1 non-sense mutation and 11 non-synonymous mutations in 12 ORFs (tick marks, CTL...). All recombinants were generated from a single co-infection between M407 and a wild type strain. The genotype of each individual recombinant strain (row) was assessed within each indicated ORF for presence of the M407 parental (variant, dark gray boxes) or wild type (light gray boxes) allele. F-actin at inclusions was assessed for each recombinant strain (row) and grouped according to phenotype. Note that all recombinant progeny lacking F-actin at inclusions inherited the *CTL0184* mutant allele.

Western blot analysis and immunofluorescence microscopy with antibodies raised against the inclusion membrane protein CT813, the homolog of *CTL0184* in *C. trachomatis* Serotype D (Chen et al., 2006; Li et al., 2008) confirmed the absence of *CTL0184* in M407 (Figure 6A and B). Given the genetic link between the *CTL0184*^{C307T} allele, the lack of detectable *CTL0184* gene product, and the loss of F-actin assembly to the inclusion, we renamed *CTL0184* as *InaC* (Inclusion membrane protein for actin assembly), to reflect its role in F-actin remodeling.

2.2.3.1 Expression of full-length InaC in M407 rescues F-actin assembly

To confirm InaC's role in F-actin rearrangements, I transformed M407 with a plasmid shuttle vector encoding wild type *inaC* under the control of its endogenous promoter. Transformation restored InaC production in M407 (Figure 6B and 7C) and F-actin assembly at the inclusion (Figure 6C). The amount (Figure 6D) and the frequency (Figure 6E) of F-actin structures at M407 inclusions were restored to wild type levels after transformation with an InaC expressing plasmid but not an empty vector control. This demonstrates that InaC is required for F-actin assembly around the *C. trachomatis* inclusion.

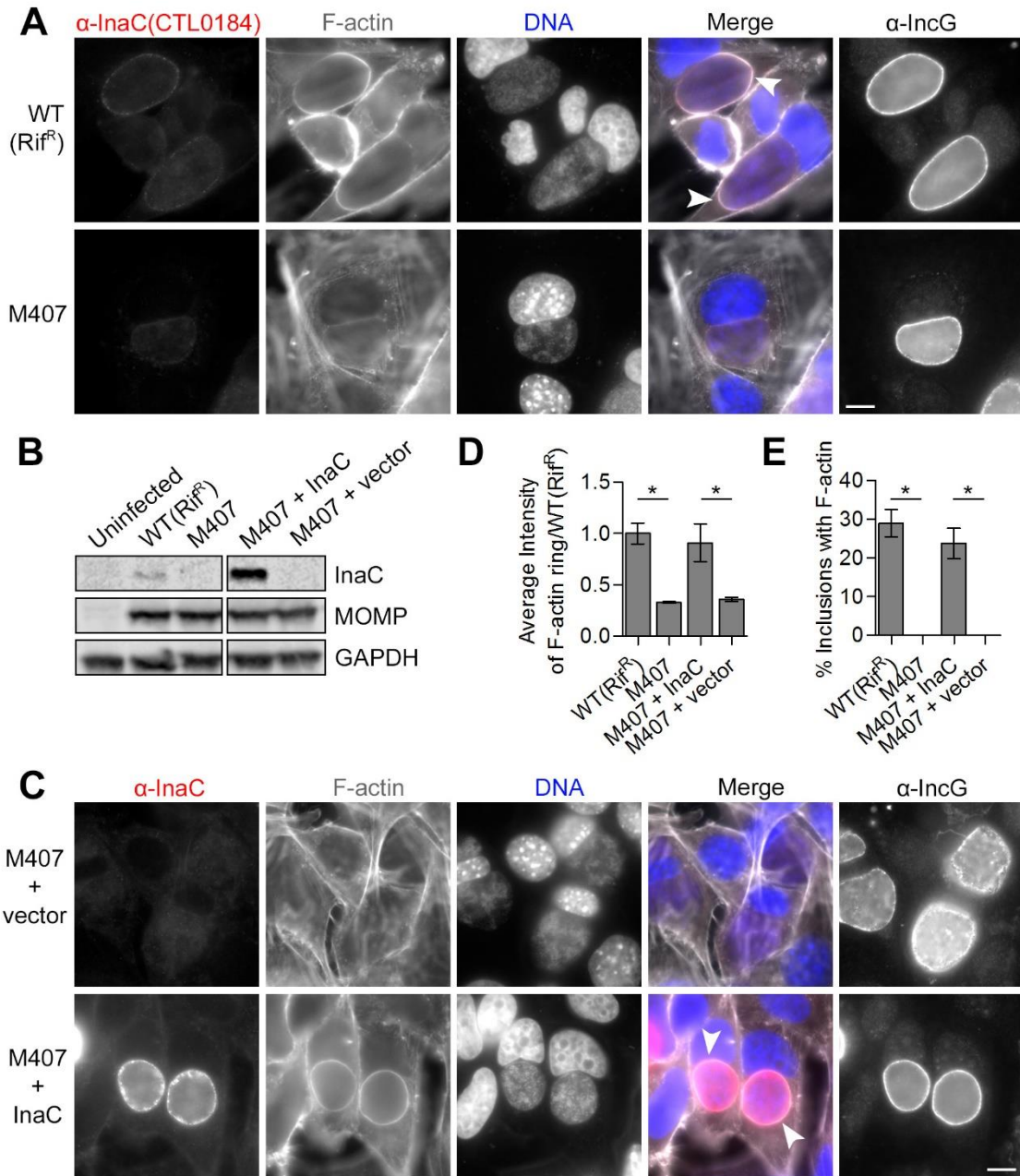


Figure 6. The inclusion membrane protein InaC (CTL0184) is required for F-actin assembly at the inclusion. (A) F-actin assembly at inclusions (arrowhead) is absent in HeLa cells infected with M407. F-actin (grayscale) and *C. trachomatis* (red) were detected by indirect immunofluorescence at 30 hpi using rhodamine-phalloidin and anti-MOMP antibodies respectively. DNA (blue) was stained with Hoechst. (B–E) F-actin assembly in M407 inclusions is rescued upon expression of wild type InaC. InaC expression is restored in M407 mutants transformed with a plasmid expressing wild type

inaC from its own promoter as assessed by immunoblot (C) and immunofluorescence (red, D) analysis and without affecting the distribution of another inclusion membrane protein, IncG. F-actin assembly at the inclusion (white arrowheads, (C)) is restored in M407 transformed with a plasmid encoding inaC but not an empty vector. Note that the average intensity (D) and frequency (E) of F-actin around complemented inclusions is comparable to wild type. Mean \pm SEM for three independent experiments is shown. At least 50 (F) or 300 (E) inclusions were enumerated in each triplicate for each experiment. * indicates $P < 0.05$ by one-way ANOVA and Newman-Keuls post hoc. Scale bars represent 10 μ m.

2.2.3.2 Primary sequence analysis of InaC

CTL0184/InaC is 264 amino acids in length and has two predicted transmembrane domains (Figure 7). This bi-partite hydrophobic domain is characteristic of a class of *Chlamydial* proteins called Incs, which are secreted by the type three secretion system (T3SS) into the host cytoplasm and associate with the inclusion membrane (Rockey et al., 2002). Topology predictions indicate that the bi-partite transmembrane regions would form a membrane spanning hairpin structure with both N- and C-terminal regions on the same side of a membrane – presumably within the cytosol. The C-terminal region appears to have a heptad *hxxhcxc* repeat (where *h* is a hydrophobic residue, *c* is charged, and *x* is any amino acid) characteristic of coiled-coils (Mason and Arndt, 2004), and indeed, regions 151-201 and 206-251 are predicted at a 90% threshold with Marcoil (Delorenzi and Speed, 2002) to participate in a coiled-coil (Figure 7). Likely because of this, InaC appears to have putative homology domains with numerous other coiled-coil proteins, such as tropomyosin, as annotated in the KEGG SSDB (Sequence Similarity DataBase). InaC is highly conserved in all serovars of *C. trachomatis*, including ocular, genital and LGV strains (at >92% identity) and orthologs can be found in other *Chlamydia*, including *C. muridarum* and *C. suis* (at 44% identity),

C. pneumoniae (at 33% identity), and the remaining *Chlamydia* species at approximately 25% identity.

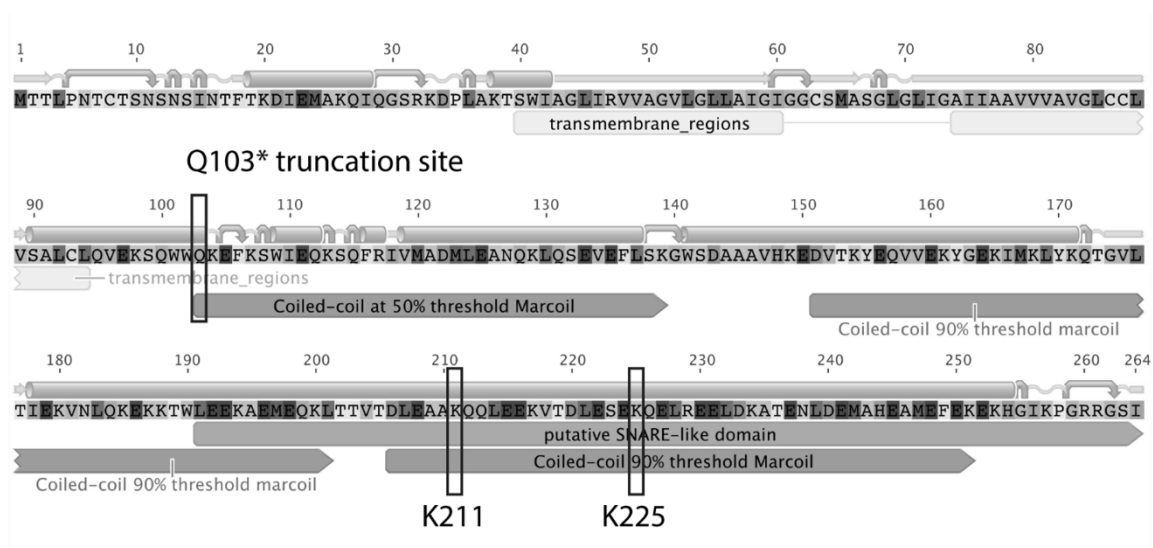


Figure 7. Schematic of InaC protein. Amino acids are displayed as single letters. Predicted secondary structures are displayed above the protein sequence, including beta strands (arrow), turns (curved arrow), alpha helices (cylinder), and coils (curvy line), with labeled boxes for transmembrane regions, and coiled-coils. The previously reported putative SNARE-like region (Delevoye et al., 2008) is labeled. Modified amino acids are highlighted with black rectangles, including the residue of truncation in M407 (Q103), and two lysines mutated to assess potential SNARE activity (see Section 2.9). Figure created with the assistance of Geneious Software (Biomatters).

2.3 Mechanisms of *F-actin* assembly at the inclusion

2.3.1 Filamins and α -actinin co-assemble with *F-actin* at inclusions

Rho-family GTPases are master switches that can dynamically control the formation of distinct *F-actin* structures. Of the three most studied mammalian Rho-family GTPases, Rac1, Cdc42, and RhoA, only RhoA is required for *F-actin* assembly at inclusions (Kumar and Valdivia, 2008a), indicating that RhoA pathways are involved in assembling or maintaining this structure at the inclusion. Consistent with this, EGFP-rGBD, which selectively binds active GTP-bound Rho, is recruited at the inclusion periphery (Figure 8A) and active GTP-bound RhoA levels increase nearly six-fold during

infection but remain at basal levels after infection with M407 which lacks F-actin assembly at inclusions (Figure 8B). Together, these data suggest that *Chlamydia* is manipulating RhoA activation for F-actin assembly at the inclusion.

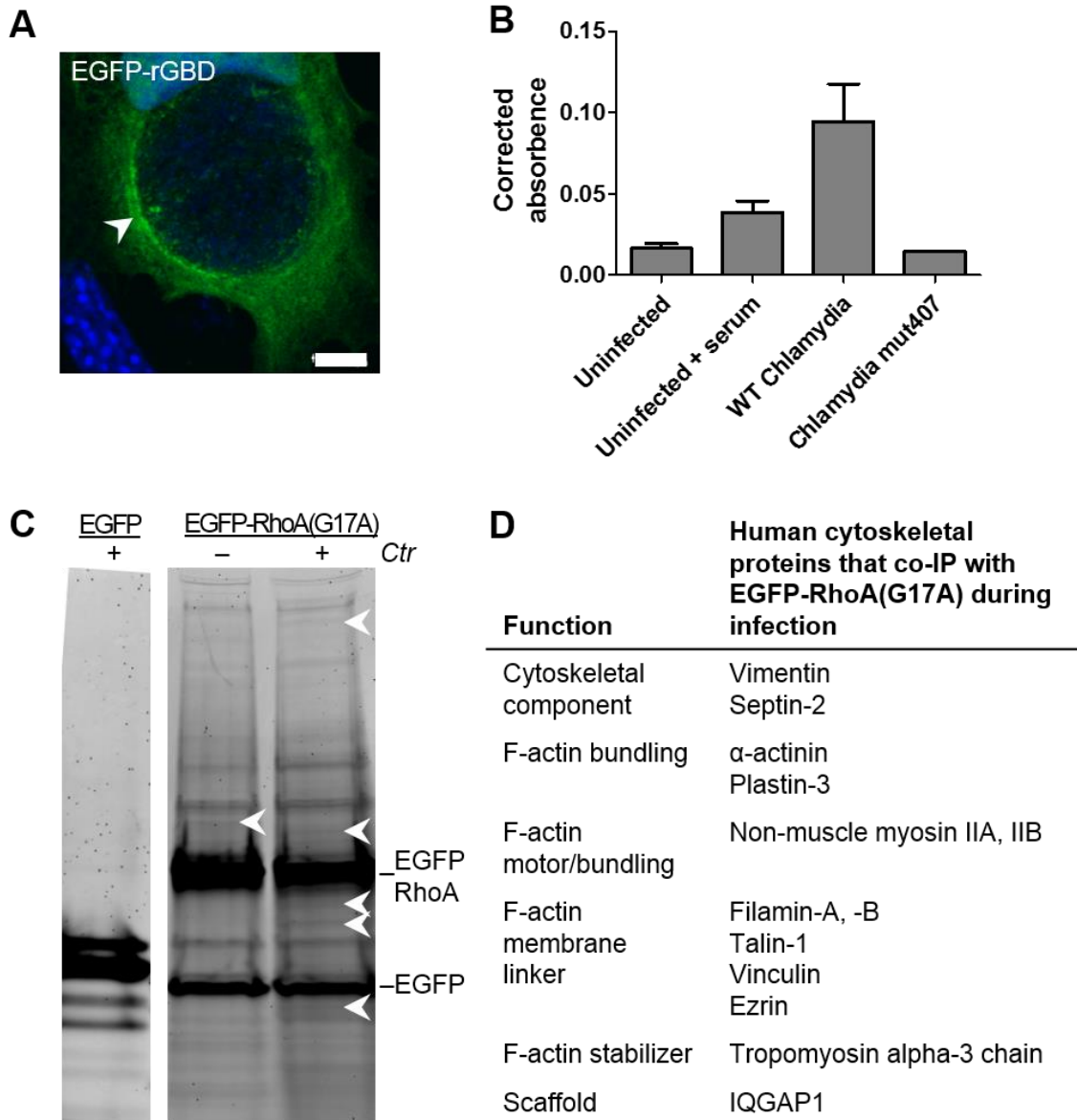


Figure 8. RhoA is active during *Chlamydia* infection and interacts with a subset of cytoskeletal proteins specifically during infection. (A) RhoA is active at the inclusion periphery. HeLa cells were infected with *C. trachomatis* for 30 hours, transfected with EGFP-rGBD for 24 hours, fixed and stained with Hoescht for DNA (blue). EGFP-rGBD

(green) binds to RhoA only when it is GTP-bound and active. Note EGFP-rGBD enrichment at the inclusion edge (arrowhead). Scale bar represents 5 μ m. (B) RhoA is activated during *Chlamydia* infection in an InaC-dependent manner. Swiss albino 3T3 fibroblasts were serum-starved and infected with *C. trachomatis* WT or M407 for 30 hours. As a positive control, uninfected cells were treated with 20% serum to induce RhoA activity for 5 minutes. Protein lysates were harvested, equalized for total protein content, and assessed by GLISA (Cytoskeleton, Inc.) for levels of active GTP-bound RhoA. Mean \pm SD of two replicates are shown. (C and D) Proteins that uniquely interact with EGFP-RhoA(G17A) in *Chlamydia*-infected cells. Lysates from HEK 293T cells transiently expressing either EGFP or EGFP-RhoA(G17A) and infected with *C. trachomatis* LGV L2 (*Ctr*) for 30 hours were incubated with GFP-Trap resin. Bound proteins were eluted, resolved by SDS-PAGE, and visualized by Sypro Orange (Invitrogen) protein staining. Note the presence of bands unique to infected or uninfected EGFP-RhoA(G17A) immunoprecipitations (arrowheads). Numerous human cytoskeletal proteins were identified (D).

Rho-family GTPases elicit F-actin rearrangement when activated to the GTP-bound form through functional interaction with GEFs. To investigate what could regulate RhoA activity during infection, I identified interacting proteins by immunoprecipitation (IP) of an EGFP-tagged RhoA(G17A) variant transiently expressed in HEK 293T cells either uninfected or infected with a wild-type *C. trachomatis* (Figure 8C). RhoA(G17A) cannot bind nucleotides, thus mimicking an intermediate state which binds to RhoA GEFs at a higher affinity. Several known RhoA GEFs were identified, which validates the technique (data not shown), albeit in an infection independent manner. However, many of the fifty-nine interacting proteins unique to infection were proteins known to participate in F-actin dynamics (Figure 8D). It remains unclear why these proteins would co-IP with RhoA as a direct interaction with RhoA has not been described.

Many of the cytoskeletal proteins that co-IP with EGFP-RhoA(G17A) specifically during infection are known to play structural roles in F-actin dynamics (Figure 8D). Thus these proteins could be components of the F-actin structure assembled around the inclusion. To address this possibility, I assessed the localization of each protein during infection either via immunofluorescence and/or by transient transfection of fluorescent

protein-tagged constructs (Figure 9). Filamin and α -actinin consistently colocalized with F-actin around inclusions. IQGAP1 also colocalized with F-actin at inclusions, although less prominently. Talin, vinculin, and both non-muscle myosin heavy chain IIA and IIB were recruited to the inclusion in large patchy regions that did not always colocalize with F-actin. All proteins were lacking around M407 inclusions (which lack F-actin assembly, Figure 3) but only filamin and α -actinin appeared enhanced around M338 inclusions (which display enhanced F-actin recruitment (Figure 3) (data not shown)). Taken together, these data suggest that α -actinin and filamin are components and novel markers of the F-actin structure assembled at the inclusion. Talin, vinculin, IQGAP1 and non-muscle myosin II may play upstream regulatory roles or define sub-regions of assembled F-actin at the inclusion. Notably, many of these proteins are known to be involved in adhesion where they connect the intracellular F-actin network to plasma-membrane-spanning adhesion complexes which themselves are attached to the extracellular matrix or other cells (Parsons et al., 2010). Thus, adhesion-like complexes may form a signaling and structural basis of F-actin assembled at the inclusion.

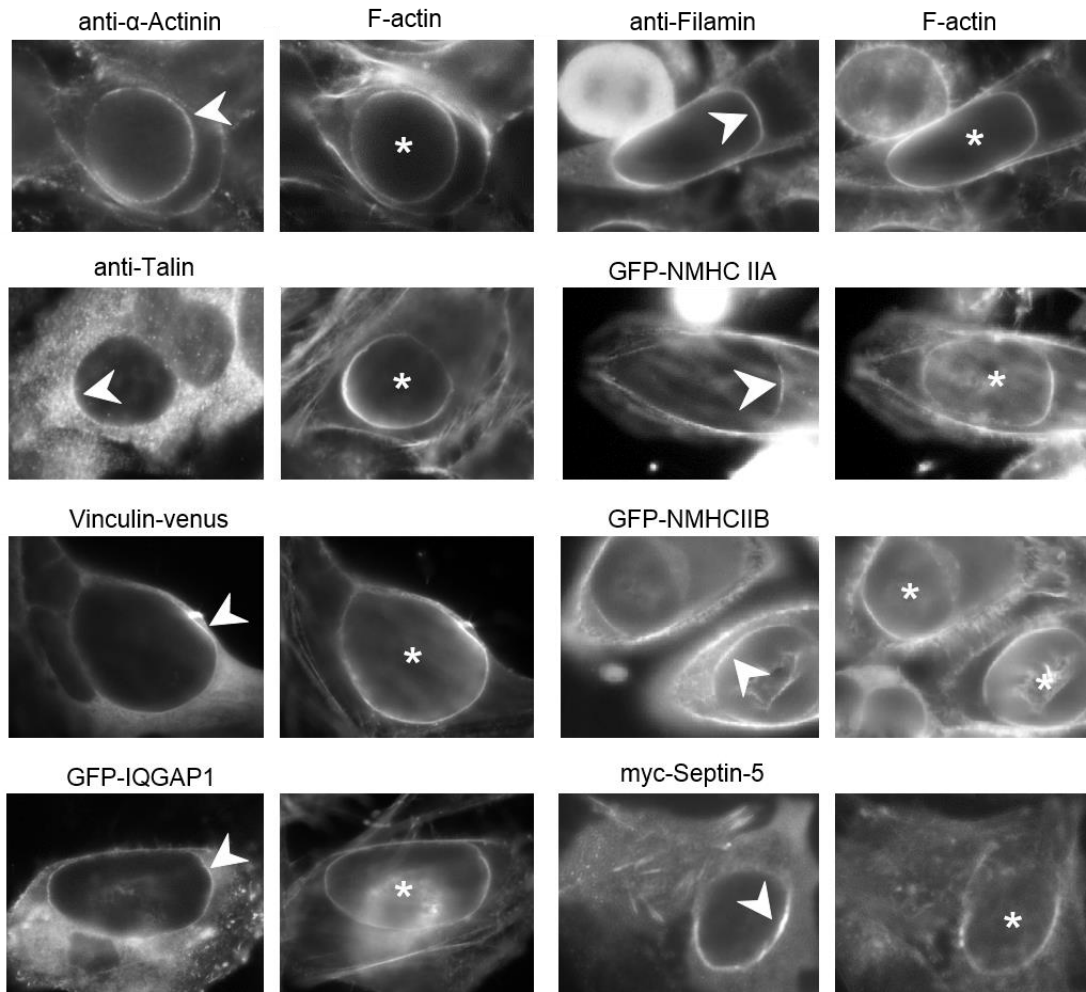


Figure 9. Host cytoskeletal proteins that co-IP with EGFP-RhoA(G17A) during infection colocalize with F-actin at inclusions. HeLa cells were infected with *C. trachomatis* LGV L2, transfected to express the indicated fusion proteins, and processed at 30 hpi for immunofluorescence using the indicated antibodies and rhodamine-phalloidin to label F-actin (right panels). Note co-localization with F-actin (arrowheads) at the inclusion. Inclusions are marked with an asterisk.

2.3.2 InaC recruits ARF and 14-3-3 proteins to the inclusion

In addition to the host GTPase RhoA, the chlamydial protein InaC is required for F-actin assembly at the inclusion (Figure 6). Since InaC localizes to the cytoplasmic surface of the inclusion membrane, InaC could interact with and recruit host proteins to activate actin-related pathways for assembly at the inclusion. To investigate how InaC

interfaces with host cellular pathways, I identified interacting host proteins by immunoprecipitating (IP) a GFP-tagged full-length InaC transiently expressed in HEK 293T cells. Ten of the 19 interacting proteins identified by mass spectrometry (Table 1) belong to two protein families – human ADP-ribosylation factors (ARF1, 4 and 5), and 14-3-3 proteins (Figure 10A). I confirmed the interaction of GFP-InaC with endogenous 14-3-3 β , 14-3-3 ϵ , and ARF1 by immunoblot analysis (Figure 10B). ARFs are small GTPases that function in vesicular trafficking and secretory organelle function (Donaldson and Jackson, 2011) and 14-3-3s are a family of conserved regulatory proteins that bind and regulate signaling proteins in numerous cellular pathways (Morrison, 2009). Given that ARF1-GFP and 14-3-3 β localize to the inclusion periphery (Moorhead et al., 2010; Scidmore and Hackstadt, 2001), I tested whether InaC mediates the recruitment of ARFs and 14-3-3s by assessing the localization ARF-GFP (ARF1, 4, 5, and 6 with C-terminal EGFP) and endogenous 14-3-3 β and 14-3-3 ϵ in cells infected with wild type *C. trachomatis* or InaC mutants (Figure 10C). 14-3-3 β and 14-3-3 ϵ are enriched around wild type inclusions yet are barely detectable around inclusions lacking InaC. ARF1-, ARF4-, and ARF5-GFP are recruited to wild type inclusions in a uniform ring which is absent around inclusions lacking InaC. Strikingly, the localization of ARF1, 4, 5 and 14-3-3 to inclusions is markedly increased in strains over-expressing InaC (Figure 10C).

ARF-family GTPases fall into three classes. Class I (ARF1, ARF3) and Class II (ARF, ARF5) are involved in secretory trafficking and localize primarily to the Golgi, while Class III (ARF6) localizes to the plasma membrane and endosomes where it functions in endocytic membrane trafficking and actin dynamics (Donaldson and Jackson, 2011; D'Souza-Schorey and Chavrier, 2006). We failed to identify any peptides

mapping to the Class III ARF6 (Table 1), which is also the most divergent ARF, and suspected that InaC may selectively recruit only Class I and Class II ARFs to the inclusion. Indeed, ARF6-GFP failed to localize to inclusions that are wild type, lacking InaC, and over-expressing InaC (Figure 4C). In contrast, ARF3-GFP localized to inclusion in an InaC-dependent manner similar to ARF1-GFP (data not shown). These data suggest that InaC is necessary for and mediates the recruitment of 14-3-3s and Golgi-specific ARFs to the inclusion.

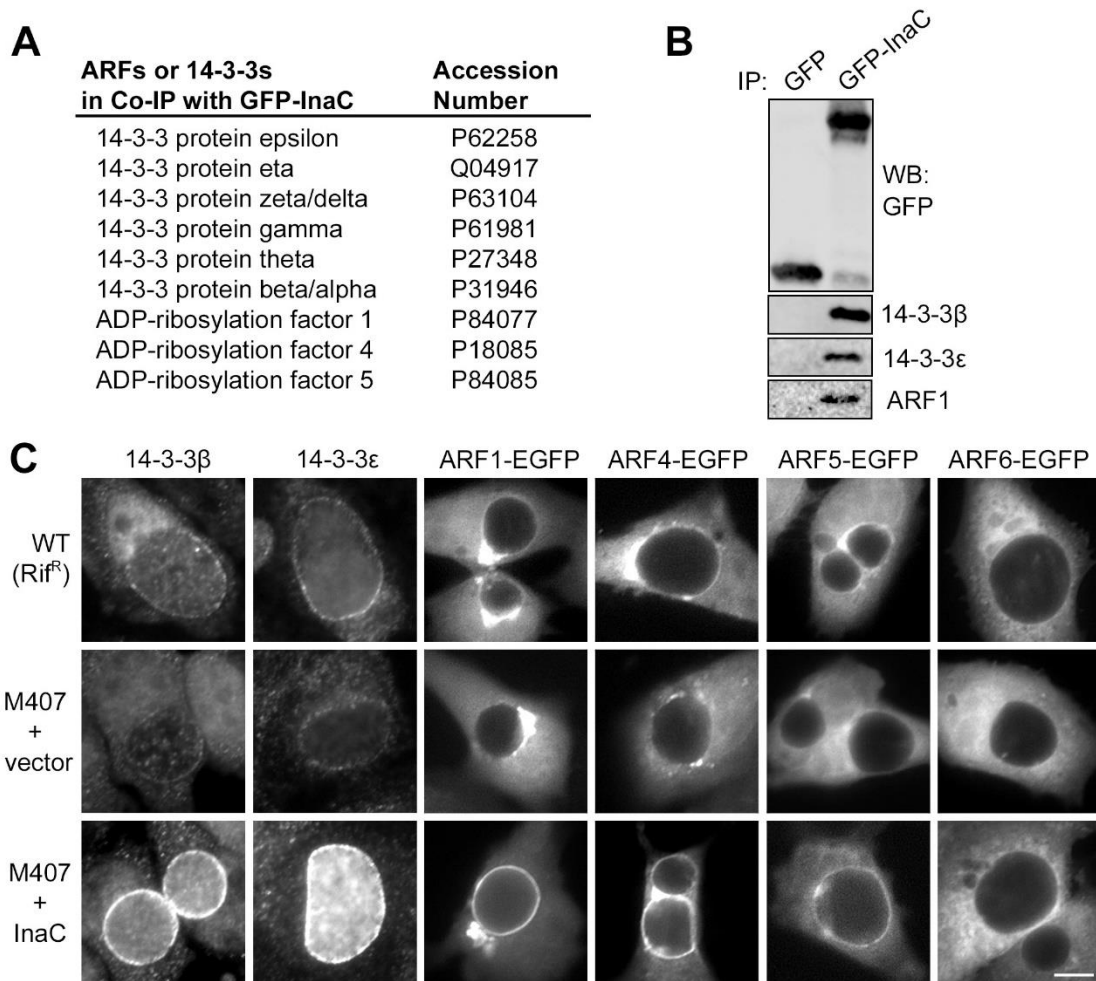


Figure 10. InaC recruits 14-3-3 and Golgi-specific ARF proteins to the inclusion. (A and B) ARF and 14-3-3 proteins interact with InaC. Lysates from HEK 293T cells transiently expressing either GFP or a GFP-InaC fusion protein were incubated with GFP-Trap resin. Bound proteins were digested on-resin with trypsin and identified by LC-MS/MS (Table 1). Only proteins of ARF and 14-3-3 families are shown with corresponding accession numbers (A). The specificity of these interactions was confirmed by SDS-PAGE followed by western blot with specific antibodies as indicated (B). (C) InaC mediates the recruitment of 14-3-3 β , - ϵ , and Golgi-specific ARF GTPases to the inclusion. HeLa cells were infected with the indicated strains and either processed at 30 hpi for immunofluorescence using anti-14-3-3 antibodies (left) or transfected with different ARF-EGFP isoforms for 24 hours before processing at 30 hpi for microscopy (right). Note that the intensity of 14-3-3 and ARF1, 4 and 5 recruitment to inclusions correlates with InaC expression. Note that untransformed M407 appeared indistinguishable from M407 + InaC (data not shown). Scale bars represent 10 μ m.

Table 1. Proteins that co-IP with GFP-InaC as identified by LC-MS/MS

Identified Proteins	Protein Name	Accession Number	Total Spectrum Count		Exclusive Unique Peptide Count	
			GFP	GFP InaC	GFP	GFP InaC
hypothetical protein CT813 [Chlamydia trachomatis D/UW-3/CX]	CT813/InaC	GI:15605547	0	101	0	20
14-3-3 protein epsilon	1433E	P62258	0	68	0	21
14-3-3 protein zeta/delta	1433Z	P63104	0	58	0	12
14-3-3 protein beta/alpha	1433B	P31946	0	47	0	8
14-3-3 protein gamma	1433G	P61981	0	41	0	10
ADP-ribosylation factor 1	ARF1	P84077	0	38	0	7
14-3-3 protein theta	1433T	P27348	0	36	0	9
14-3-3 protein eta	1433F	Q04917	0	32	0	13
Transcription intermediary factor 1-beta	TIF1B	Q13263	0	30	0	19
ADP-ribosylation factor 4	ARF4	P18085	0	29	0	6
ADP-ribosylation factor 5	ARF5	P84085	0	27	0	3
Probable ATP-dependent RNA helicase DDX49	DDX49	Q9Y6V7	0	18	0	11
Transcription elongation factor SPT5	SPT5H	O00267	0	11	0	10
Acidic leucine-rich nuclear phosphoprotein 32 family member A	AN32A	P39687	0	11	0	7
Nucleophosmin	NPM	P06748	0	5	0	3
ATPase family AAA domain-containing protein 3B	ATD3B	Q5T9A4	0	5	0	2
ATPase family AAA domain-containing protein 3C	ATD3C	Q5T2N8	0	5	0	0
Protein SET	SET	Q01105	0	4	0	4
Acidic leucine-rich nuclear phosphoprotein 32 family member B	AN32B	Q92688	0	4	0	2
ATPase family AAA domain-containing protein 3A	ATD3A	Q9NVI7	0	4	0	0

2.3.2.1 InaC selectively recruits a GTP-locked ARF1 variant to the inclusion

Molecular mimicry is one mechanism by which pathogens manipulate host pathways (Cossart et al., 2005), and InaC could mimic known ARF-interacting proteins

to recruit it to the inclusion. As a small GTPase, ARF-protein interactions can be simplified into three groups (Donaldson and Jackson, 2011): effectors (signaling proteins), inhibitors (GTPase activating proteins, GAPs), and activators (guanine nucleotide exchange factors, GEFs). I investigated which forms of ARF1 (GTP- or GDP-bound) are recruited to the inclusion. I transfected HeLa cells with different ARF1-GFP variants that are mutated to mimic either GTP-bound ARF1 (Q70L prevents GTP hydrolysis), or GDP-bound ARF1 (T31N prevents nucleotide binding). I found that WT ARF1 and ARF1(Q70L), but not ARF1(T31N) were recruited to the inclusion in an InaC-dependent manner (Figure 11). Since InaC-mediated recruitment is selective to the variant which mimics GTP-bound ARF, InaC may mimic effectors or GAPs to recruit ARFs to the inclusion. It is important to note that, in addition to effectors, GEFs and GAPs are typically multi-domain proteins and can scaffold protein complexes at specific subcellular sites to create a vast and dynamic signaling network around ARF GTPases (Donaldson and Jackson, 2011). Thus, ARF may recruit host effectors and/or GAPs to promote signaling complexes to the inclusion.

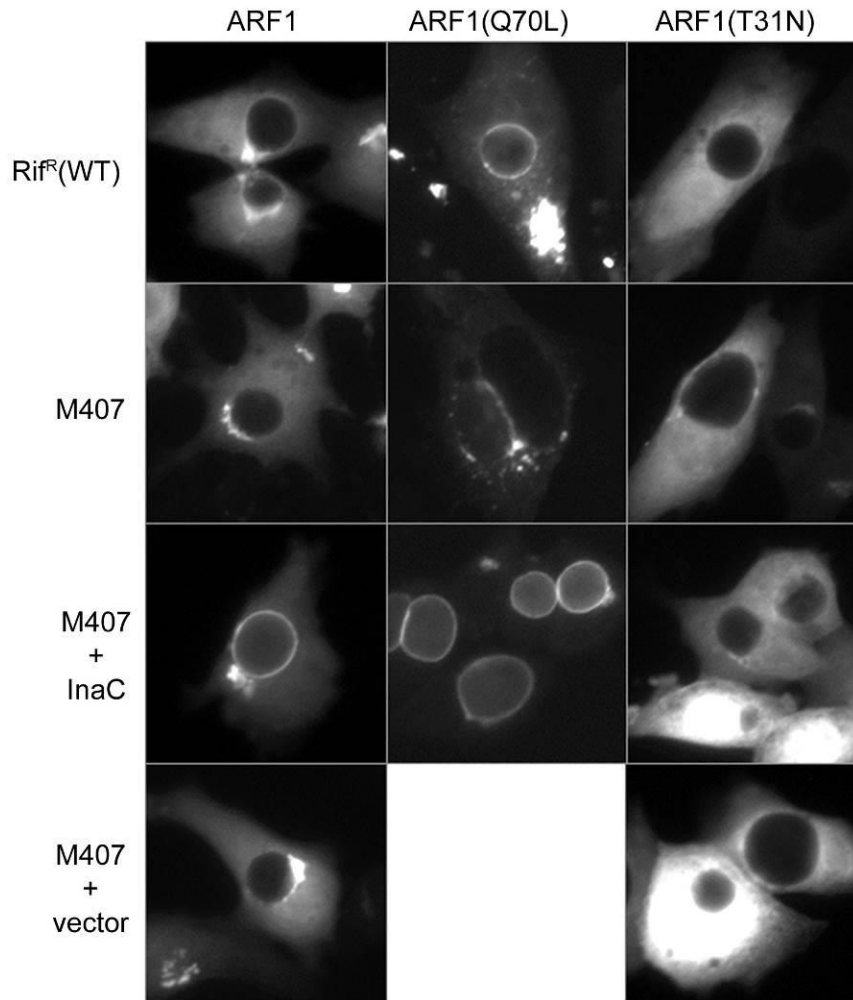


Figure 11. InaC recruits GTP-locked ARF1(Q70L)-GFP to inclusions. HeLa cells were infected with the indicated strains and transfected with different ARF1-EGFP variants as indicated for 24 hours before processing at 30 hpi for microscopy. Note strong recruitment of ARF1(Q70L), intermediate recruitment of WT ARF1, and no recruitment of ARF1(T31N). Inclusions are evident as dark circular regions centered within images.

2.3.2.2 Different aspects of InaC mediate interactions with ARF and 14-3-3 proteins

To investigate the role of InaC protein regions in interactions with ARF and 14-3-3 proteins, I created three versions of GFP-InaC that differed from each other by the

presence or absence of the N-terminal soluble region (aa 1-41), the bi-partite hydrophobic motif (aa 42-95), or the larger soluble C-terminal region (aa 96-264) (Figure 12A). I transiently expressed each in HEK 293T cells and assessed the presence of ARF and 14-3-3 upon anti-GFP IP (Figure 12B). The C terminal region (aa 96-264) was necessary and sufficient to pull-down both 14-3-3 β and 14-3-3 ϵ , while all domains tested were required for interaction with ARF1. These results reveal a differential requirement for regions of InaC for interaction with 14-3-3s and ARFs.

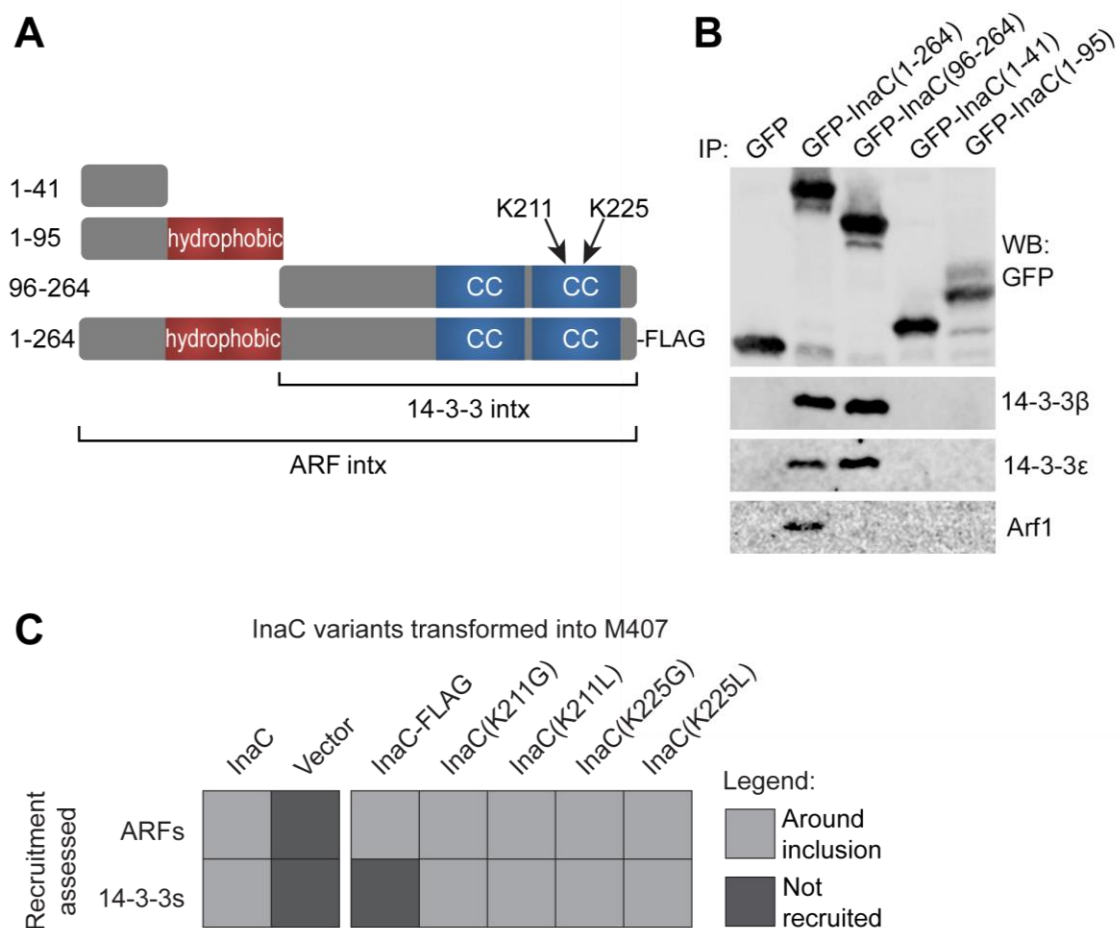


Figure 12. InaC domains and residues are differentially involved in interactions with ARF and 14-3-3 proteins. (A) Schematic of InaC domains tested and residues mutated. (B) Lysates from HEK 293T cells transiently expressing each GFP-tagged InaC

domain-containing protein were precipitated with GFP-Trap resin. Precipitates were resolved by SDS-PAGE probed with specific antibodies as indicated to assess efficiency (GFP) and interactions. (C) Amino acid changes in the C-terminal region of InaC differentially affect ARF and 14-3-3 recruitment. HeLa cells were infected with M407 strains expressing the indicated variants of InaC, and assessed at 30 hpi for inclusion localization of ARF1, ARF3, ARF4, ARF5, and ARF1(Q70L)-EGFP, and 14-3-3 β and 14-3-3 ϵ . Light gray boxes indicate a lack of recruitment and dark gray boxes indicate recruitment to inclusions.

The N-terminal region of InaC is predicted to encode a secretion signal, and *trans*-complementation with *inaC* containing large deletions in M407 could interfere with protein secretion and localization to the inclusion. Thus I took an alternative approach to investigate potential differential InaC requirements for ARF and 14-3-3 recruitment to the inclusion. I introduced point mutations (K211 to L and G, K225 to L and G) designed to disrupt a putative SNARE-like domain of InaC (Delevoye et al., 2008). However, the effect of these mutations on putative InaC SNARE-like activity was confounded since phenotypes proposed to be due to SNARE-like InaC activity (Vamp-7 and -8 recruitment to inclusions) were unaffected by the absence of InaC (data not shown). Additionally, in an attempt to identify proteins that interact with InaC in the context of infection, I fused a FLAG epitope tag to the C-terminus of InaC and transformed it into M407. I assessed ARF and 14-3-3 recruitment to M407 strains expressing these InaC variants (Figure 12C). While all five variants recruited ARF1, 3, 4, and 5, InaC-FLAG failed to recruit 14-3-3 β and ϵ , suggesting an important role for the very C-terminus of InaC selectively in interactions with 14-3-3s.

2.4 Functions of F-actin assembly at the inclusion

2.4.1 Golgi redistribution around the inclusion requires InaC and F-actin

The Golgi apparatus is a critical component of the secretory system in eukaryotic cells that consists of a dynamic membrane system in which organelle architecture and membrane traffic are fundamentally linked (Lippincott-Schwartz et al., 1998). ARFs are critical mediators of vesicular traffic within this system and maintain Golgi structure and identity (Donaldson and Jackson, 2011; D'Souza-Schorey and Chavrier, 2006). The actin cytoskeleton supports membrane traffic within the secretory system and is directly involved in the maintenance of Golgi architecture (Egea et al., 2006). In *C. trachomatis* infected cells, the Golgi fragments into ministacks that envelop the inclusion (Heuer et al., 2009). Since InaC recruits ARFs and is required for F-actin assembly at the inclusion, I tested whether InaC plays a role in modulating Golgi architecture during *C. trachomatis* infection. The Golgi appeared distributed at least halfway around 40% of wild type inclusions (Figure 13A and 13B). In contrast, the Golgi retained a compact morphology at a perinuclear region adjacent to inclusions lacking InaC. Furthermore, the Golgi was no longer distributed around wild type inclusions treated with the F-actin polymerization inhibitor Latrunculin B (Figure 13C). These results indicate that Golgi redistribution around *C. trachomatis* inclusions requires InaC and intact actin filaments. Additionally, I assessed F-actin assembly and Golgi redistribution around M407 inclusions expressing five InaC variants (Figure 13D). The same three variants failed to recruit F-actin and redistribute the Golgi around the inclusion, further supporting a link between these InaC-dependent processes.

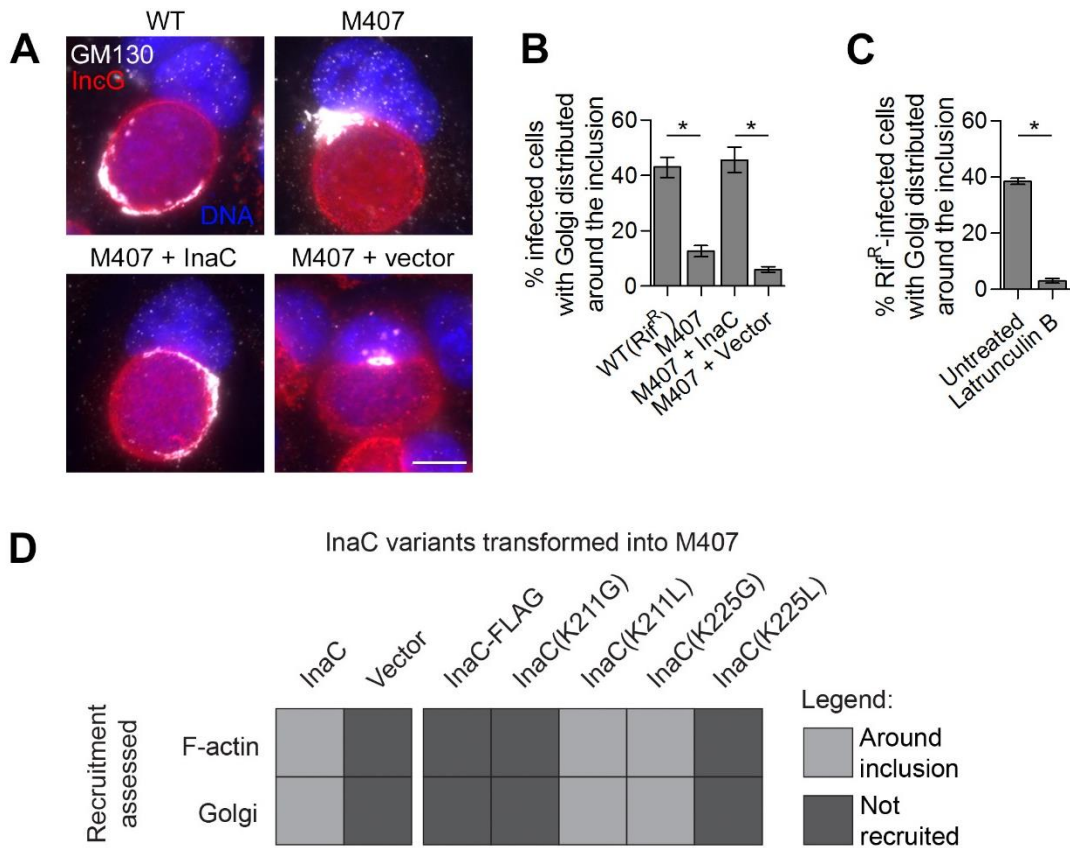


Figure 13. F-actin and InaC mediate Golgi redistribution around the inclusion. (A and B) Golgi redistribution around the inclusion requires InaC. HeLa cells were infected with the indicated *C. trachomatis* strains and processed at 30 hpi for immunofluorescence (A) using anti-GM130 (white) anti-IncG (red) antibodies and Hoechst (blue), and the frequency of Golgi distribution was quantified (B). (C) F-actin assembly is required for Golgi redistribution at inclusions. HeLa cells were infected with a wild type LGV-L2 strain and treated with 500nM Latrunculin B for 30 minutes before processing as in (B) at 30 hpi. Mean \pm SEM for three independent experiments is shown. At least 40 (B) or 90 (C) inclusions were enumerated in each triplicate for each experiment. * indicates $P < 0.05$ by one-way ANOVA and Newman-Keuls *post hoc* (B) or Student's t test (C). Scale bar represents 10 μ m. (D) Amino acid changes in the C-terminal region of InaC similarly affect Golgi redistribution and F-actin recruitment around inclusions. HeLa cells were infected with M407 strains expressing the indicated variants of InaC, and quantitatively (data not shown) assessed at 30 hpi for inclusion localization rhodamine-phalloidin (F-actin), and GM130 (Golgi). Light gray boxes indicate a lack of recruitment and dark gray boxes indicate recruitment around inclusions.

InaC(K211G) and InaC(K225L) efficiently recruit ARFs and 14-3-3s but fail to rescue Golgi and F-actin redistribution, indicating that ARF or 14-3-3 localization to the

inclusion is not sufficient to recruit F-actin and redistribute the Golgi. These substitutions may disrupt the nature of any possible signal transduction that may occur upon ARF or 14-3-3 recruitment. For instance, WT InaC could recruit ARF which could recruit downstream effectors, but K211G or K225L substitution may result in ARF recruitment in such a way that InaC now interferes with the availability or conformation of a downstream effector binding site. Alternatively, these substitutions may disrupt the recruitment of an unidentified InaC-recruited factor involved in these processes. K211G or K225L could interfere with putative homo-oligomerization (Gauliard et al., 2015), which could be important for select InaC functions. Finally, if F-actin assembly and Golgi redistribution are exquisitely sensitive to the levels of InaC on the inclusion, this could explain the pattern of rescue since InaC was more highly expressed in the strains that did not rescue F-actin and Golgi redistribution (data not shown). Because the effect of these substitutions on InaC structure and biochemistry is unclear, there are caveats to broad interpretations as to the nature of their impact on InaC function and pathways.

2.4.2 InaC-mediated Golgi redistribution is dispensable for *Chlamydia* sphingolipid acquisition and growth

Sphingolipids are delivered to *Chlamydia* through Golgi-dependent vesicular trafficking and via ARF-regulated pathways (Elwell et al., 2011; Hackstadt et al., 1996) and Golgi redistribution around inclusions has been proposed to facilitate sphingolipid acquisition by *Chlamydia* (Heuer et al., 2009; Rejman Lipinski et al., 2009). Therefore, I assessed whether InaC contributes to *Chlamydia* growth and its ability to acquire sphingolipids.

Sphingolipids are synthesized in the ER as ceramide precursors, processed in the Golgi, and accumulate at the plasma membrane (Perry and Ridgway, 2005).

Chlamydia intercepts these lipid transport pathways and acts as a sink for sphingomyelin (Hackstadt et al., 1996). Because sphingomyelin biosynthesis is important for the generation of infectious progeny (Robertson et al., 2009), I first assessed if expression of InaC in mutant M407 would restore this strain's growth potential as compared to M407 transformed with an empty vector. While I found a significant decrease in the recovery of infectious progeny due to background mutations in M407 compared to its wild type Rif^R parent, I detected no significant difference in either the recovery of infectious progeny from infected cells (Figure 14A), or the average area of inclusions (Figure 14B) upon restoring InaC expression in M407. These data suggest that InaC is dispensable for inclusion expansion and replication of *C. trachomatis* in cultured epithelial cells.

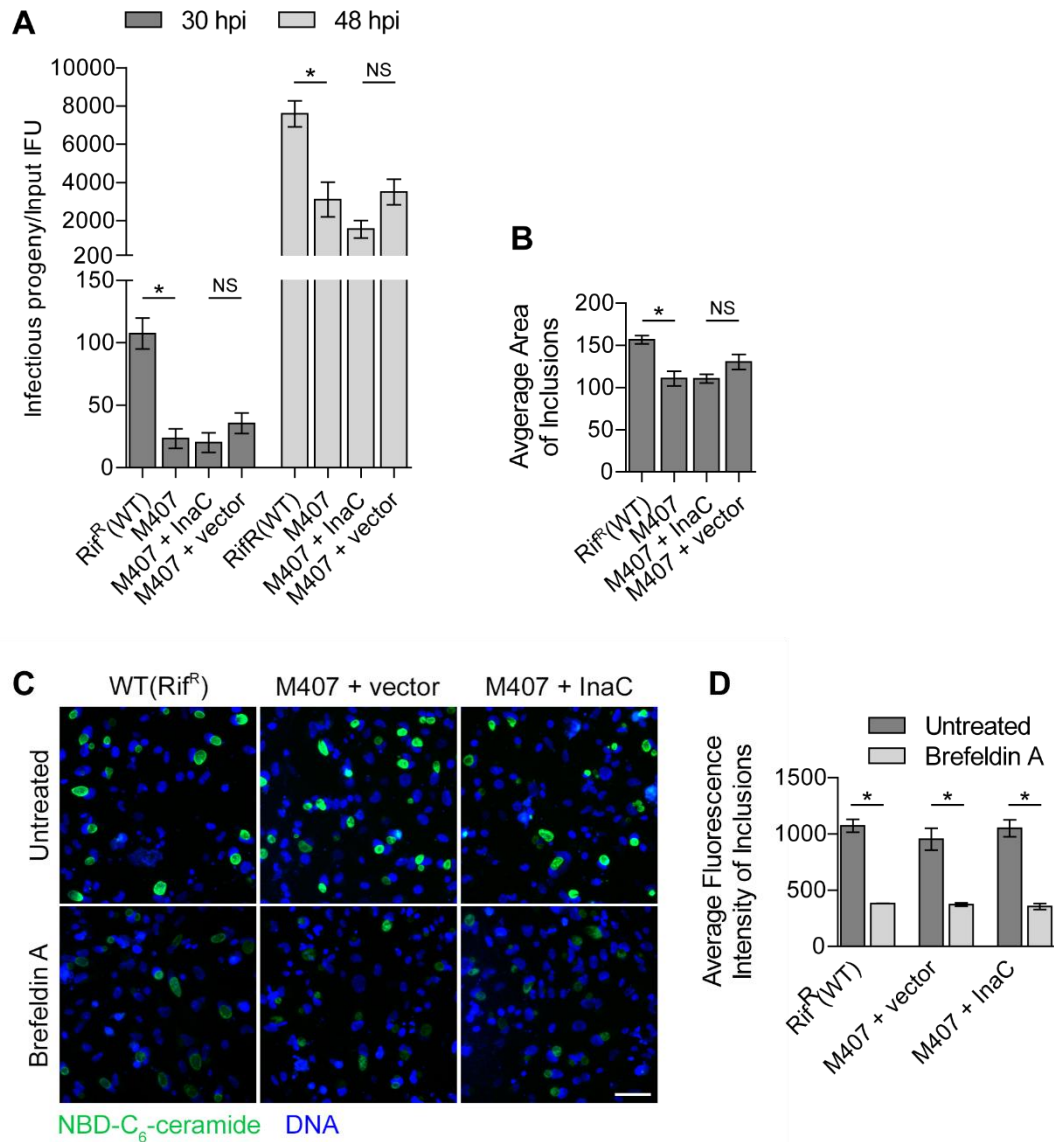


Figure 14. InaC is dispensable for sphingolipid traffic to the *C. trachomatis* inclusion, bacterial growth, and inclusion expansion. (A) The recovery of infectious progeny is not significantly different between M407 transformed with a plasmid encoding *inaC* or an empty vector. At 30 and 48 hpi, HeLa cells infected with the indicated strains at a multiplicity of infection (MOI) of 0.6 were harvested and the resulting infectious progeny were enumerated and normalized to the number of input bacteria. (B) InaC expression in M407 does not alter inclusion size. At 24 hpi, cells infected as in (A) were processed for immunofluorescence with anti-Slc1 antibodies to define inclusions. The average area of at least 100 inclusions was measured. (C and D) Accumulation of fluorescent sphingolipids within inclusions is not significantly different between wild type or M407 transformed with an empty vector or a plasmid encoding *inaC*. HeLa cells were

infected at an MOI of 3 with the indicated strains and at 23 hpi, labeled with NBD-C6-ceramide (green) followed by a 6 hour back-exchange, stained with Hoechst (blue), imaged (C), and assessed for the mean fluorescence intensity (D) of at least 90 inclusions in each triplicate. As a control, cells were incubated with 3 $\mu\text{g}/\text{mL}$ Brefeldin A for 30 minutes prior to labeling and throughout the back-exchange. Mean \pm SEM for three independent experiments, each done in triplicate, is shown. * indicates $P < 0.05$ and NS indicates $P > 0.05$ by one-way ANOVA and Newman-Keuls *post hoc* (A and B), or two-way ANOVA with Bonferroni *post hoc* (D). Scale bar represents 50 μm .

Chlamydia can acquire sphingomyelin through vesicular and non-vesicular pathways, but only the vesicular pathway affects bacterial growth (Derré et al., 2011; Elwell et al., 2011; Hackstadt et al., 1996). Therefore, I assessed the role of InaC in the delivery of sphingolipids to inclusions. When incubated with a fluorescent ceramide analog, wild type, InaC-deficient, and InaC-restored infected cells displayed no significant differences in inclusion fluorescence intensity (Figure 14C and 14D). As a positive control, I treated infected cells with Brefeldin A, which inhibits vesicular-mediated sphingolipid acquisition by *Chlamydia* (Elwell et al., 2011; Hackstadt et al., 1996) and observed a significant decrease in the fluorescent ceramide acquisition (60%) consistently in all strains tested (Figure 14C and 14D). Collectively, these data demonstrate that InaC itself, including InaC-mediated ARF recruitment and Golgi redistribution around the inclusion, is not required for *C. trachomatis* replication, inclusion expansion, and efficient sphingolipid trafficking to the inclusion in cultured epithelial cells.

2.4.2.1 Mutant 338 is defective in the generation of infectious progeny but forms wild-type-sized inclusions

The identification of two different chlamydial proteins that modulate F-actin assembly at the inclusion reveals that *Chlamydia* has evolved a fine-tuned control and can dynamically alter this structure, suggesting that adjusting F-actin assembly at the inclusion may influence the success and pathogenesis of *Chlamydia*. While promising

mouse models of *C. trachomatis* infection continue to be developed (Gondek et al., 2012), I chose to assess the success of M338 in a tissue culture system of infection. While M338 inclusions reached a size comparable to WT at 24 hpi, the generation of infectious progeny was reduced 10-fold at 30 hpi and 3-fold at 48 hpi (Figure 15). These results indicate that M338 has a reduced growth potential, but do not delineate whether the mutation in CTL0496 or other mutations in M338 contribute to reduced growth.

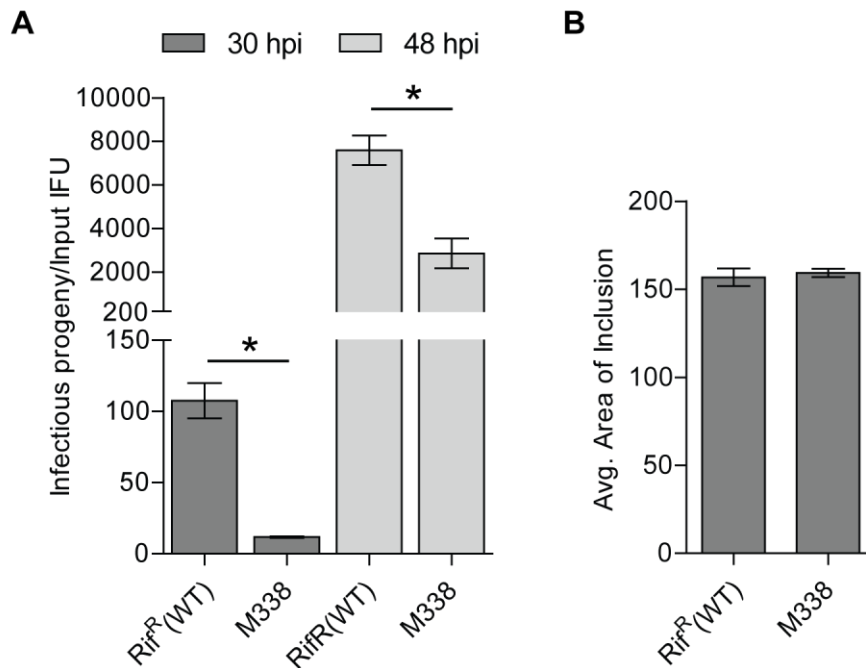


Figure 15. M338 has a reduced replication potential but WT-sized inclusions. (A) At 30 and 48 hpi, HeLa cells infected with the indicated LGV-L2 strains at a multiplicity of infection (MOI) of 0.6 were harvested and the resulting infectious progeny were enumerated and normalized to the number of input infectious units. (B) M338 inclusions were the same size as WT. HeLa cells were infected with the indicated strains. At 24 hpi, cells infected as in (A) were processed for immunofluorescence with anti-Slc1 antibodies to define inclusions. Mean \pm SEM for three independent experiments is shown. At least 100 inclusions were enumerated in each triplicate for each experiment. * indicates $P < 0.05$ by one-way ANOVA and Newman-Keuls *post hoc*.

2.4.3 InaC may affect the distribution of various organelles

Actin is highly dynamic and supports the dynamic remodeling of cells.

Accordingly, InaC and F-actin are required for redistribution of Golgi minstacks around inclusions (Figure 12), which is consistent with a model in which InaC facilitates F-actin assembly which in turn redistributes the Golgi around inclusions. Numerous other organelles are enriched at or associated with the inclusion periphery (Chapter 1), and InaC-dependent F-actin could play a role more broadly in organelle redistribution around inclusions. I surveyed the effect of InaC on the distribution and dynamics of several organelles around mid to late cycle inclusions by expressing a panel of fluorescent protein-tagged markers in cells infected with InaC expressing or deficient strains (Figure 18). Organelle distribution was recorded over time using live cell spinning disk confocal microscopy. Markers of the Golgi (GFP-GalTase), recycling endosomes (REs) (Rab11-GFP), and lysosomes (Lamp1-GFP) displayed InaC-dependent differential association with inclusions (Table 2). The Golgi remained compact in the absence of InaC but was redistributed around M407 inclusions expressing InaC (Figure 18), consistent with other findings (Figure 16A). Lysosomes appeared evenly distributed around InaC-expressing inclusions, but more compactly and polarly localized near inclusions lacking InaC (data not shown), suggesting that InaC may affect lysosome distribution similar to the effect on Golgi distribution. In contrast, RE association was enhanced around inclusions lacking InaC (Figure 16A).

Table 2. Organelle markers assessed for InaC-dependent effects on inclusion association.

	Marker	Localization	Observations in M407 + vector
Altered	GFP-GalTase	Golgi	Compact
	Lamp1-GFP	Lysosomes	Compact
	Rab11-GFP	Recycling endosomes	Enhanced
Unchanged	ER-RFP	ER	Recruited
	Sec61 β -GFP	ER	Recruited
	DsRed-Mito	Mitochondria	Recruited
	GFP-PI4KII α	Punctate at inclusion	Recruited
	GFP-Rac1	Inclusion	Recruited
	Rab1-GFP	Inclusion	Recruited

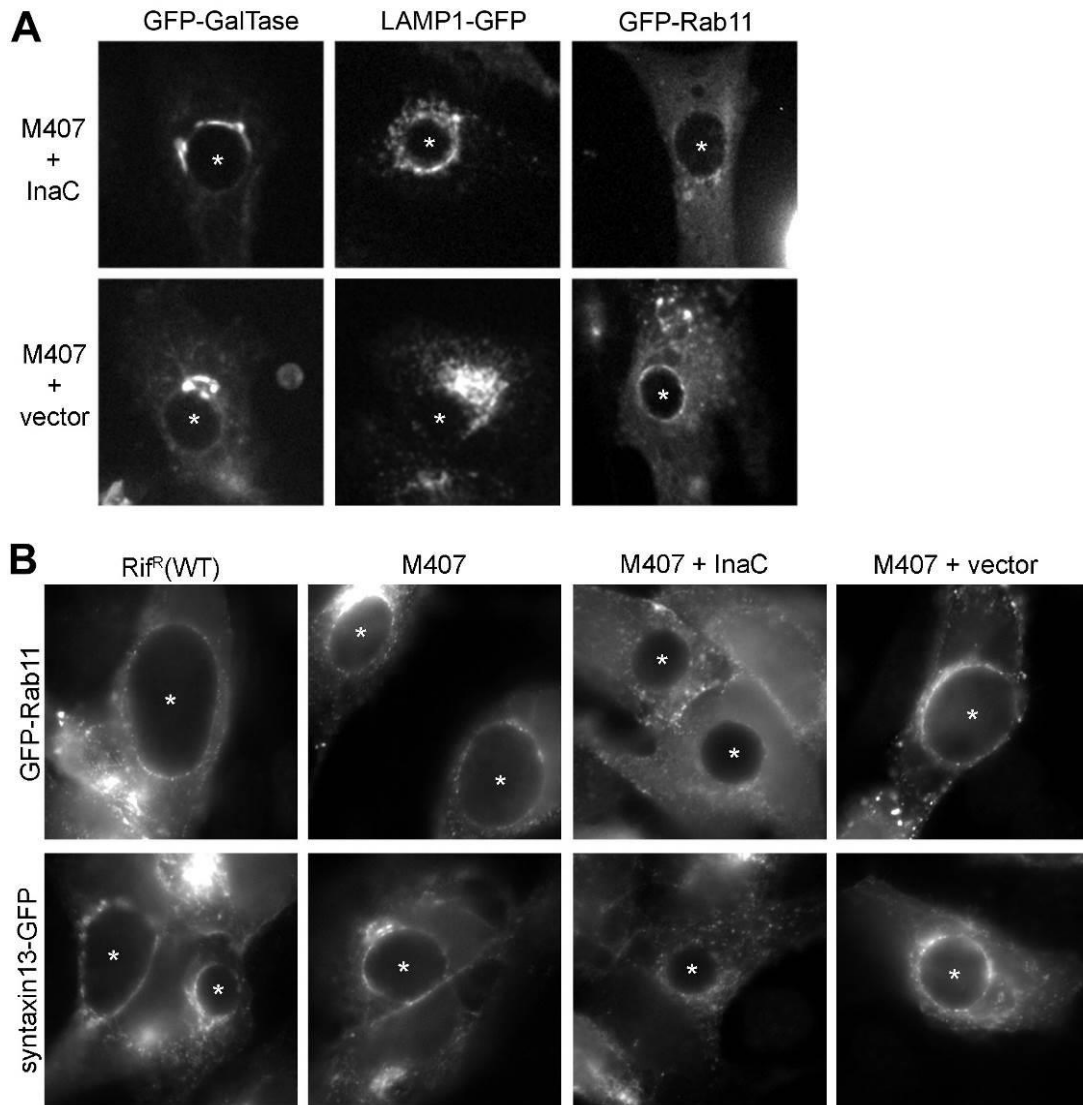


Figure 16. Recycling endosomes and lysosome localization around inclusions is altered by InaC. (A) HeLa cells were infected with the indicated strains and transfected with markers of the Golgi (GFP-GalTase), lysosomes (LAMP1-GFP), and recycling endosomes (GFP-Rab11) and imaged via live cell spinning disk confocal microscopy from 20-36 hpi. Note that Golgi and lysosomes are more widely distributed around inclusions in the presence of InaC, and recycling endosome recruitment is enhanced in absence of InaC. (B) InaC overexpression reduces recycling endosome recruitment to inclusions. HeLa cells were infected with the indicated and transfected with different Rab11-GFP or syntaxin13-GFP for 24 hours before processing at 30 hpi for widefield microscopy. Note that punctate recycling endosomes are recruited to the inclusion similarly across strains except M407 + InaC displays reduced recruitment. * marks inclusions.

2.4.3.1 InaC affects recycling endosome accumulation at the inclusion

To further investigate RE recruitment to WT inclusions and the potential role of InaC in RE recruitment, I assessed the localization of two RE markers, Rab11-GFP and Syntaxin13-GFP, around WT, M407, and M407 transformed with empty vector or rescued with InaC at 30 hpi at higher magnification (Figure 16B). Surprisingly, in the absence of InaC, REs were recruited to inclusions to a degree similar to WT, but InaC over-expression resulted in reduced RE recruitment to inclusions (Figure 16B). These data suggest that InaC overexpression interferes with RE-inclusion interactions. While IncG and IncA levels and localization to inclusions appear unaffected by InaC overexpression (data not shown), it is possible that global Inc interactions could be altered in the rescue strain. Alternatively, enhancement of an InaC-dependent pathway could more directly interfere with RE accumulation or enhance RE turnover at inclusions. However, it should be noted that while ARF and 14-3-3 recruitment is enhanced upon InaC overexpression (Figure 10), the intensity and frequency of F-actin at inclusions does not (Figure 6) which suggests that enhanced F-actin assembly does not interfere with RE accumulation at inclusions.

2.4.3.2 InaC alters STING translocation kinetics

The ER-resident and integral membrane protein STING is important for the induction of type I IFNs in *Chlamydia*-infected cells (Prantner et al., 2010). STING can directly bind to bacteria-specific cyclic di-AMP, and this is the predominant pathway of type I IFN induction in response to *C. trachomatis* (Barker et al., 2013). Because InaC affects Golgi redistribution and recycling endosome recruitment to inclusions, ER-localized STING recruitment around inclusions might be affected by InaC, which could potentially impact the immune response to *C. trachomatis*. To assess the localization of

STING, I used immortalized mouse lung fibroblasts derived from a mouse strain with destabilized STING, functionally complemented with HA-tagged STING (Barker et al., 2013). STING-HA was equally recruited to inclusions independently of InaC (Figure 17A), consistent with no change to ER recruitment to inclusions (Figure 16). However, to promote IFN induction, upon activation, STING must translocate from the ER to the Golgi apparatus, and then to punctate structures in the cytoplasm that colocalize with autophagy-related proteins (Saitoh et al., 2009). Because the Golgi is compactly distributed in the absence of InaC (Figure 13), the rate of translocation of STING through the Golgi and into cytoplasmic puncta could be altered, potentially affecting the generation of IFN responses. Upon infection with wild-type *C. trachomatis*, a quarter of cells displayed STING localization with some evidence of translocation from the ER (Figure 17, B and C). In the absence of InaC, STING translocation to puncta was notably more frequent, and almost all cells displayed evidence of translocation. These data suggest that InaC dampens the efficiency of STING translocation from ER to Golgi to cytoplasmic puncta. It remains unclear whether this InaC-dependent effect on STING translocation is mediated through InaC-mediated changes to Golgi morphology, ARF recruitment, or F-actin assembly. Finally, enhanced STING translocation in the absence of InaC could alternatively occur if the inclusion membrane is destabilized resulting in a greater release of bacterial patterns into the cytosol and increased STING activation.

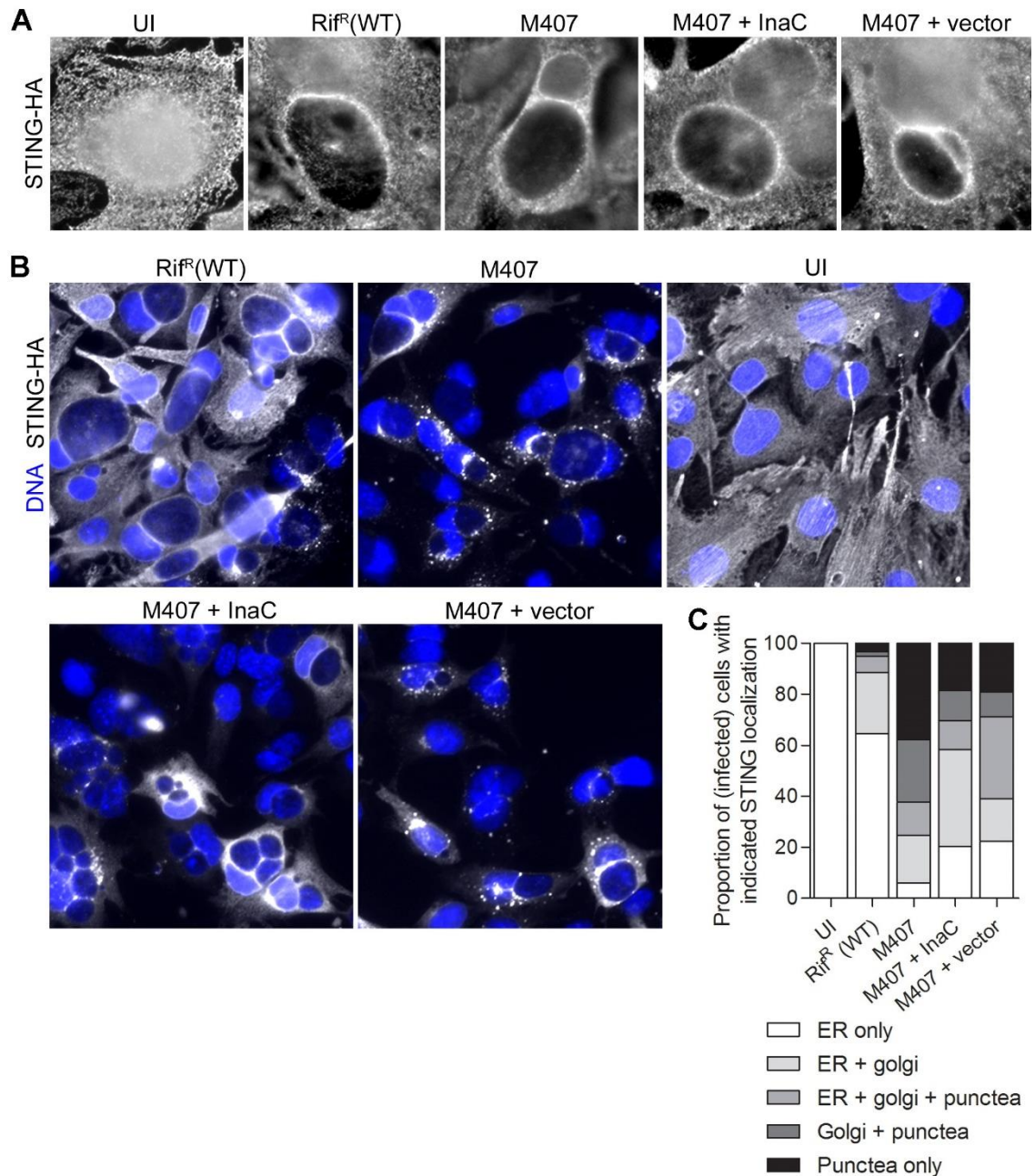


Figure 17. STING translocation is enhanced in the absence of InaC. (A) STING recruitment to the inclusion is independent of InaC. *Goldenticket* mouse lung fibroblasts expressing STING-HA (Barker et al., 2013) were infected at an MOI of 0.1 with the indicated strains and processed for immunofluorescence at 30 hpi. Inclusions are visualized as large dark oval regions centered in images and surrounded by enhanced STING recruitment. (B) Cells were infected as in (A) but at an MOI of 5 and processed for immunofluorescence at 32 hpi. (C) Proportion of cells displaying the indicated STING

localization in cells infected with strains as in (B). Average values from three replicates are displayed as a proportion of 100. Note that in most cells, STING retains reticular ER and some Golgi localization when InaC is present but appears to have largely translocated out of the ER and to Golgi or cytosolic puncta in the presence of InaC.

2.4.4 InaC is dispensable for maintenance of gross inclusion integrity and morphology

Global F-actin depolymerization during infection results in a loss of inclusion membrane integrity, bacterial spillage into the host cell cytosol, and a resulting increase in the abundance of pro-inflammatory cytokine IL-8 transcripts, presumably due to enhanced detection and cell autonomous immune responses (Kumar and Valdivia, 2008a). These data support a model in which F-actin assembled at the inclusion functions to support inclusion integrity. However, pharmacological F-actin disruption affects all F-actin structures within cells beyond just the F-actin assembled immediately around the inclusion, and it is unclear which F-actin structures or functionally-linked processes affect inclusion membrane integrity. In the absence of InaC, only F-actin assembly at the periphery of the inclusion appears to be disrupted while other subcellular F-actin structures, such as stress fibers and focal adhesions appear unperturbed (Figure 6 and data not shown). I did not detect any evidence of inclusion membrane disruption, bacterial spillage into the cytosol, or changes to the abundance of IL-8 transcripts during infection of InaC-deficient strains (Figure 18 and data not shown). These data suggest that InaC itself or InaC-dependent processes, including F-actin assembly at the inclusion, are not involved in maintaining large-scale inclusion integrity during infection.

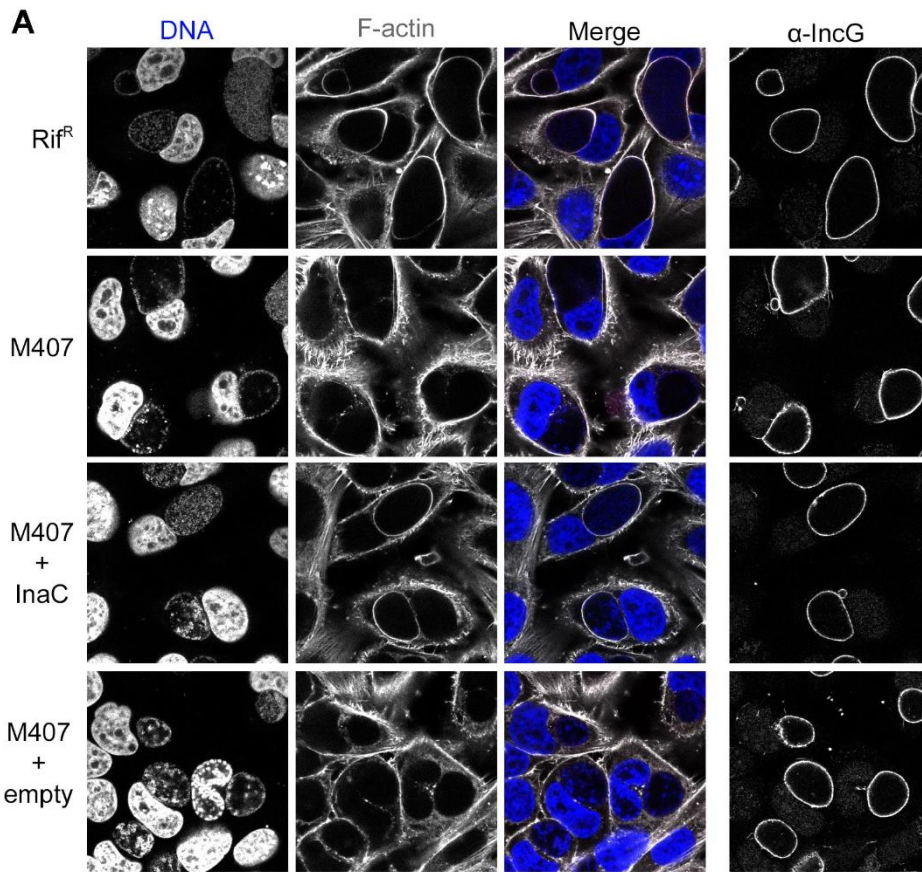


Figure 18. InaC does not grossly affect inclusion membrane integrity. (A) HeLa cells were infected with the indicated strains and processed for immunofluorescence at 30 hpi. Cells were stained with Hoescht (DNA, blue) to visualize host nuclei (very bright regions) and *C. trachomatis*, rhodamine-phalloidin (grayscale) to identify cellular boundaries and define the host cell cytosol, and anti-IncG antibodies to label the inclusion membrane. Note the absence of cytoplasmic bacteria and the intact nature of the inclusion membrane upon infection with all strains.

2.4.5 InaC does not globally affect IFN transcriptional responses during *C. trachomatis* infection

InaC is not required for inclusion expansion and the generation of infectious progeny in a tissue culture model (Figure 14). However, InaC could affect parameters of pathogenesis that are absent in tissue culture models, such as eliciting immune responses that require the action of other effector immune cells. For instance, enhanced

detection of cytosolic bacteria or bacterial patterns could lead to increased expression of immune pathways but not effect replication in a cell model, as occurs upon global F-actin disruption (Kumar and Valdivia, 2008a; Y. Kumar and R. H. Valdivia, unpublished).

While an absence of gross disruptions to inclusion morphology (Figure 18) suggests that InaC does not affect inclusion stability and segregation of bacteria from the host cytosol, subtle defects in inclusion integrity may not be apparent in this assay. To assess if InaC may prevent subtle leakage of bacterial patterns out of the inclusion and the subsequent activation of host detection pathways, I took an unbiased approach to measure InaC-dependent changes to host mRNA transcripts. I chose to use an immortalized epithelial cell line (A2EN) derived from an endocervical tissue explant because they respond appropriately to numerous immune signals and functionally resemble endocervical epithelial cells (Buckner et al., 2011). Briefly, I infected A2ENs with M407 transformed with an empty vector or one encoding *inaC*, harvested total RNA at 30 hpi in three independent experiments, and had the samples enriched for mRNA and analyzed by RNA-seq. Principle component analysis of the data showed clustering by batch of paired samples rather than by the presence of absence of InaC, which can occur when batches vary widely or when the RNA differences by treatment are minimal. After controlling for the effect of batch variance, only four protein-coding transcripts were found to be significantly different at a false discovery rate (FDR) at less than 0.05 (Table 3). These data indicate that InaC, and InaC-dependent processes including F-actin assembly, Golgi rearrangement, and ARF and 14-3-3 recruitment to the inclusion, have a minimal effect on the transcriptome.

Table 3. Coding transcripts with InaC-dependent change in abundance at FDR<0.05

GeneID	Gene Name	Fold Change (M407+vector/ M407+InaC)	Log ₂ FC	P-value	FDR
COX6A1P2	Protein COX6A1P2	0.218038	- 2.19735	1.11E- 09	1.03E- 05
NME3	Nucleoside diphosphate kinase 3	0.172799	- 2.53283	1.24E- 07	0.00045 8
ODF3B	Outer dense fiber protein 3B	0.309236	- 1.69322	1.38E- 05	0.02121 2
IFI6	Interferon alpha- inducible protein 6	0.630768	- 0.66482	2.3E-05	0.03029 6

Interferon alpha-inducible protein 6 (IFI6) was one of the four genes that was significantly reduced in the InaC-deficient mutant (with a less than 2-fold decrease) and is induced in response to interferons (IFNs). *C. trachomatis* induces type I IFNs in many cell types, and *Chlamydia*-induced type I IFN responses are mediated predominantly by host cell detection of the bacteria-specific small molecule c-di-AMP (Barker et al., 2013). Thus, altered inclusion integrity could alter IFN responses to infection, and when assessing putative transcript abundance changes of a variety of genes in the IFN pathway, I noted that all appeared consistently decreased in the strain lacking InaC (Figure 19A). Furthermore, when I performed cluster analysis of the 234 coding transcripts at p<0.05 I found numerous IFN pathway genes within a clustered group of transcripts that consistently decreased across all three batches of samples (Figure 19B) perhaps because statistical significance can be difficult to achieve by RNA-seq with three paired samples. I next assessed changes mRNA transcript abundance of a panel of twelve of these genes, selected based on a combination of significance values, fold-change, abundance, and functional diversity within the IFN pathway. However, over half

of these genes appeared to have no change in abundance or an increase rather than decrease in abundance in the absence of InaC (Figure 19C), and only to a mild degree. Additionally, I observed no InaC-dependent difference in type I IFN induction using a luminescence reporter-based assay (Figure 19D). These demonstrate that while IFI6 mRNA abundance is decreased less than 2-fold in the absence of InaC, there is no consistent InaC-dependent effect on the IFN pathway.

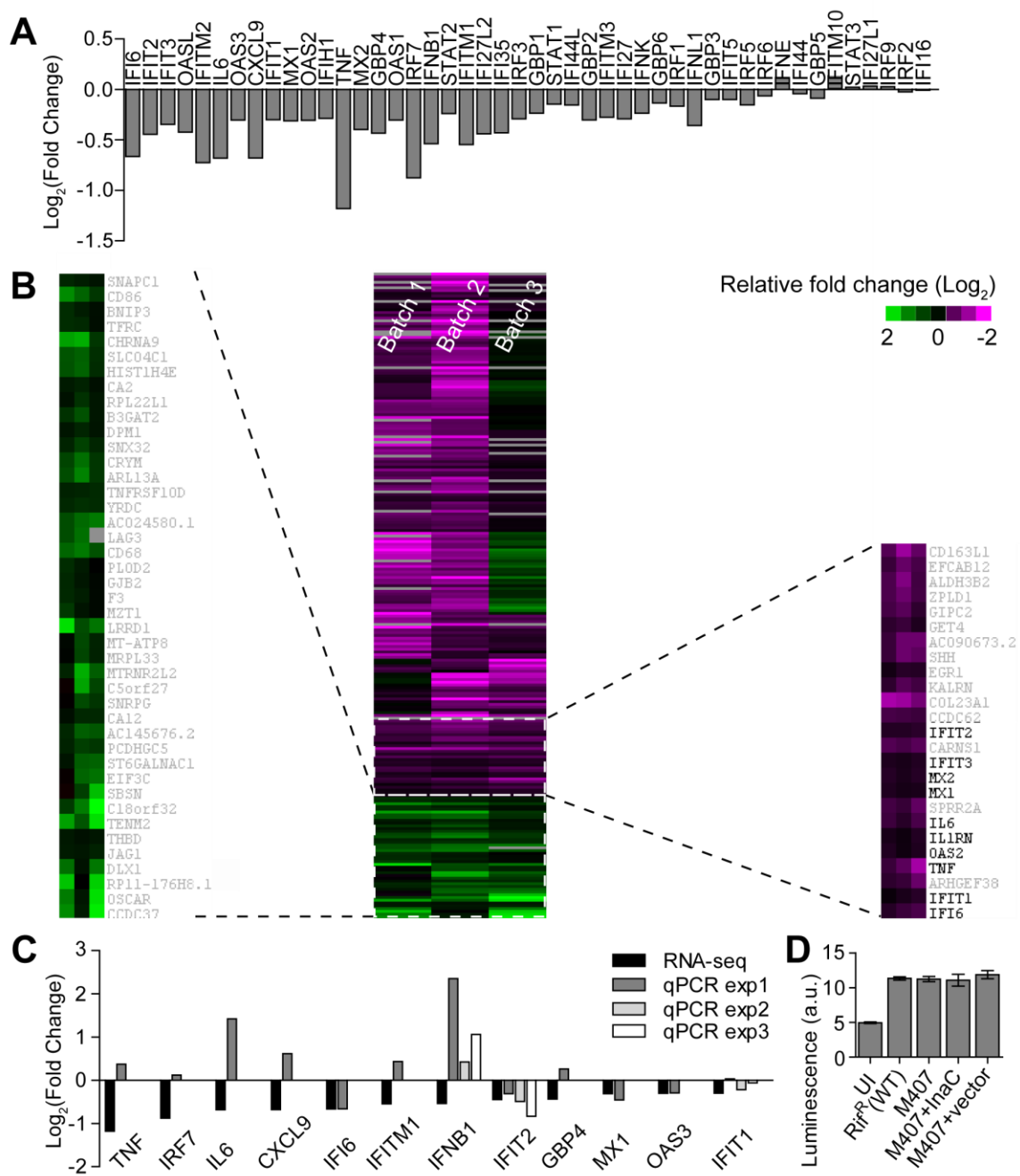


Figure 19. Assessment of IFN-related transcript abundance. (A) Transcripts of genes in the IFN pathway are similarly reduced in an InaC-dependent manner. A2EN cells were infected with M407 + vector or M407 + InaC and host mRNA transcripts sequenced by RNA-seq at 30 hpi. Only change in IFI6 was statistically significant difference at FDR<0.05, and the remaining genes are ranked by p-value. Values are displayed as Log₂(M407+vector/M407+InaC). Values are calculated from the average of three independent experiments. (B) A cluster of consistently decreased transcripts

contains numerous IFN-related genes. Log₂(Fold Change) of the 234 coding transcripts different at p<0.05 values from each RNA-seq sample batch were analyzed by hierarchical clustering (Cluster 3.0). In the heat map (TreeView), magenta represents a decrease or negative value, green represents an increase, gray represents values of zero, and geneIDs are displayed to the right of enlarged heat maps. (C) qPCR-based quantification of IFN-related mRNA transcripts does not consistently replicate RNA-seq results. A2EN cells were infected as in (A) and host mRNA transcript abundance measured by qPCR as indicated. qPCR was performed more than once only for IFIT1, IFIT2, and IFNB1. (D) InaC is not required for Type I IFN induction in response to *C. trachomatis* infection. A2ENs stably transduced with a plasmid encoding luciferase downstream of an ISRE (IFN-stimulated response element) region and infected with the indicated strains. At 30 hpi, cells were lysed and measured for luciferase activity (luminescence). Mean±SD of six replicates.

2.5 Discussion

2.5.1 Insights into mechanisms of F-actin assembly at the inclusion

As a fundamental and highly conserved aspect of eukaryotic cell biology, pathogens co-opt the host cytoskeleton (Haglund and Welch, 2011). The best studied examples involve rapid and short-term changes to F-actin dynamics for entry or motility within host cells. In contrast, very little is known about the mechanisms by which pathogens elicit the formation and maintenance of F-actin structures that are sustained over a longer period, as well their function.

Pathways and interactions involved in forming cytoskeletal structures are complex and under tight spatial and temporal regulation. Actin monomers polymerize into helical filaments, and through the coordinated activity of hundreds of actin-binding proteins, can be directed to form complex higher order structures. These structures play important roles in various cellular processes, such as motility, cytokinesis, phagocytosis, and sensing mechanical forces (Chhabra and Higgs, 2007). The coordinated regulation of actin and actin-associated proteins is typically performed by Rho-family GTPases to regulate the formation of distinct actin structures (Etienne-Manneville and Hall, 2002). By identifying cytoskeletal proteins that interact with RhoA specifically during *C. trachomatis*

infection, I identified host filamin and α -actinin as markers and potential structural components of F-actin assembled at the inclusion. α -actinin cross-links actin filaments and localizes in an alternating beads-on-a-string pattern with non-muscle myosin in contractile stress fibers (Hotulainen and Lappalainen, 2006; Naumanen et al., 2008). Non-muscle myosin II is recruited to patches on the inclusion (Lutter et al., 2013) where it does not consistently co-localize with F-actin, and its pharmacological inhibition does not disrupt or prevent F-actin assembly at the inclusion (Kumar and Valdivia, 2008a). This suggests that while there are some common factors, F-actin assembled at the inclusion is not merely re-localized stress fibers. Filamins are mechanosensors that serve to link F-actin to membranes and are enriched at sites of increased tension across membranes (Razinia et al., 2012). Continuous expansion of the inclusion during infection could exert tensile forces on the cytoplasmic surface of the inclusion and enveloping F-actin structures. As is the case with tension-sensitive focal adhesions that form between extracellular substrates on the internal F-actin network in cells (Parsons et al., 2010), tension across the inclusion membrane could influence the nature or maturation of the F-actin structure at the inclusion, and filamins could play a part in this.

By employing a forward genetics screen, I identified the bacterial protein InaC as a necessary factor for the assembly of an F-actin structure surrounding the inclusion. I find that InaC interacts with and recruits host ARF and 14-3-3 proteins to the inclusion, and these interactions are further supported by findings in a recent study (Mirrashidi et al., 2015). 14-3-3s are ubiquitous proteins that act in numerous pathways by scaffolding different proteins (over 200 known binding partners) together to propagate signaling (Morrison, 2009). In this capacity, 14-3-3s often bind specific phosphorylated motifs within their ligands, and homo- and hetero-dimerize to scaffold signaling components

together. InaC lacks any predicted 14-3-3 binding phosphorylation motifs so this interaction is likely phosphorylation-independent, which has been reported for several other 14-3-3-binding partners. Interestingly, 14-3-3 recruitment to the inclusion is significantly reduced in the absence of InaC, but not completely diminished which may be due to a phospho-dependent interaction with another inclusion membrane protein, IncG (Scidmore and Hackstadt, 2001). 14-3-3s can act in cell death pathways, and while it has been suggested that 14-3-3 recruitment to the inclusion would interfere with its pro-apoptotic function (Verbeke et al., 2006), we find no defect in *C. trachomatis*-mediated resistance to apoptosis, or induction of apoptosis in the absence of InaC (B. S. Sixt and R. H. Valdivia, unpublished data). Even though mediated by two different *Chlamydia* effectors, the significance of 14-3-3 recruitment to the inclusion remains unclear.

Golgi-specific ARF GTPases and 14-3-3 proteins, which are recruited to the inclusion by InaC, are not canonical regulators of F-actin dynamics, but both have been found to influence F-actin processes. For instance, ARF1 at the Golgi stimulates actin assembly via recruitment and regulation of Cdc42 (Myers and Casanova, 2008) and 14-3-3 proteins can modulate T-cell adhesion by binding to an intracellular region of integrins which are membrane receptors that bridge the intracellular F-actin network and the extracellular matrix (Takala et al., 2008). The precise mechanism by which InaC, potentially through ARF and/or 14-3-3s interactions, regulates F-actin assembly and Golgi redistribution at the inclusion remains to be determined. Since regions or residues of InaC are differentially required for interactions with ARF and 14-3-3s, I propose that chimeras between InaC and another inclusion membrane protein, such as IncA or IncG, could be generated that would be functionally secreted and localize to the inclusion and

selectively recruit only 14-3-3s or ARFs when expressed in M407, thereby facilitating pathway separation in future investigations. Additionally, knock-down or knockout of ARFs and 14-3-3s could reveal a requirement for F-actin assembly, although the results could be difficult to interpret since ARFs can be functionally redundant and frequently act in pairs or cascades, requiring combinatorial knock-down (Volpicelli-Daley et al., 2005).

Moreover, as cytoskeletal structures are highly complex, dynamic, and diverse in eukaryotic cells, we must move forward considering that multiple distinct cytoskeletal structures may be induced during *C. trachomatis* infection, in distinct subcellular locations and at distinct times, to perform distinct functions. For example, one can imagine an inclusion at mid to late stages of infection, surrounded by an F-actin structure which forms scaffold to physically redistribute organelles around the inclusion, and simultaneously, F-actin is co-assembled with septins in stress fiber-like structures underneath the inclusion which could help anchor the inclusion with respect to the cell and extracellular substrate. Indeed, perhaps these co-assembled filaments are the particular F-actin structures that stabilize the inclusion membrane (Kumar and Valdivia, 2008a). One can further imagine that at very late stages of infection when the inclusion takes up nearly all the cytosolic space of the cell and is closely abutted to the cellular cortex underlying the plasma membrane, that a network of contractile actomyosin fibers may form in this space and work in concert to push the inclusion out of the cell, condensing into a contractile ring-like structure associated with septins that pinches off the inclusion, leaving the infected cell intact. To best investigate the biogenesis and function of each of these distinct structures, rather than using a “sledgehammer” and disrupting all F-actin structures, we must use a molecular “scalpel” to disrupt only one

structure, such as the M407 *Chlamydia* mutant lacking InaC and F-actin assembled at inclusions.

2.5.2 Impact of F-actin assembly at the *C. trachomatis* inclusion on subcellular architecture and function

Cellular F-actin contributes to the stability of the inclusion (Kumar and Valdivia, 2008a) and to the extrusion of inclusions at late stages of infection upon bacterial cell exit (Chin et al., 2012; Hybiske and Stephens, 2007), and thus the F-actin structure assembled specifically at the inclusion periphery has been proposed to contribute to both of these actin-dependent processes. Using a microscopy-based screen, I identified the *C. trachomatis* hypothetical protein CTL0496 as a modulator of F-actin assembly at the inclusion – an amino acid substitution that led to enhanced F-actin assembly. F-actin at the inclusion becomes progressively more prominent over the course of mid to late inclusion expansion, and inclusions that are undergoing the non-lytic form of exit termed extrusion (Hybiske and Stephens, 2007) appear heavily coated with F-actin (Chin et al., 2012). *Chlamydia* could encode InaC to initially form F-actin at the inclusion and CTL0496 to modulate this structure at later times to initiate and facilitate extrusion. However, InaC was not required for the extrusion mode of exit (data not shown), suggesting that the F-actin structure assembled at the inclusion during mid cycle is not required for extrusion, although it was unclear whether M338 displayed increased frequency or early extrusion, which could link CTL0496 to extrusion via F-actin modulation.

Cell-autonomous IFN immune responses to *C. trachomatis* remain unchanged and the inclusion membrane is intact in the absence of InaC, indicating that InaC-dependent F-actin assembled at the inclusion does not stabilize the inclusion

membrane. Maintenance of membrane integrity was proposed to be the prevailing role of cytoskeletal structures assembled at the surface of pathogenic vacuoles (Kumar and Valdivia, 2009). This model was based largely on results in which global F-actin disruption lead to a loss of integrity of the *Chlamydia* and *Salmonella* pathogenic vacuoles. However, as is the case with InaC and *Chlamydia*, in contrast to global interference of F-actin, deletion of the *Salmonella* kinase SteC, which is required for F-actin remodeling selectively around the *Salmonella*-containing vacuole, did not result in any loss of vacuolar integrity (Poh et al., 2008). Besides playing structural and supportive roles in cells, F-actin is highly dynamic and facilitates subcellular organization and organelle positioning within cells, and these dynamic faces of actin should be considered as we re-evaluate the roles of cytoskeletal structures surrounding pathogenic vacuoles.

In addition to remodeling F-actin at the inclusion periphery, InaC remodels the distribution of organelles around the inclusion. InaC acts to uniformly distribute lysosomes but inhibit recycling endosome recruitment around the inclusion. Whether InaC-mediated F-actin assembly or ARF-recruitment mediate these functions remains unclear. However, both cellular F-actin and InaC are required for Golgi redistribution to surround the inclusion, suggesting that InaC-dependent F-actin remodeling may mediate Golgi positioning during infection.

The Golgi plays a central role in the secretory pathway, which *Chlamydia* manipulates to intercept ER-synthesized sphingolipids destined for the plasma membrane both by engaging the ceramide transporter CERT at ER-inclusion membrane contact sites (Derré et al., 2011; Elwell et al., 2011) and by hijacking Golgi-dependent vesicular traffic (Elwell et al., 2011; Hackstadt et al., 1995, 1996). Disruption of Golgi

vesicular traffic and interference with ARF regulated pathways using Brefeldin A or by depletion of the ARF nucleotide exchange factor GBF1 disrupts sphingolipid acquisition by *Chlamydia* (Elwell et al., 2011; Hackstadt et al., 1996). In addition to vesicular traffic, Golgi morphology and localization may affect sphingolipid trafficking to the inclusion since inhibition of Golgi dispersal during infection using a caspase inhibitor or by depletion of Rab6 or Rab11 impairs sphingolipid acquisition by *Chlamydia* (Heuer et al., 2009; Rejman Lipinski et al., 2009). Surprisingly, we find that InaC-mediated Golgi redistribution or ARF recruitment does not appear to have any discernable effect on the delivery of sphingolipids to the inclusion. Importantly, disruption of vesicular trafficking with Brefeldin A leads to the same decrease in sphingolipid acquisition in the absence of InaC, indicating that both the Golgi-dependent and non-vesicular pathways of lipid acquisition are both fully functional in the absence of InaC.

InaC-mediated Golgi redistribution or ARF recruitment may affect cellular processes during infection other than sphingolipid trafficking to the inclusion. Indeed, the kinetics of STING translocation through the Golgi are altered in the absence of InaC. Besides lipid trafficking to the plasma membrane, the Golgi and ARFs are also critical in secretory trafficking of cytokines. Effectors of other pathogens, including EspG encoded by enterohemorrhagic *E. coli* (EHEC) (Selyunin et al., 2014) and IpaJ encoded by *Shigella flexneri* (Burnaevskiy et al., 2013) alter Golgi distribution and consequently disrupt cytokines secretion into the extracellular milieu. InaC could similarly disrupt the secretion of cytokines during *C. trachomatis* infection. Critical steps of surface protein glycosylation occurs at the Golgi, and surface proteins are incompletely glycosylated during *C. trachomatis* infection, which has been suggested to be due to changes to Golgi morphology (Heuer et al., 2009), and could be InaC-dependent. Moreover, the

positioning and orientation of the Golgi is critical for directed cell migration, which is disrupted in *C. trachomatis*-infected cells (Heymann et al., 2013; Kumar and Valdivia, 2008b) which could be attributed to InaC-mediated Golgi redistribution. Finally, the full consequence of F-actin assembly or Golgi redistribution on the pathogenesis of chlamydial disease may not become apparent until the development of appropriate tissue and animal infection models for *C. trachomatis*.

2.6 Materials and Methods

2.6.1 Cell lines, *Chlamydia* strains, growth conditions, and antibodies

Vero cells (ATCC CCL-81), HeLa cells, HEK 293T, and the indicated mouse lung fibroblasts (Barker et al., 2013) were grown in high glucose DMEM supplemented with L-glutamine, sodium pyruvate (Gibco, Life Technologies) and 10% FBS (Mediatech, CellGro), and A2EN cells (Buckner et al., 2011) were grown Keratinocyte-SFM supplemented with L-Glutamine, EGF and BPE (Gibco, Life Technologies), and 300 µM calcium chloride and 10% FBS (Mediatech, CellGro) at 37 °C in a 5% CO₂ humidified incubator.). Rifampin resistant (Rif^R) and spectinomycin resistant (Sp^c^R) *C. trachomatis* LGV biovar L2 434/Bu strains have been previously described ((Nguyen and Valdivia., 2012), Supplementary table S3 in (Snively and Kokes et al., 2014)). All *Chlamydia* strains were maintained as frozen stocks in SPG buffer (0.25 M sucrose, 10 mM sodium phosphate, 5 nM glutamic acid). LGV L2 infections were performed with EBs from crude cell lysates of infected cells, synchronized by centrifugation (2,500 x g for 30 minutes at 10 °C) onto Vero and HeLa cell monolayers, and incubated for indicated times. EB titers were determined by infecting Vero cell monolayers seeded in a 96 well plate. At 30 hpi cells were fixed and stained with anti-Slc1 antibodies. The number of Inclusion forming

units (IFUs) were determined using a Cellomics ArrayScan automated fluorescence imaging system (Thermo Scientific). Antibody and plasmid sources: rabbit monoclonal anti- α -actinin (EMD Milipore), mouse monoclonal anti-Filamin (Sigma Aldrich), mouse monoclonal anti-Talin (Sigma Aldrich), rabbit polyclonal anti-*Chlamydia* MOMP (Kenneth Fields, University of Kentucky), mouse anti-CT813 (Guangming Zhong, University of Texas Health and Science Center), rabbit anti-GAPDH (Abcam), rabbit anti-Slc1 (Chen et al., 2014), rabbit anti-IncG (Ted Hackstadt, NIAID Rocky Mountain Laboratories), rabbit anti-14-3-3 ϵ (Cell Signalling), rabbit anti-14-3-3 β (Santa Cruz), mouse anti-GM130 (BD Biosciences), mouse anti-GFP (Clontech), EGFP-RhoA vectors, GFP-Rac1, and Lamp1-GFP (Soman Abraham, Duke University), ARF-EGFP vectors and GFP- PI4KII α (Marci Scidmore), and *C. trachomatis* Serovar D Gateway ORFeome (Roan and Starnbach, 2008), ER-RFP and DsRed-Mito (Richard Youle, NIH), Sec61 β -GFP (Addgene 15108, Tom Rapoport, Harvard Medical School), GFP-Rab1 (Craig Roy, Yale), and the following plasmids are from Addgene: GFP-GalT (11929), GFP-NMHC IIA (11347), Vinculin-venus (27300), GFP-NMCHIIB (11348), GFP-IQGAP1 (30112), myc-Septin-5 (27272), GFP-rGBD (26732).

2.6.2 Forward genetics screen for F-actin recruitment altered mutants

HeLa cells were grown to 50% confluency in 96-well plates and infected with 10 μ l of crude cell lysates derived from each mutant in the library. As controls, cells were infected with varying amounts of density gradient purified wild type EBs at MOIs ranging from 0.1-100. At 30 hpi, cells were fixed and stained with rabbit anti-Slc1 antibodies followed by Alexa488 conjugated Goat anti Rabbit IgG (Life Technologies), Rhodamine-Phalloidin (Life Technologies), and Hoechst. Cells were imaged with Cellomics HTC Arrayscan (Thermo Scientific) and images viewed with Cellomics vHCS: View Software

v1.6 (Thermo Scientific) to visually assess F-actin at the periphery of inclusions. The MOIs of infections with mutant strains ranged from 0.1 to 50.

2.6.3 Identification of lesions in CTL0184 and CTL0496 as causal

Whole genome sequencing: *Chlamydia* DNA was isolated from M407 and M338 as described above and sequenced in a MiSeq sequencing platform (Illumina Inc.). Read mapping and SNV calling was performed by reference-based assembly to the *C. trachomatis* L2/434/Bu (GenBank NC_010287) genome with Geneious Pro v6 software (Biomatters).

Generation of recombinants: Vero cells were co-infected with M407 or M338 (Rif^R) and a Spc^R strain at an MOI ratio of 3:3. At 44 hpi, progeny were harvested by hypotonic lysis and Rif^R/Spc^R doubly resistant recombinant strains isolated by plaque assay as described in (Nguyen and Valdivia, 2012). All recombinants isolated were assessed for F-actin assembly at inclusions.

Genotyping: Seven recombinants lacking F-actin assembly at inclusions and one recombinant displaying wild-type actin recruitment were genotyped for all M407 encoded SNVs through TILLING as previously described (Colbert et al., 2001; Kari et al., 2011), and by Sanger sequencing for the SNV in CTL0299.

2.6.4 Complementation of M407 with wild type and variants of InaC

Vector construction and transformation: The CTL0184 ORF (*inaC*) and 250 b. p of upstream sequence were amplified from *C.t* LGV L2 genomic DNA by PCR and inserted into the shuttle vector p2TK2-SW2 (Agaisse and Derré., 2013). A Q5 site-directed mutagenesis kit (NEB) was used according to manufacturers instructions to introduce amino acid substitutions and a 3xFLAG tag. M407 was transformed with each

vector as previously described (Wang et al., 2011). Transformants were plaque purified under Penicillin G selection (1 U/mL).

Immunoblot: HeLa cells grown to 50% confluency were infected with the indicated strains at an MOI of 1 and at 30 hpi cell lysates prepared in 1% SDS buffer (1% SDS, 150 mM NaCl, 50 mM Tris–HCl, pH 7.5). Equal amounts of lysates were resolved by SDS-PAGE followed by immunoblot analysis with anti-CT813 (anti-InaC), anti-MOMP, and anti-GAPDH antibodies using a LI-COR (Odyssey) infrared imaging system.

2.6.5 Visual and quantitative analysis of F-actin assembly at inclusions

High-resolution imaging: HeLa cells grown on glass coverslips were infected with indicated *C. trachomatis* strains at an MOI of five. At 30 hpi, cells were fixed and stained with mouse anti-CT813 (anti-InaC) antibodies, rabbit anti-IncG, Alexa conjugated secondary antibodies (Life Technologies), Rhodamine-Phalloidin (Life Technologies), and Hoechst, and mounted onto glass slides with Slow Fade Gold (Invitrogen). Images were captured on an Axio Observer Z1 (Zeiss) inverted widefield fluorescence microscope with a 63X objective (Zeiss). Images were minimally processed with Image J (NIH) and Photoshop CS6 (Adobe).

Visual quantification: HeLa cells grown in 96-well plates were infected with indicated strains at an MOI of five. At 30 hpi, cells were fixed and stained as above with rabbit anti-Slc1 antibodies, Alexa488 conjugated Goat anti Rabbit IgG (Life Technologies), Rhodamine-Phalloidin (Life Technologies), and Hoechst. Cells were imaged with a Cellomics HTC Arrayscan (Thermo Scientific) and a 20x objective and images viewed with Cellomics vHCS: View Software v1.6 (Thermo Scientific) to quantify

number of inclusions surrounded by F-actin for at least 60 inclusions per well. Images were analyzed with a custom-designed algorithm in Cellomics Scan Software v5.6 (Thermo Scientific) to assess average intensity of F-actin. All images were background subtracted with a 3D surface-fitting model. Inclusions were defined by anti-Slc1 staining, and 2 μm -wide ring-shaped regions were further defined by expanding out from 1 μm within the inclusion object edge. Average intensity of Rhodamine-Phalloidin fluorescence (F-actin) was measured in these regions as a mean value of all objects in a well. Background intensities were measured by defining similar ring-shaped objects around Hoechst-positive nuclei in uninfected wells, and subtracted from the average intensities of F-actin around inclusions in each experiment. At least 350 inclusions or nuclei were analyzed per well.

Statistics: Three technical triplicate wells were combined in each of three independent experiments. Within each experiment, values were normalized to values observed in wild-type inclusions. Statistically significant differences were assessed by a one-way ANOVA followed by Newman-Keuls Multiple Comparison *post-hoc* analysis with a p-value < 0.05 considered significant. Graphs were prepared with Prism (GraphPad Software) and Photoshop (Adobe).

2.6.6 Identification of host proteins that interact with InaC or RhoA(G17A)

Vector construction: To create a plasmid for mammalian transient expression of a full-length CT813 tagged at the N-terminus with cycle 3 GFP, a Gateway entry clone containing the *C. trachomatis* Serovar D ORF CT813 from a *C. trachomatis* Gateway ORFeome library (Roan et al., 2006) was used as a donor for Gateway transfer into the destination vector pDEST53. The NEB Q5 Site-Directed Mutagenesis Kit was used to

insert a stop codon at the end of the CT813 ORF. EGFP-RhoA(G17A) was obtained from Soman Abraham (Duke University).

Immunoprecipitation: HEK 293T cells grown to 50% confluency in 10 cm dishes coated with poly-L-Lysine (Sigma-Aldrich), infected as indicated with wild type *C. trachomatis* LGV L2, were transfected with either a GFP-only vector (pDEST53) or a GFP-InaC plasmid using jetPRIME (Polyplus transfection) with a fresh media exchange after 4 hr. At 24 hr post transfection, cells were chilled and scraped in lysis buffer (25 mM Tris-HCl [pH 8.0], 150 mM NaCl, 1 mM EDTA, and 0.5% NP-40) supplemented with a broad protease inhibitor cocktail (Roche Diagnostics) and a broad phosphatase inhibitor (Pierce). After mechanical lysis by vigorous pipetting three times over 30 min and high speed centrifugation to remove insoluble debris, GFP-Trap (ChromoTek) resin was added and incubated overnight at 4°C. After washing thoroughly with lysis buffer, bound resin was analyzed by LC-MS/MS at the Duke Proteomics Core facility to identify proteins, or bound proteins were eluted in 0.2 M glycine [pH 2.5] and resolved by SDS PAGE and subjected to immunoblot analysis as described above.

2.6.7 Assessing ARF, 14-3-3, recycling endosome markers, and RhoA-interacting protein recruitment to inclusions

HeLa cells grown on glass coverslips were infected with indicated *C. trachomatis* strains at an MOI of five and transfected with the indicated plasmids using jetPRIME (Polyplus transfections). At 30 hpi, cells were fixed and stained with the indicated antibodies, Hoeschst, and rhodamine-phalloidin. Images were captured on an Axio Observer Z1 (Zeiss) inverted widefield fluorescence microscope with a 63X objective (Zeiss). Images were minimally processed with Image J (NIH) and Photoshop CS6 (Adobe). 14-3-3 micrographs were acquired at the same exposures across all samples.

A Gaussian de-blur algorithm was applied uniformly to only ARF-GFP micrographs to reduce background from out of focus signal.

2.6.8 Visual and quantitative analysis of Golgi redistribution around inclusions

High-resolution imaging: HeLa cells grown on glass coverslips were infected with indicated *C. trachomatis* strains at an MOI of five. At 30 hpi, cells were fixed and stained with mouse anti-GM130 antibodies (BD Biosciences), rabbit anti-IncG, Alexa conjugated secondary antibodies (Life Technologies), and Hoechst. Images were captured on an Axio Observer Z1 (Zeiss) inverted widefield fluorescence microscope with a 63X objective (Zeiss). Images were minimally processed with Image J (NIH) and Photoshop CS6 (Adobe).

Visual quantification: HeLa cells grown in 96-well plates were infected with indicated strains at an MOI of five. At 30 hpi, cells were fixed and stained with rabbit anti-Slc1 antibodies, Alexa conjugated secondary antibodies (Life Technologies), and Hoechst. F-actin was depolymerized with a 30 min treatment of 500 nM Latrunculin B (Life Technologies) prior to fixation, as indicated. Samples were imaged with a Cellomics HTC Arrayscan (Thermo Scientific) and a 20x objective and images viewed with Cellomics vHCS: View Software v1.6 (Thermo Scientific) to quantify the number of inclusions with Golgi distributed half-way or more around the inclusion for at least 50 inclusions in each well.

Statistics: Three technical triplicate wells were combined in each of three independent experiments. Values are expressed as a percent. Statistically significant differences were assessed by Student's t test or a one-way ANOVA followed by Newman-Keuls Multiple Comparison *post-hoc* analysis with a p-value < 0.05 considered

significant. Graphs were prepared with Prism (GraphPad Software) and Photoshop CS6 (Adobe).

2.6.9 Inclusion forming units (IFU) and inclusion size analysis

Confluent monolayers of HeLa cells in 96-well plates were infected with various *Chlamydia* strains at an MOI of 0.6. At 24 hpi samples were fixed and inclusions were detected by immunostaining with anti-Slc1 antibodies. Bacteria in infected cells were harvested at 30 and 48 hpi by hypotonic lysis as previously described (Nguyen and Valdivia., 2012) in duplicate. Serial dilutions of the cell lysates were used to infect a new monolayer of confluent HeLa cells and inclusions were detected by immunostaining with anti-Slc1 antibodies at 24 hpi. Cells were imaged with a Cellomics HTC Arrayscan (Thermo Scientific) and a 20x objective and images were analyzed with a custom-designed algorithm in Cellomics Scan Software v5.6 (Thermo Scientific) to analyze the total count, or IFUs, and the average area of inclusions. The total number of IFUs obtained at 30h and 48h (output) was divided by the number of input IFU to derive number of infectious progeny per input IFU. The average area reported was assessed only from input samples, which were infected uniformly at an MOI of 0.6 and are expressed as arbitrary units.

Three technical triplicate wells were combined in each of three independent experiments. Statistically significant differences were assessed by Student's t test or a one-way ANOVA followed by Newman-Keuls Multiple Comparison *post-hoc* analysis with a p-value < 0.05 considered significant. Graphs were prepared with Prism (GraphPad Software) and Photoshop CS6 (Adobe).

2.6.10 Visual and quantitative analysis of sphingolipid trafficking to inclusions

We adapted a published protocol (Moore., 2012). HeLa cells grown to 50% confluency in 96-well plates were infected with the indicated LGV-L2 strains at an MOI of 3. At 23 hpi, plates were chilled to 12°C for 15 min and rinsed with cold Hanks balanced salt solution (HBSS) prior to incubation with pre-chilled 5µM NBD-C₆-ceramide (Life Technologies) in DMEM supplemented with 0.034% defatted BSA (Sigma) at 12°C for 30 min. Cells were rinsed twice with 37°C HBSS and incubated for 6 hr with DMEM supplemented with 0.7% defatted BSA for back-exchange at 37°C. Prior to imaging, cells were incubated with 2 µg/mL Hoechst in HBSS at 37°C for 10 min. Live cells were imaged with a Cellomics HTC Arrayscan (Thermo Scientific) and a 20x objective and images were analyzed with a custom-designed algorithm in Cellomics Scan Software v5.6 (Thermo Scientific) to analyze the average intensity of objects defined by an intensity threshold in the NBD-detecting channel (inclusions). As a control, cells were incubated with 3 µg/mL Brefeldin A (Sigma-Aldrich) for 30 minutes prior to labeling and throughout the back-exchange and processed identically. Images were minimally processed with Cellomics vHCS: View Software v1.6 (Thermo Scientific) and Photoshop CS6 (Adobe).

Three technical triplicate wells were combined in each of three independent experiments. Statistically significant differences were assessed by two-way ANOVA with Bonferroni *post hoc* analysis with a p-value < 0.05 considered significant. Graphs were prepared with Prism (GraphPad Software) and Photoshop CS6 (Adobe).

2.6.11 Screen of InaC-dependent changes to organelle distribution

HeLa cells were grown to 50% confluency in 96-well plates glass-bottom plates (Corning 4680), infected with M407 transformed with empty vector or the vector harboring wild type InaC at an MOI of 1, and transfected with the indicated plasmids using jetPRIME (Polyplus transfections). Living cells were imaged with spinning disk confocal microscopy using the Operetta (Perkin Elmer) at 40x magnification every hour from 20 to 36 hpi. Images were viewed using ImageJ.

2.6.12 Quantitative measurement of RNA transcript abundance

RNA-seq: Approximately 5×10^5 A2EN cells were seeded per well in 6-well plates the day before experiment. Cell samples were infected with the M407 transformed with empty vector or the vector harboring wild type InaC at an MOI of 3. Infections were synchronized by centrifugation at 2500 x g for 30 min at 10 C. Samples were collected at 30 hpi using QIAGEN RNeasy Plus Mini Kit (QIAGEN) as described by the manufacturer. RNA integrity was assessed with Agilent 2100 Bioanalyzer G2939A (Agilent Technologies) and quantified with a Nanodrop 8000 spectrophotometer (Thermo Scientific/Nanodrop). This was repeated for three independent experiments. 12 μ g of total RNA of each sample was submitted to the Duke University Genome Sequencing & Analysis Core Resource for RNA-seq. Samples were enriched for mRNA by creating TruSeq mRNA-seq individually barcoded libraries were created and sequenced in two lanes of an Illumina HiSeq 2500. The resulting data was initially analyzed by David Corcoran, PhD at the Duke University Integrative Genomic Analysis Shared Resource as following: RNA-seq data was processed using the TrimGalore toolkit which employs Cutadapt and FastQC to trim low quality bases and Illumina sequencing adapters from

the 3' end of the reads. Only reads 20nt or longer were kept for further analysis. Reads were mapped to the GRCh37r73 version of the human genome and transcriptome using the STAR RNA-seq alignment tool. Reads were kept for subsequent analysis if they mapped to a single genomic location. Gene counts were compiled using the HTSeq tool. Only genes that had at least 10 reads in any given library were used in subsequent analysis. Normalization and differential expression was carried out using the EdgeR Bioconductor package in the R statistical programming environment. A negative binomial generalized linear model was employed to identify differentially expressed genes across conditions. An additional factor was added to the model to control for the batch. The false discovery rate was calculated to control for multiple hypothesis testing.

Quantitative real-time PCR (qPCR): Q-PCR was performed using Power SYBR Green RNA-to-CT 1-Step Kit and StepOne Real-Time PCR system as described by the manufacturer (Applied Biosystems, Grand Island, NY, USA). Primers were designed using the Roche Universal Probe Library (Roche). Primers against Chlamydia 16S rRNA were used to confirm equal amounts of bacteria and primers against human HPRT1 were used as a standard for normalization.

Type I IFN expression: Expression of type IFNs was assessed either with reporter cell lines. For reporter cell line construction, lentiviruses containing an IFN-stimulated response element (ISRE)-luciferase reporter (SABiosciences) was used to stably transduce A2ENs. These cells were seeded into 96-well plates and infected with the indicated strains of *C. trachomatis* in triplicate. After 30 hours, the medium was removed and cells were washed once with calcium chloride and magnesium chloride-free phosphate-buffered saline (PBS). Cells were lysed in 50 µl of britelite plus reagent per well (PerkinElmer), and the samples were transferred to a white OptiPlate

(PerkinElmer) for measurement of luminescence on an EnSpire 2300 Multilabel Plate Reader (PerkinElmer).

3. Reassessing the role of the secreted protease CPAF in *Chlamydia trachomatis* infection through genetic approaches¹

The secreted *Chlamydia* protease CPAF cleaves a defined set of mammalian and *Chlamydia* proteins *in vitro*. As a result, this protease has been proposed to modulate a range of bacterial and host cellular functions. However, it has recently come into question the extent to which many of its identified substrates constitute *bona fide* targets of proteolysis in infected host cell rather than artifacts of post lysis degradation. Here we clarify the role played by CPAF in cellular models of infection by analyzing *Chlamydia trachomatis* mutants deficient for CPAF activity. Using reverse genetic approaches, we identified two *C. trachomatis* strains possessing nonsense, loss-of-function mutations in *cpa* (CT858), and a third strain containing a mutation in Type II secretion (T2S) machinery that inhibited CPAF activity by blocking zymogen secretion and subsequent proteolytic maturation into the active hydrolase. HeLa cells infected with T2S⁻ or CPAF⁻ *C. trachomatis* mutants lacked detectable *in vitro* CPAF proteolytic activity, and were not defective for cellular traits that have been previously attributed to CPAF activity, including Golgi fragmentation. In addition, we provide compelling evidence in live cells that CPAF-mediated protein processing of at least two host protein targets, vimentin filaments and the nuclear envelope protein Lamin-associated protein 1

¹ Parts of Chapter 3 are reused and edited with permission of the following published article of which I am co-first author: Snavelly, E.A., Kokes, M., Dunn, J.D., Saka, H.A., Nguyen, B.D., Bastidas, R.J., McCafferty, D.G., and Valdivia, R.H. (2014). Reassessing the role of the secreted protease CPAF in *Chlamydia trachomatis* infection through genetic approaches. *Pathog Dis*.

(LAP1), occurs rapidly after the loss of the inclusion membrane integrity, but before loss of plasma membrane permeability and cell lysis. CPAF-dependent processing of host proteins correlates with a loss of inclusion membrane integrity, and so we propose that CPAF plays a role late in infection, possibly during the stages leading to the dismantling of the infected cell prior to the release of EBs during cell lysis.

3.1 Introduction

To modulate host cellular functions, *Chlamydia* employs a type III secretion (T3S) system to translocate “effector” proteins that mediate cell invasion, re-routing of lipid transport, and manipulation of signaling pathways important in immunity (Valdivia, 2008). In addition, some chlamydial virulence proteins contain “classical” signal peptides and presumably use the Sec secretory system to cross the bacterial cytoplasmic membrane (Chen et al., 2010). How these signal peptide-containing proteins are further translocated from the bacterial periplasmic space to the inclusion lumen and eventually across the inclusion membrane is unclear. Potential delivery pathways include outer membrane vesicles (Giles and Wyrick, 2008; Giles et al., 2006) and Type II secretion (T2S) machinery, which in gram-negative bacteria is required to secrete a subset of folded proteins across the outer membrane (Sandkvist, 2001). One prominent example of a protein that may follow this secretion pathway is the chlamydial protease-like activity factor (CPAF), a serine protease (Zhong et al., 2001). Late in infection, CPAF localizes to the inclusion lumen and the host cell cytoplasm as assessed by immunofluorescence microscopy and subcellular fractionation (Shaw et al., 2002; Zhong et al., 2001).

CPAF was the first *Chlamydia* virulence factor for which a biochemical activity (protease) and a target (transcription factors) had been established (Zhong et al., 2001).

CPAF-mediated degradation of the transcription factors RFX-5 and USF-1 were linked to the loss of expression of MHC Class I and II - a cellular phenotype that had been observed in infected cells (Zhong et al., 2000). CPAF has also been reported to cleave the pro-apoptotic factors Bim and Puma (Pirbhai et al., 2006; Zhong et al., 2001), p65/RelA, a transcription factor required for NF κ B signaling (Christian et al., 2010), intermediate filaments vimentin, and keratins 8 and 18, (Dong et al., 2004a; Kumar and Valdivia, 2008a), the adherence junction protein nectin1 (Sun and Schoborg, 2009), the MHC-like lipid presentation protein CD1d (Kawana et al., 2007), the pro-inflammatory mediator HMGB1 (Yu et al., 2010), the mitotic cell cycle regulator CyclinB1 (Paschen et al., 2008), securin (Brown et al., 2012; Christian et al., 2011), the Golgi tethering factor Golgin 84 (Christian et al., 2011), and PARP – a mediator of DNA-damage during apoptosis (Paschen et al., 2008). Because of CPAF's apparent preference for proteins important in host immunity and signaling, it has been proposed that CPAF-mediated proteolysis represents a core strategy employed by *Chlamydia* to modify host-signaling pathways and usurp the cellular machinery for its own benefit (Zhong, 2009, 2011). Additional functions of CPAF may include death of the infected host cell as ectopic over expression of CPAF in mammalian cells initiates a host cell death pathway that mimics the necrotic cell death observed at the end of the *Chlamydia* life cycle (Paschen et al., 2008). Similarly, *Chlamydia* proteins have also been reported to be targets of CPAF-mediated processing including early T3S effectors, which we postulated plays a role in protection from re-infection (Jorgensen et al., 2011), and the abundant outer membrane protein OmcB (Hou et al., 2013), which may represent a mechanism to generate soluble form(s) of OmcB that can access the host cell cytoplasm (Qi et al., 2011).

As more CPAF targets began to emerge, similar correlations were made between the degradation of these factors and cellular phenotypes of *Chlamydia*-infected cells. This list includes, but is not limited to, Golgi fragmentation, inclusion expansion, resistance to re-infection, modulation of apoptosis and pro-inflammatory signaling pathways, disruption of the cell cycle, cell junction defects, and centrosomal abnormalities (Zhong, 2011). Because molecular genetic tools to specifically inactivate chlamydial genes were not available, many of these correlations could not be formally tested in CPAF-deficient mutants. The development of small molecule and peptide inhibitors that blocked CPAF activity *in vitro* and *in vivo* promised to be helpful in assessing some of these questions (Jorgensen et al., 2011). Indeed, cell-permeable inhibitors blocked CPAF activity in cell culture infection models, decreased the replicative potential of *Chlamydia* (Christian et al., 2011; Hou et al., 2013; Jorgensen et al., 2011) and often reversed cellular phenotypes of infected cells that have been associated with CPAF. However, these CPAF inhibitors also varied in their effect in cells and displayed varied levels of toxicity (Christian et al., 2011; Jorgensen et al., 2011).

CPAF is fairly selective in its target specificity and broad degradation of proteins is not observed when crude cell lysates are treated with recombinant CPAF (Jorgensen et al., 2011). However, the significance of CPAF-dependent proteolysis *in vivo* has recently come into question since, in principle, post-cell lysis sample preparation could expose putative substrates under examination to degradation by nonspecific proteases that are commonly released upon cellular lysis (Chen et al., 2012). As such, the extent to which CPAF cleaves reported substrates in intact infected cells remains unclear (Chen et al., 2012). Definitive experimental evidence for the *in vivo* target specificity of CPAF and the consequences of its proteolytic activity has been hampered by the difficulty in

identifying CPAF substrate recognition sites that can be mutated, the redundancies in the function of host cell targets, and the lack of a system to generate defined mutations in *Chlamydia*. Furthermore, although cell permeable inhibitors of CPAF demonstrated a role in chlamydial pathogenesis, off-target effects are difficult to anticipate or control and thus limit their usefulness as compared to genetic knockout approaches (Christian et al., 2011; Hou et al., 2013; Jorgensen et al., 2011).

In this study, we sought to clarify the role played by CPAF by performing a phenotypic analysis of *C. trachomatis* mutants that are either defective for CPAF secretion or have loss-of-function mutations in *cpa*. We report that many of the cellular phenotypes of *Chlamydia*-infected cells that had been previously ascribed to CPAF, including Golgi fragmentation, are not CPAF-dependent. However, it is important to note that this does not mean that all identified CPAF substrates are not targeted for proteolysis *in vivo*. We provide compelling evidence for CPAF-mediated processing of vimentin as well as a new CPAF substrate recently identified *in vitro*, the nuclear envelope protein Lamin Associated protein-1 (LAP1). These proteolytic events occurred in intact live cells late in infection soon after loss of inclusion membrane integrity, suggesting that the bulk of active CPAF is sequestered within the inclusion lumen.

3.2 A *Chlamydia* mutant defective for Type II secretion accumulates unprocessed CPAF zymogen

C. trachomatis remains poorly characterized because of its history of intractability to routine molecular genetic manipulation. Recently we developed a combinatorial approach to rapidly generate a comprehensive library of genetically defined mutants (Nguyen and Valdivia, 2012). Chemical mutagenesis coupled with whole genome sequencing (WGS) was used to generate *Chlamydia* mutants with distinct phenotypes

and to map the underlying genetic lesions. As a result, we identified a *C. trachomatis* LGV-L2 variant (RSTE4 (T2S⁻)) bearing a point mutation in the Type II secretion ATPase GspE (Nguyen and Valdivia, 2012). This mutant is attenuated for growth and accumulates insoluble glycogen granules within inclusions, presumably as a result of the impaired secretion of glycogen processing enzymes (Nguyen and Valdivia, 2012). Given the known role of T2S in the export of folded hydrolases from the bacterial periplasm (Sandkvist, 2001), we hypothesized that this secretion system is also responsible for the export of CPAF. Indeed, immunofluorescence analysis with anti-CPAF antibodies of HeLa cells infected with *C. trachomatis* RSTE4 (T2S⁻) mutants revealed that all CPAF was exclusively associated with bacteria within the inclusion and no immunoreactive material was present in the host cytoplasm (Figure 20A-B). An immunoblot analysis of total protein lysates from cells infected with RSTE4 (T2S⁻) further showed that the processed 35kDa and 29kDa bands of mature CPAF (Dong et al., 2004b), which are prominent in cells infected with wild type *C. trachomatis*, are absent. Instead, a higher molecular weight 70kDa band consistent with the size of unprocessed CPAF zymogen (Dong et al., 2004b) was detected, albeit at lower abundance (Figure 20C). Lysates from cells infected with an unrelated *C. trachomatis* slow-growing mutant (SPQ6-2 (TrxB*)) (Nguyen and Valdivia, 2012) also showed the processed forms of CPAF, indicating that the accumulation of unprocessed CPAF in cells infected with the T2S⁻ mutants is not due to a slower replication rate. Consistent with this observation, crude lysates from cells infected with a *gspE* mutant lacked *in vitro* CPAF activity against a purified substrate (recombinant GST-CT695) (Figure 20D). Overall these results suggest that CPAF is a substrate of T2S and that secretion is coupled to its processing into an active form.

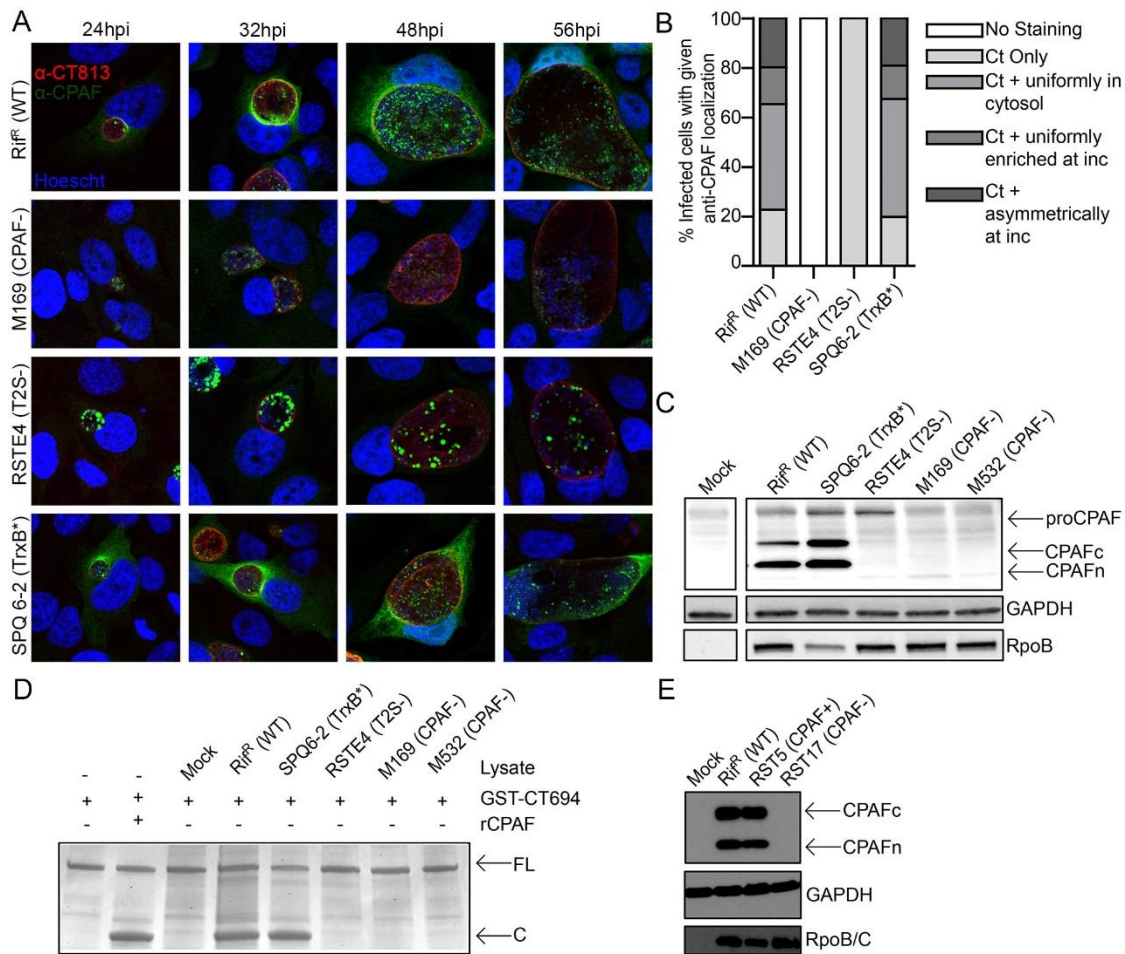


Figure 20. Identification of *C. trachomatis* strains deficient in CPAF secretion or expression. A-B). CPAF fails to accumulate in the cytoplasm of cells infected with a T2S-deficient mutant and is not detectable in a CPAF-truncation mutant (M169). The subcellular localization of CPAF in HeLa cells infected with the indicated *C. trachomatis* mutant strains was assessed by indirect immunofluorescence with polyclonal anti-CPAF antibodies (green), DNA with Hoescht (blue), and the inclusion membrane with anti-CT813 antibodies (red). Immunoreactive anti-CPAF material could not be detected in cells infected with a CPAF-deficient strain, or in the cytoplasm of cells infected with a T2S-deficient strain. The relative distribution of CPAF at 32 hpi in infected cells (n=100) is shown in panel B. C) T2S-deficient mutants fail to process CPAF into its active form. Immunoblot analysis of total protein lysates from HeLa cells infected with the indicated strains at 48 hpi. Strains containing mutations in *cpa* that do not express CPAF and T2S-deficient strains exhibit accumulation of a larger molecular weight band consistent with the size of unprocessed CPAF (proCPAF). The C terminal fragment and N terminal fragment of CPAF are indicated by “CPAFc” and “CPAFn”, respectively. D) Lysates from cells infected with CPAF or T2S-deficient *C. trachomatis* mutants do not process CPAF substrates in vitro. Purified recombinant CPAF (rCPAF) or lysates from HeLa cells that

were mock infected or infected with the indicated strain were harvested at 40 hpi and incubated with recombinant GST-CT695, an *in vitro* CPAF substrate. Cleavage products were monitored by SDS PAGE and staining with Coomassie Blue. FL: full length GST-CT695; C: cleavage product. E) M169-derived recombinant *C. trachomatis* strains retaining the *cpa* mutation do not express CPAF. Immunoblot analysis of total protein lysates of HeLa cells infected with RST17 (CPAF-) or its nearly co-isogenic recombinant sibling RST5 (CPAF+) for 48 hours. CPAF expression is restored in RST5 (CPAF+) bacteria but still absent in the RST17 (CPAF-) strain. The genotypes of these strains are shown in Tables 2 and Table S2.

3.3 Identification of *Chlamydia* strains with loss-of-function mutations in CPAF

The finding that RSTE4 (T2S⁻) mutants did not possess CPAF activity suggested that CPAF is not absolutely essential for bacterial viability. This is consistent with previous observations made with CPAF-inhibitors, where 5-10 fold differences in the yield of infectious units were reported (Christian et al., 2011; Hou et al., 2013; Jorgensen et al., 2011). We subsequently generated a bank of chemically mutagenized *C. trachomatis* LGV-L2 strains and screened for mutants that consistently formed small plaques on Vero cell monolayers overlaid with soft agar. We isolated ~1000 small plaque forming mutants, which were amplified in Vero cells, and their DNA isolated and sequenced (Kokes et al., 2015). Among this collection of mutants, we identified two strains (M169 and M532) with nonsense mutations in *cpa* (Snaveley et al., 2014). We determined that a representative CPAF truncation mutant (M169) had no detectable CPAF protein by immunofluorescence microscopy (Figure 20A-B) or western blots (Figure 20C). Furthermore, as observed for the T2S-deficient *Chlamydia* mutant, lysates of HeLa cells infected with the strains M169 and M532 lacked *in vitro* protease activity (Figure 20D).

3.4 HeLa cells infected with CPAF-deficient *Chlamydia* mutants display normal Golgi fragmentation

C. trachomatis infection leads to fragmentation of the Golgi apparatus into mini-stacks (Heuer et al., 2009), a phenotype that can be recapitulated by expression of active CPAF in infected cells (Christian et al., 2011; Heuer et al., 2009). Golgi fragmentation in infected cells correlates with the cleavage of golgin-84 (Heuer et al., 2009). The levels of Golgi fragmentation in cells infected with wild type LGV-L2 or M532 (CPAF⁻) were assessed by quantifying the number of GM130-positive Golgi structures, using previously described methods (Christian et al., 2011; Heuer et al., 2009). No significant differences between the wild type and the *cpa* mutant were observed, as both strains exhibited Golgi fragmentation (Figure 21A-B). As a control, I treated infected cells with the caspase-1 inhibitor z-WEHD-fmk, which has been reported to block CPAF activity, and to inhibit golgin-84 cleavage and Golgi fragmentation (Christian et al., 2011). z-WEHD-fmk treatment inhibited Golgi fragmentation in both wild type and the *cpa* mutant (Figure 21C) suggesting that its effect on Golgi fragmentation is not mediated by CPAF. Golgin-84 was not cleaved in cells infected with *cpa* mutants (data not shown). These experiments suggest that CPAF is not essential for the Golgi fragmentation phenotype observed in *Chlamydia* infected cells.

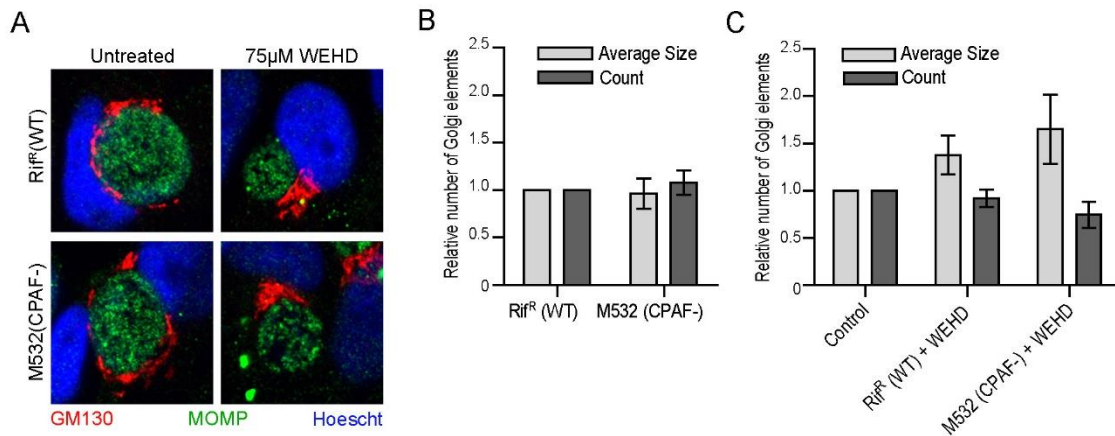


Figure 21. *C. trachomatis*-induced Golgi fragmentation occurs in a z-WEHD-fmk-dependent manner in the absence of CPAF. HeLa cells were infected with the indicated strains for 24 hpi and processed for immunofluorescence to visualize the Golgi apparatus (GM130, red), *C. trachomatis*, (MOMP, green) and DNA (Hoescht, blue). No difference was observed in Golgi fragmentation as assessed visually and by post-acquisition processing to assess size and number of Golgi elements between wild-type and a CPAF-deficient strain infections (panels A and B). In the same experiment, cells were treated with 75 μM z-WEHD-fmk from 9hpi, which inhibited Golgi fragmentation in cells infected with wild-type and a CPAF-deficient strain (panels A and C). Mean±SEM of three independent experiments.

3.5 CPAF mediates cleavage of intermediate filaments late in infection

CPAF cleaves the head domain at the amino terminus of intermediate filaments in vitro (Bednar et al., 2011; Dong et al., 2004a; Kumar and Valdivia, 2008a). Given the possibility that post lysis proteolysis may mask the extent to which CPAF-dependent processing truly occurs in live cells (Chen et al., 2012; Goodchild and Dauer, 2005), we reassessed our protein harvesting protocols to minimize post-lysis proteolysis. In particular, because of the intrinsic liability of its parent thioester to long term storage that likely explains batch to batch variability on the effectiveness of some commercial batches of lactacystin (data not shown), we shifted to performing lactacystin-free protein extractions either in hot 1% SDS at pH 7.0 or in normal sample buffer supplemented with a CPAF-inhibitory peptide (termed Pep2, which is cell permeable and inhibits CPAF

reversibly with a 50 nM K_i) (Bednar et al., 2011; Jorgensen et al., 2011). Under either of these lysis conditions, the activity of recombinant CPAF activity is completely inhibited (Figure 22A). We therefore performed a time course of infection with *C. trachomatis* from 12-56h and harvested total protein under these conditions. An immunoblot analysis of total protein lysates indicated that a vimentin cleavage product is detected as compared to the CPAF⁻ control strain, and this degradation occurred at a later timepoint during infection. We also observed that the vimentin degradation occurred to a lesser extent than previously described (Kumar and Valdivia, 2008a). This difference could be attributed to the degree to which the vimentin is proteolyzed intracellularly versus postlysis or to other factor such as the degree to which vimentin fragments are extracted in 1% SDS. To exemplify the dynamic range of CPAF-mediated cleavage of vimentin occurred, the example shown in Figure 22B highlights an experiment where the *least* amount of vimentin proteolytic processing was observed. In parallel, we monitored the release of lactate dehydrogenase (LDH) from wells with infected cells and did not observe significant differences in LDH release suggesting that cells remained intact during the course of infection (Figure 22C). These findings are consistent with vimentin and other CPAF targets (see below) being processed late during the course of infection.

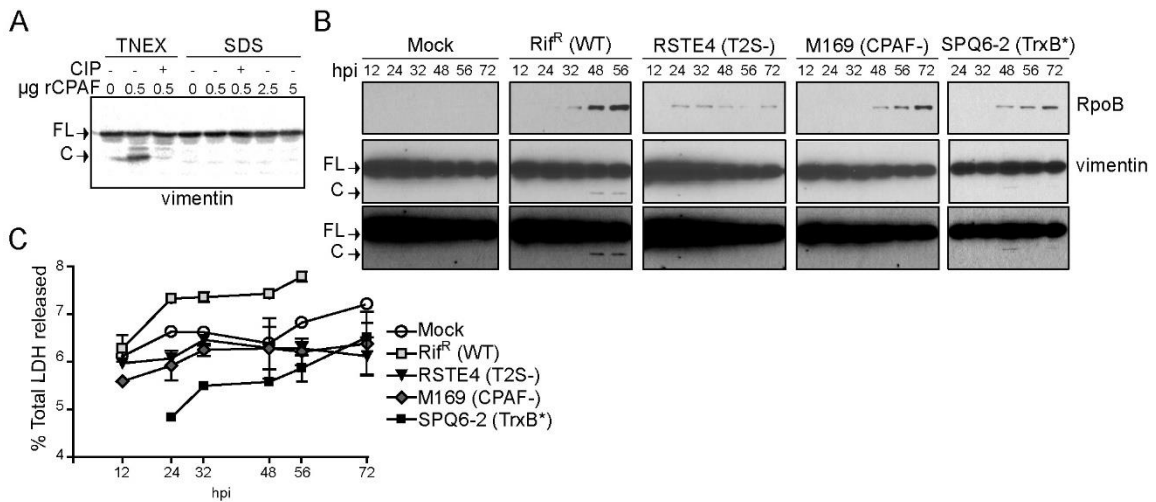


Figure 22. Evidence for CPAF mediated processing of vimentin in intact cells. A) CPAF is not active in 1% SDS buffer. HeLa cell lysates prepared under denaturing conditions in 1% SDS buffer were incubated with the 0.5, 2.5, and 5 μg recombinant CPAF (rCPAF) for 20 minutes at 37°C. As a positive control, rCPAF was also incubated with HeLa lysates prepared under non-denaturing conditions in TNEX buffer. Where indicated, 100 μM CPAF inhibitor peptide Pep2 (CIP) was included as a control. CPAF activity was assessed by monitoring the generation of vimentin cleavage products by immunoblot analysis. B) Proteolytic processing of vimentin at later stages of infection is dependent on CPAF. The bottom panel represents an increased exposure (OE) of the middle panel. FL: full-length vimentin; C: cleavage product C) LDH release by cells infected with wild type and CPAF-deficient *C. trachomatis* strains. The supernatants of infected cells were collected at the indicated time points and the amount of LDH release was measured and compared to total LDH levels. Mean±SD of three replicates.

We previously observed that extraction of live cells with 0.5% Triton X-100 on ice for 5 minutes preferentially extracted filaments proximal to the inclusion, but not those at the periphery within the same cell or within adjacent cells (Kumar and Valdivia, 2008a). These findings were interpreted as evidence of spatially constrained alteration of the cytoskeletal properties of intermediate filaments by CPAF. Although these detergent extractions were performed in the presence of lactacystin, the effectiveness of this inhibitor is somewhat difficult to control since the active form omuralide contains a beta lactone which is labile over longer periods of time in aqueous buffers. To address potential issues arising from CPAF proteolysis during the detergent extraction process, I

repeated these experiments in the presence of the CPAF inhibitory peptide Pep2 (Bednar et al., 2011; Jorgensen et al., 2011). HeLa cells were infected with *C. trachomatis* for 44, 52 and 60h, chilled on ice and extracted with 0.5% Triton X-100 with excess amounts of the Pep2. Under these conditions, no solubilization of filaments adjacent to the inclusion for the majority of infected cells was observed (Figure 23A lower left panel). These results indicate that either processing does not occur in all infected cells or that the extent of processing in the averaged infected cell does not lead to gross alterations in the physical properties of filaments.

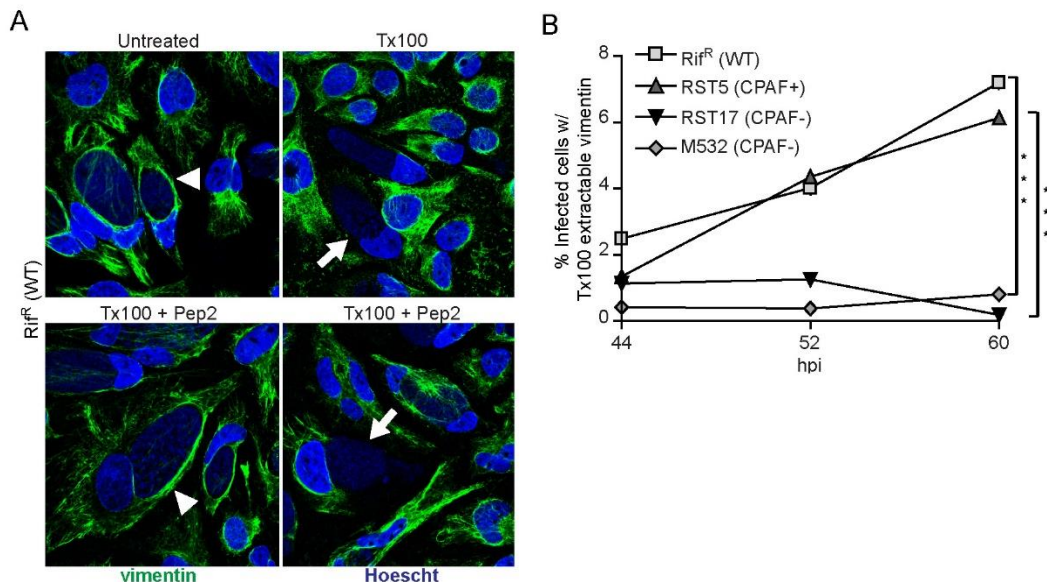


Figure 23. The solubility of vimentin filaments are altered in a CPAF-dependent manner at late stages of infection. A) A subset of infected cells contain vimentin filaments that are sensitive to detergent extraction. Top panel: Immunofluorescence images of HeLa cells infected with Rif^R (WT) at 52 hpi. Infected cells were either untreated or treated with 0.5% Tx100 for 5 minutes on ice, prior to fixation and immunostaining for vimentin localization. Vimentin cage forms around the inclusion of infected cells (arrowhead), which are sensitive to Tx100 extraction (arrow). Bottom panel: Infected HeLa cells were treated with 0.5 % Tx100 in the presence of 100 μ M CPAF-inhibitory peptide (Pep2). Note the presence of inclusions with both detergent resistant (arrowhead) and detergent sensitive (arrow) vimentin filaments. Blue: Hoescht; Green: vimentin. B) The proportion of inclusions with detergent extractable vimentin filaments increases with infection times in a CPAF-dependent manner. Cells were

infected with Rif^R (WT) or CPAF-mutant strains and the percentage of infected cells with Tx100 extractable vimentin (Figure 5A, bottom right) was quantified at 44 hpi, 52 hpi, and 60 hpi. All extractions were done in the presence of 100 μ M Pep2. Cells with extractable intermediate filaments were not apparent in HeLa cells infected CPAF-deficient mutants. *** $p < 0.001$ by two-way ANOVA with Bonferroni *post hoc*, mean \pm SEM of three independent experiments.

Nonetheless, in a significant subset of infected cells, the vimentin filament network was completely extractable with Triton X-100 even when CPAF activity was carefully inhibited during the extraction process (Figure 23A lower right panel). The proportion of these cells increased to ~7% of all cells as infection progressed to >60h (Figure 23B). To determine if CPAF played a role in this processing, we infected HeLa cells with RST5 (CPAF⁺) or the CPAF-deficient mutants RST17 and M532 and recorded the number of cells with Tx100-extractable vimentin filaments in the presence of Pep2 (Figure 23B). The presence of these “detergent-sensitive” soluble vimentin filaments in infected cells was completely dependent on CPAF. These results suggest that at late stages of infection a subset of infected cells display CPAF-mediated modification of one of its well-described substrates.

3.6 CPAF-dependent modification of vimentin filaments occurs after inclusion rupture

Given the observation that brief extractions (<5 min) of live cells with cold Triton X-100 in the absence of robust inhibition of CPAF lead to the preferential solubilization of filaments at the inclusion periphery post-lysis, we infer that the bulk of active CPAF resides within inclusion lumen where it may access chlamydial substrates, and then host substrates in a live cell when the integrity of the inclusion membrane is compromised. To formally test this premise, I performed live cell microscopy in HeLa cells co-expressing EGFP-vimentin and tdTomato during infection with either wild type (Rif^R) or a CPAF-

deficient mutant (M532). tdTomato is a red fluorescent protein that localizes to the host cell cytoplasm and is excluded from the inclusion lumen. Upon loss of inclusion membrane integrity, tdTomato becomes evenly distributed throughout the infected cell. Similarly, loss of plasma membrane integrity can be monitored as the overall loss of cell-associated red fluorescence, when cytoplasmic proteins rapidly diffuse into the extracellular media. In this manner, I determined that on average, plasma membrane integrity is not compromised until >30 min after the loss of inclusion membrane integrity (data not shown). Time-lapse events captured by fluorescence microscopy showed that in cells infected with wild type Chlamydia, loss of inclusion membrane integrity at late stages of infection preceded the rapid (<7 min) processing of vimentin filaments (Figure 24). In contrast, in CPAF-deficient mutants, the vimentin network remained unaltered upon loss of inclusion membrane integrity or even after loss of plasma membrane integrity.

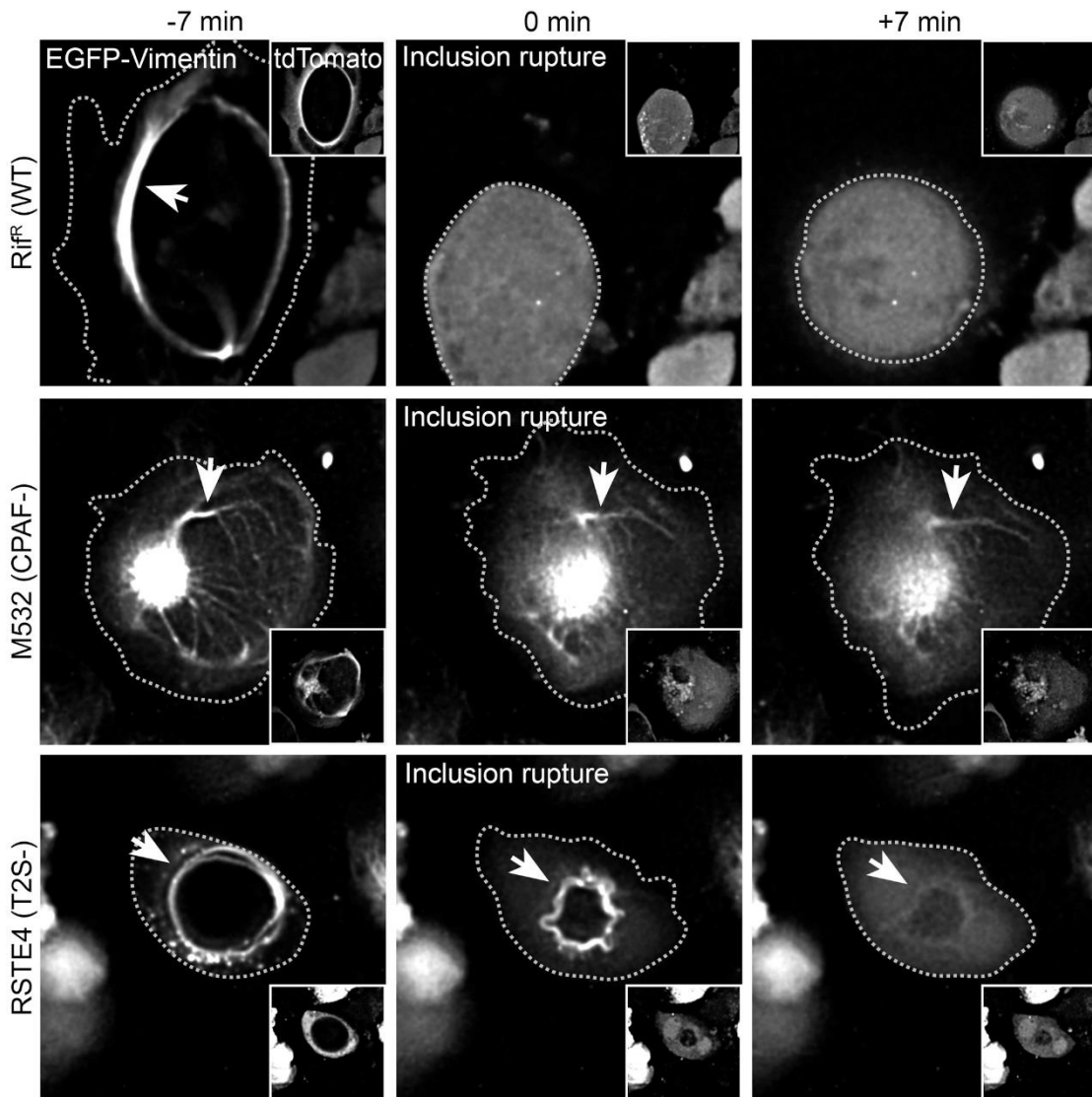


Figure 24. Cleavage of vimentin in live infected cells occurs after inclusion rupture and is dependent on CPAF and T2S. HeLa cells were infected with the indicated strains and transfected with N-terminally EGFP-tagged vimentin and tdTomato vectors and imaged using widefield deconvolution live-cell microscopy every seven minutes after 54 hpi for 14 hours. Inclusion rupture was assessed by the influx of dTomato signal into the inclusion lumen. Images acquired 7 min before and after inclusion rupture are shown. In cells infected with Rif^R (WT) LGV-L2, the filamentous EGFP-vimentin signal became diffuse immediately after inclusion rupture. EGFP-vimentin remained in a filamentous form after loss of inclusion integrity in cells infected with CPAF or T2S-deficient strains (arrows).

3.7 CPAF-dependent processing of LAP1 occurs after inclusion rupture

Based on our observations with vimentin processing in live cells, we predicted that cleavage of the newly-identified *bona fide* CPAF substrate, LAP1 (Snively et al., 2014), would also occur upon loss of inclusion membrane integrity late in infection, where CPAF is released into the host cytosol. I formally tested this prediction by infecting cells that had been co-transfected with tdTomato and EGFP-LAP1 with either RST17 (CPAF⁻) or RST5 (CPAF⁺) *Chlamydia* strains. As previously described (Goodchild and Dauer, 2005), EGFP-LAP1 prominently labeled the nuclear envelope (Figure 25). This localization pattern was not altered in infected cells. Time lapse microscopy of live infected cells revealed that upon loss of inclusion membrane integrity, as assessed by the influx of tdTomato into the inclusion lumen, the localization of EGFP-LAP1 rapidly changed from the nuclear envelope to the cytoplasm, which most likely resulted from the cleavage of the EGFP moiety from the portion of the protein anchored to the nuclear membrane (Figure 25). As with vimentin cleavage, these proteolytic events occurred within cells in which the integrity of the plasma membrane was not compromised and were dependent on CPAF.

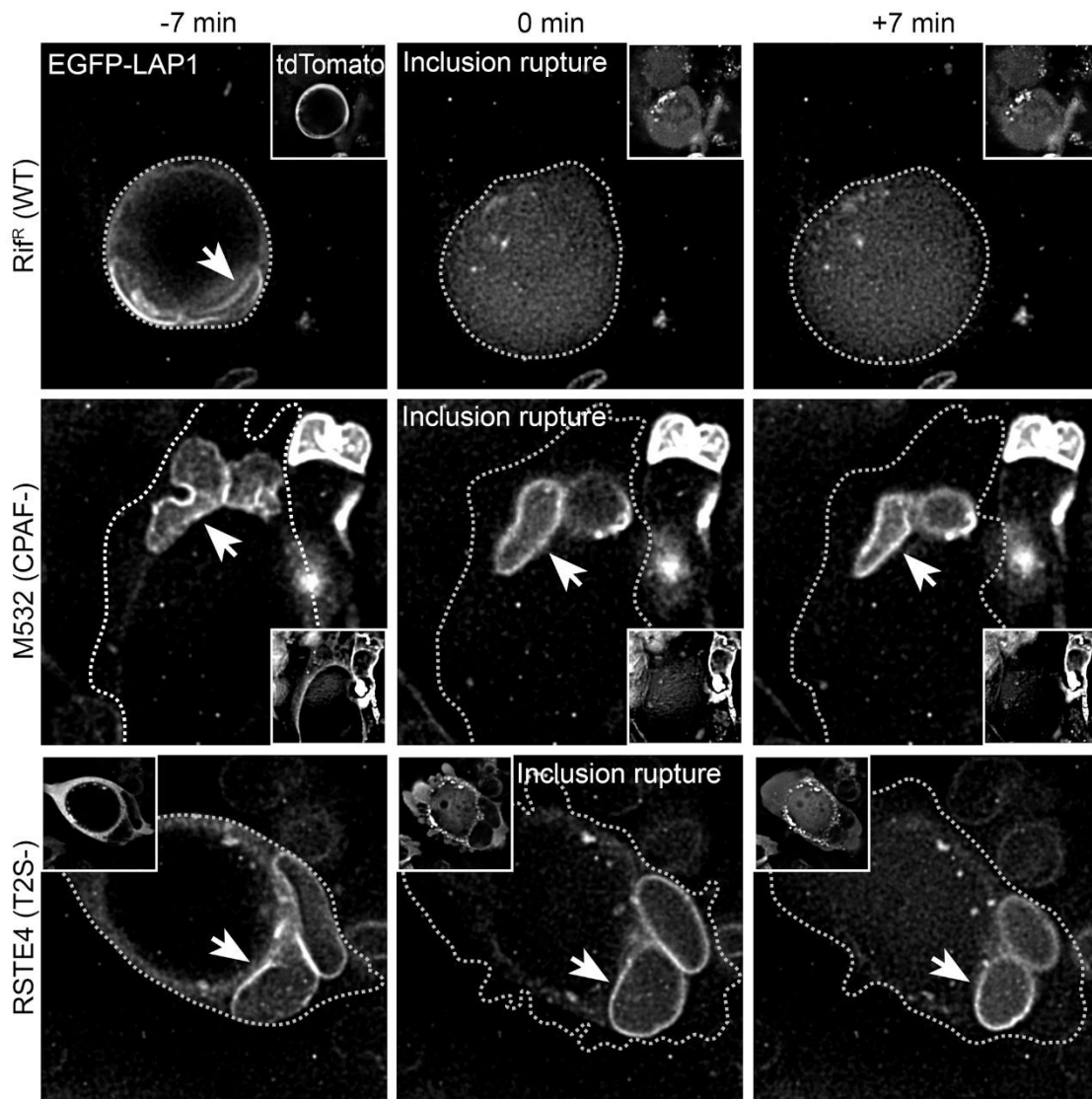


Figure 25. Cleavage of LAP1 in live infected cells occurs after inclusion rupture and is dependent on CPAF and T2S. HeLa cells were infected with the indicated strains and transfected with N-terminally EGFP-tagged LAP1 and tdTomato vectors and imaged using widefield deconvolution live-cell microscopy every seven minutes after 54hpi for 14 hours. Inclusion rupture was assessed by the influx of dTomato signal into the inclusion lumen. Images acquired 7 min before and after inclusion rupture are shown. Loss of EGFP-LAP1 localization to the nuclear membrane (arrows) occurred rapidly following inclusion rupture in cells infected with Rif^R (WT) but not in cells infected with CPAF or T2S-deficient strains.

3.8 Discussion

In the last two years there have been remarkable advances in the development of systems for genetic analysis in *C. trachomatis*. This includes the generation and mapping of chemically generated mutants as well as the stable delivery of recombinant DNA into *C. trachomatis* (A Conrad et al., 2013; Kari et al., 2011; Nguyen and Valdivia, 2012; Wang et al., 2011). We had previously identified and characterized a mutant defective in T2S (Nguyen and Valdivia, 2012), which we now report is also defective for CPAF secretion. In addition, we identified two *C. trachomatis* LGV-L2 strains with nonsense mutations in *cpa*. Equipped with these mutants we can now clarify the role that CPAF plays in the various unique cellular phenotypes that have been attributed to *Chlamydia* infections. Overall, our findings suggest that CPAF is not essential for Golgi fragmentation. However, while CPAF does not appear necessary for this cellular processes to occur, we cannot exclude the possibility that this protease plays an auxiliary role or whether there are redundant factors contributing to these cellular phenotypes.

Tan and colleagues brought to the forefront the issue that the unique challenges of inhibiting CPAF's proteolytic activity post lysis can confound the degree of proteolytic activity that occurs within live infected cells (Chen et al., 2012). Indeed, the level of true CPAF-mediated proteolysis that occurs within infected cells has come into doubt with an understandable impulse to label most proteolytic events observed to date as artifacts (A Conrad et al., 2013). Our findings indicate that it is premature to assume that traditional targets of CPAF are not cleaved during infection. We presented evidence that the bulk of CPAF activity resides within the inclusion lumen and that CPAF rapidly cleaves at least one of its described targets when the inclusion membrane is compromised during late

stages of infection. Our results also indicate that the new CPAF substrate we recently identified, LAP1 (Snaveley et al., 2014), is similarly processed upon loss of inclusion membrane integrity. This could represent a pathogenic strategy to destroy key components in the cytoplasm or subcellular structures (e.g. nuclear envelope for LAP1) prior to bacterial exit from a lysing cell or a transient response to mechanical or immune stress on the integrity of the inclusion. Such a strategy may help degrade or modify factors that constitute danger signals to be sensed by immune cells, or modify physical barriers that limit bacterial dispersal. CPAF mutants display a small (~2.5 fold) decrease in the generation of IFUs (Snaveley et al., 2014), suggesting that CPAF also performs functions important for replication before the late exit stages. These functions could include the processing and turnover of bacterial proteins within the inclusion, as has been suggested for the outer membrane protein OmcB (Hou et al., 2013).

In addition, CPAF released from infected cells may play a prominent role in tissue colonization or dissemination in infected animals. Indeed, experimentally infected animals and human patients develop a strong humoral response to CPAF, and immunization with recombinant CPAF is protective against infections (Murthy et al., 2009, 2011), suggesting that this protein may have extracellular roles in tissue infections. It should also be emphasized that our findings are restricted to the role of CPAF in strain LGV L2. At present we do not know if CPAF plays different roles in urogenital and ocular *C. trachomatis* serovars.

At this stage, there are many unresolved questions as to the function of CPAF, yet these mutant strains offer a distinct advantage to deconstruct the function of CPAF, especially in light of very recent advances in transformation and genetic manipulation of *Chlamydia* (Wang et al., 2011). Work ongoing in our laboratory seeks to address several

issues, prominent among these is what are the cytosolic substrates of CPAF and what are their roles in supporting pathogenesis? Is CPAF activity in the host cytosol regulated? Could there be additional structural motifs that are only present in a subset of 'true' CPAF substrates that are cleaved in the cytoplasm of cells with intact inclusions? In such a scenario, CPAF in the cytoplasm could act to specifically modify host cellular processes and act more broadly once inclusion membrane integrity is compromised and the bulk of active CPAF is released into the cytoplasm. Indeed, a role for chlamydial proteases in the dissolution of the infected host cell late in infection was first reported by Gerald Stokes almost 40 years ago (Stokes, 1973). Preliminary analyses of the sequence specificity of CPAF (D. G. McCafferty, unpublished data) indicates a capacity for this enzyme to conduct endoproteolysis at multiple sites, as well as the participation of CPAF in complexes with other proteases. Therefore, CPAF may exhibit additional interactions with host proteins, mediated by intrinsic substrate specificity or by release into subcellular compartments that may lead to the proteolytic activation of host hydrolases (or removal of inhibitory factors) to promote lytic egress, as has been observed in viral and parasitic infections. Future work with *Chlamydia* expressing modified forms of CPAF should help address some of the outstanding questions remaining as to the function of this unusual protease.

3.9 Materials and Methods

3.9.1 Reagents

Reagents were obtained from the following sources: mouse anti-GM130 (BD Biosciences), rabbit anti-*Chlamydia* MOMP (gift of K. Fields, U. of Kentucky), mouse anti-CT813 (gift of G. Zhong, U. of Texas Health and Science Center), mouse anti-

vimentin (Invitrogen, clone V6630), rabbit anti-GAPDH (Abcam), mouse anti-EGFP monoclonal antibody (Clontech), rabbit anti-RpoB/C (gift of M. Tan, UC Irvine), rabbit anti-CPAF (27), Alexa Fluor 555-conjugated anti-mouse, Alexa Fluor 488-conjugated anti-rabbit, Hoescht 33258 (Invitrogen), FluorSave Reagent (Calbiochem), Cyclohexamide (Sigma-Aldrich), Rifampicin (Sigma-Aldrich), Trimethoprim (Sigma-Aldrich), Slow Fade Gold Antifade Reagent (Invitrogen), JetPrime (Polyplus transfection). Enhanced green fluorescent protein (EGFP)-tagged rat vimentin was provided by Ronald Liem (Columbia University, NY), and tandem dimer Tomato (tdTomato) was provided by Marc Caron (Duke University, NC). Full-length lamin-associated protein 1 (LAP1) was PCR-amplified from MGC Human sequence-verified cDNA clone 3458117 (Thermo Fisher) and inserted into pLEGFP-C1 (Clontech) downstream of EGFP to express an EGFP-LAP1 fusion protein.

3.9.2 Cell Culture and *Chlamydia* Infections

HeLa cells (CCL-2: ATCC) and Vero cells (CCL-81: ATCC) were maintained in DMEM HG supplemented with 10% FBS (CellGro Mediatech). *C. trachomatis* LGV-L2 434/Bu and *C. trachomatis* mutant strains were propagated by infecting HeLa cells with elementary bodies (EBs) that had been stored in sucrose-phosphate-glutamate (SPG) buffer (0.25 M sucrose, 10 mM sodium phosphate, 5 mM L-glutamic acid, pH 7.0) and purified on Omnipaque (GE Healthcare) density gradients (Saka et al., 2011). EBs were added to HeLa cells at the indicated multiplicities of infection (MOIs), and infections were synchronized by centrifugation at 2500 × *g* for 30 min at 10°C. Rifampin, spectinomycin, and trimethoprim resistant *C. trachomatis* LGV-L2 variants were generated as previously described (Nguyen and Valdivia, 2013). The mutations leading to antibiotic resistance in these strains were determined by whole genome sequencing: H471Y

in *CTL0567* (*rpoB*), G1197 in *CTL_r01/CTL_r02* (16S rRNA copies 1 and 2), and G408R in *CTL0369* lead to Rif^R, Spc^R, and Tmp^R, respectively.

3.9.3 Identification and whole genome sequencing of CPAF-deficient LGV-L2 strains

Identification of cpa mutant: LGV-L2 strains containing the null alleles *C127T* (Q43*) and *G882A* (W294*) in *cpa* (*CTL0233*) were initially identified by whole genome sequencing of pools of chemically-mutagenized and plaque-purified *C. trachomatis* LVG-L2 434/Bu strains (Kokes et al., 2015). Strain CTL2-M532 harboring the *cpaC127T* allele and strain CTL2-M169 harboring the *cpaG882A* allele were identified from among two independent pools of mutants and the mutations in the *cpa* locus (*CTL0233*) were confirmed by Sanger sequencing.

Whole genome sequencing: Strains were harvested from infected Vero cells grown in a 6-well cell culture plate by hypotonic lysis of host cells with 800 μ l of dH₂O per well (for 20 minutes) followed by addition of 200 μ l of 5X SPG buffer. Lysates were sonicated (2 x 10 seconds in ice water) and bacterial cells spun down at 14,000 rpm, for 15 minutes at 4 °C. Bacterial pellets were pooled and resuspended in 1X DNase I buffer (New England Biolabs, Ipswich, MA, USA). Depletion of host DNA was achieved by treating cell suspensions with 4 units of DNase I (New England Biolabs) for 1 hour at 37 °C. Bacterial pellets were washed with PBS buffer and total DNA isolated with a DNA isolation kit (DNeasy tissue and blood kit, Qiagen) following the manufacturer's instructions. M169 (1 μ g) and M532 enriched DNA (1 μ g) were each sheared with an Adaptive Focused Acoustics S220 instrument (Covaris). DNA sequencing libraries were prepared with a library construction kit (TruSeq DNA Sample Preparation Kit v2, Illumina, Inc. San Diego, CA, USA) according to the manufacturer's instructions.

Libraries were sequenced in a MiSeq DNA Sequencing Platform (Illumina) at the Duke University IGSP DNA Sequencing Core facility. Genome assembly and single nucleotide variant (SNV) identification was performed with Geneious Software version 6 (Biomatters - <http://www.geneious.com>). The *C. trachomatis* LGV L2 434/Bu genome (GenBank no. NC_010287) was used as reference sequence. All non-synonymous single nucleotide variants (SNVs) identified in M169 and M532 (Table 1 and Table S1) were verified by Sanger dideoxy DNA sequencing.

3.9.4 Western blot analyses

HeLa cells were grown in 6-well plates to confluency and infected with the *C. trachomatis* LGV-L2 Rif^R parent or its derived mutant strains at an MOI of 1. At the indicated hours post infection, cells were washed with 1X PBS (Invitrogen), lysed with 1% SDS buffer (1% SDS, 150 mM NaCl, 50 mM Tris-HCl pH 7.5), heated in boiling water bath immediately before addition to cells. Lysates were incubated at 65 °C for 10 minutes to solubilize and denature proteins and sonicated 2x10 seconds to shear DNA. Protein concentrations were determined by the DC protein assay (Bio-Rad). Equal amounts of lysate were loaded into SDS-PAGE 4-15% gradient gels (Bio-Rad), transferred to 0.45 µM nitrocellulose membranes using a Trans-Blot SD Semi-Dry Electrophoretic Transfer Cell (Bio-Rad), blocked in Odyssey blocking buffer (LI-COR) and incubated in primary antibodies diluted in Odyssey blocking buffer, followed by incubation with goat anti-rabbit IRDye 680LT (LI-COR) or goat anti-mouse IRDye 800CW (LI-COR). Membranes were imaged with the LI-COR Odyssey infrared imaging system.

3.9.5 *In Vitro* CPAF cleavage assays

HeLa cells grown in 6-well plates were mock-infected or infected with the *C. trachomatis* LGV-L2 Rif^R strain or with the indicated mutant strains at an MOI of 1. At 40 hours post infection (hpi) crude protein extracts were prepared by lysing infected cells in RIPA buffer (50 mM Tris pH 7.5, 150 mM NaCl, 0.1% SDS, 0.5% sodium deoxycholate, 1% NP-40) supplemented with a protease inhibitor cocktail (Roche). Purified recombinant CPAF (40 µg) (Bednar et al., 2011; Jorgensen et al., 2011) or crude protein extracts were prepared as described above and incubated with 20 µg recombinant GST-CT695 for 1hr at 37 °C, and cleavage was assessed by colloidal blue Commassie Blue staining (Invitrogen). Figures were compiled and intensities adjusted for display using Photoshop CS6.

To test the effectiveness of 1% SDS buffer in preventing post-lysis degradation by CPAF, the activity of recombinant CPAF in this denaturing buffer was assessed. Crude protein extracts were prepared from non-infected HeLa cells by rinsing monolayers with PBS, adding 1% SDS buffer pre-warmed to 100 °C, transferring to a microfuge tube, heating at 65 °C for 10 minutes, and then clarifying the lysate by centrifugation (10,000 x *g*, 15 minutes, room temperature). For the *in vitro* cleavage assays, 200 µg of total HeLa protein extract with or without 100 µM of a CPAF-inhibitory peptide (Bednar et al., 2011; Jorgensen et al., 2011) was mixed with 0.5, 2.5, or 5 µg recombinant CPAF in a final volume of 100 µl. The reactions were assembled at room temperature, incubated at 37 °C for 20 minutes, and then inactivated with SDS-PAGE sample buffer and incubation at 65 °C for 10 minutes. As a positive control, reactions were also performed under non-denaturing conditions. Crude protein extracts were generated from non-infected HeLa cells by rinsing monolayers with PBS, adding ice-cold

TNEX buffer (20 mM Tris-HCl, pH 8.0, 150 mM NaCl, 2 mM EDTA, 1% Triton X-100, complete protease inhibitor cocktail (Roche)), incubating at 4°C for 10 minutes, transferring lysates to a microfuge tube, and then clarifying the lysate by centrifugation (10,000 x g, 15 minutes, 4 °C). Reactions were assembled on ice, incubated at 37 °C for 20 minutes, and subsequently processed as described for the reactions in 1% SDS buffer. CPAF activity was determined by monitoring vimentin cleavage via western blot analysis.

In vitro cleavage assays were used to demonstrate that CPAF cleaves EGFP-LAP1. HeLa cells transfected with the EGFP-LAP1 construct were harvested in TNEX buffer, and crude protein extracts were generated as described above. For the reactions, 100 µg of transfected or non-transfected extract was incubated with either recombinant CPAF or TNEX protein extracts prepared from mock-infected or LGV-L2 -infected (44 hours post-infection) HeLa cells. The reactions were assembled on ice, incubated at 37 °C for 30 minutes, and then inactivated with SDS-PAGE sample buffer and incubation at 65 °C for 10 minutes. Cleavage was assessed by western blot analysis with mouse anti-EGFP) and rabbit anti-LAP1 antibodies.

3.9.6 Immunofluorescence

For routine indirect immunofluorescence, HeLa cells were grown on glass coverslips and infected at the indicated MOIs. Cells were fixed with 3% formaldehyde/0.025% glutaraldehyde or 4% paraformaldehyde or methanol in phosphate-buffered saline (PBS) for 20 minutes and permeabilized with 0.1-0.2% Triton X-100 for 10 minutes. After blocking with 5% bovine serum albumin (BSA) in PBS for 20 minutes, cells were stained with specific antibodies followed by Alexa-conjugated

secondary antibodies at room temperature at 20 minutes. Host and bacterial DNA were stained with 1 μ g/mL Hoechst. Coverslips were mounted with FluorSave, or Slow Fade.

3.9.7 Golgi Fragmentation Analysis

HeLa cells were seeded onto coverslips to visualize the Golgi apparatus in Rif^R or M532 (CPAF-) infected cells. A set of infected cells were treated with Z-WEHD-fmk (75 μ M, Enzo Life Sciences) for 9h after infection as a positive control for blocking Golgi fragmentation. At 24h after infection, cells were fixed with 4% paraformaldehyde for 20 minutes at room temperature, permeabilized, and blocked with BSA-PBS. Bacteria, the Golgi apparatus, and DNA were detected by incubating cells with mouse anti-GM130 antibodies and rabbit anti-*Chlamydia* MOMP for 20 minutes followed by incubation with fluorescently conjugated secondary antibodies and Hoescht for 20 minutes at room temperature. Cells were mounted with FluorSave and allowed to cure at room temperature overnight before imaging. Images were acquired with a Zeiss 780 scanning confocal microscope with the same settings for each sample with a 100x objective and processed using ImageJ. Confocal images of specific samples were used to quantify Golgi fragmentation. The number and area of Golgi elements in 18 cells at minimum per condition were counted after applying a threshold calculated with the Otsu algorithm for each image and using the Analyse Particles function in ImageJ software excluding particles smaller than 0.1 μ m. Three independent experiments were performed and imaged to analyze fragmentation. Figures were compiled and intensities adjusted for display using Adobe Photoshop CS6.

3.9.8 Detergent Extraction Assays

For immunofluorescence assays after detergent extraction, HeLa cells were seeded in 96-well plates, with three biological replicates per condition (+Triton X-100 and -Triton X-100), and infected at an MOI of 1 with the indicated strains. At 44 hpi, 52 hpi, or 60 hpi cells in the untreated condition were washed twice with ice cold PBS and fixed with 3% formaldehyde/0.025% glutaraldehyde at room temperature for 20 minutes prior to permeabilization and blocking with BSA-PBS. For live cell samples extracted with Triton X-100, infected cells were first washed twice with ice cold PBS before incubation with pre-chilled 0.5% Triton X-100 in PBS supplemented with 100 μ M anti-CPAF peptide (Bednar et al., 2011; Jorgensen et al., 2011) on ice for 5 minutes. Cells were then fixed, blocked with BSA-PBS and immunostained with mouse monoclonal anti-vimentin antibodies, followed by fluorophore conjugated secondary anti-mouse antibodies. Samples were mounted with Slow Fade Gold Antifade reagent and images from at least 5 fields for each replicate were acquired with a Zeiss Axioskop 2 upright epifluorescence microscope using Axiovision v3.0 software. The number of infected cells with altered vimentin staining was calculated for each replicate in 0.5% Triton X-100 treated and untreated samples. The average percentage of infected cells with altered vimentin (6-8% of total cells) staining in the untreated samples was subtracted from the treated control for each replicate. Figures were compiled and intensities adjusted for display using Photoshop CS6. Two-way ANOVA with Bonferroni's *post hoc* test was performed using GraphPad Prism for Windows, GraphPad Software, San Diego California USA.

3.9.9 EGFP-Vimentin and LAP1-EGFP transfection and live cell microscopy

Cells were seeded onto #1.5 glass-bottom plates, infected with Rif^R L2 434/Bu, M532 (CPAF⁻), M169 (CPAF⁻), RSTE4 (TS2⁻) strains, and co-transfected with either EGFP-Vimentin or EGFP-LAP1 and tdTomato using the lipid-based JetPrime reagent 4h after infection. Cells were imaged every seven minutes from 54-76hpi after infection at 37°C under 5% CO₂ using a motorized Zeiss Axio Observer Z1 widefield fluorescence microscope equipped with a 40x air objective. Fifteen stage positions at minimum were recorded with 6-23 instances of inclusion rupture in transfected cells observed for each condition. Only cells expressing moderate levels of the fluorescent reporters were included in the analysis. Images were viewed with Metamorph to manually assess inclusion rupture by tdTomato diffusion into the inclusion lumen and the structured or diffuse nature of the EGFP signal. Images were deconvolved using Huygens Essential, and processed with ImageJ and Photoshop for presentation.

4. The rising tide - Impacts of recent genetic tools on our understanding of *Chlamydia* infections and outlook

Chlamydia is an obligate intracellular pathogen that resides within a membrane-bound vacuole in the cytoplasm termed an inclusion (Moulder, 1991). As such all aspects of *Chlamydia* survival are intimately linked to the cell biology of its host. It is not surprising that a vast array of modifications to host cellular pathways and internal organization have been described to occur during infection (Chapter 1 and Figure 2). *Chlamydia* has evolved an intricate arsenal of effector proteins with which to manipulate the host cell. However, our inference of how these effectors affect the cell biology of the host, which has been based on correlative evidence, including biochemical and gain-of-function approaches, may not tell the whole story. This leads to important questions of how individual effectors contribute to the many documented alterations in the host and how these changes influence pathogenesis. Definitive answers to these questions require loss-of-function approaches.

In the last few years there have been landmark advances in the development of systems for genetic analysis in *C. trachomatis*. This includes the stable delivery of recombinant DNA into *C. trachomatis* (Wang et al., 2011), targeted insertional mutagenesis with Type II Introns (Johnson and Fisher, 2013), and the generation and mapping of chemically generated mutants (Kari et al., 2011; Nguyen and Valdivia, 2013). With these advances in mind, we developed a resource for forward and reverse genetic analysis in *C. trachomatis* by generating and sequencing a collection of 934 chemically mutagenized strains (Kokes et al., 2015). By characterizing strains identified with loss-of-function mutations in the secreted effector CPAF, we used this resource in reverse genetic approaches, leading us to re-evaluate the role of CPAF during infection (Chapter

3). This resource is also an ideal platform for forward genetic approaches to reveal bacterial effectors causally linked to *Chlamydia* manipulation of host cell biology. We performed a screen for mutants impaired in F-actin assembly at the inclusion and identified InaC, an inclusion membrane protein that mediates F-actin reorganization, ARF and 14-3-3 recruitment, and Golgi redistribution (Chapter 4).

The revolutionary effect that powerful genetic tools are likely to have on our understanding of *Chlamydia* infections is well exemplified in the case of CPAF. Largely through biochemical approaches, CPAF was associated with many changes during infection, ranging from inhibition of apoptosis and altering immune responses to more architectural changes such as cytoskeletal and Golgi rearrangements around the inclusion. However, through characterizing CPAF loss-of-function strains, we found that CPAF is not required for Golgi fragmentation, activation of NFκB, and resistance to apoptosis and reinfection (Snavelly et al., 2014), but found rather that CPAF may act on its biochemically-characterized targets at late stages of infection after the inclusion membrane has ruptured (Chapter 4). In the context of an *in vivo* infection, this could facilitate bacterial dispersion from the site of inclusion rupture by dismantling surrounding cytoskeletal structures through vimentin or even LAP1 cleavage. Furthermore, CPAF could act extracellularly to modulate immune responses, which is supported by the recent finding that CPAF can cleave and deactivate certain anti-microbial peptides (Tang et al., 2015) and that a strong humoral response to CPAF found in human patients (Murthy et al., 2009). In addition to directly interfacing with host proteins, CPAF could indirectly alter host cell biology through modification of other chlamydial effectors. Recent findings that the catalytic triad of CPAF is not required for its activity in cells (Yang et al., 2015) could be explained by the presence of a bacterial

co-factor. Since our work characterizing loss-of-function CPAF strains was published, other groups have used these strains to show that CPAF is required for centrosome amplification and mitotic control, which lead to multinucleation during *C. trachomatis* infection (Brown et al., 2014), although it remains unclear if this occurs by direct or indirect CPAF action on host pathways.

The types of novel mechanistic insights that powerful genetic tools are likely to have on our understanding of the cell biology of *Chlamydia* infections is well exemplified in the case of InaC. InaC is a previously under-characterized effector that localizes to the inclusion membrane. Through a microscopy-based screen and a combination of genetics, biochemistry, and cellular characterization, we find that InaC recruits host ARF and 14-3-3 proteins and is required for F-actin assembly and redistribution of select organelles around the inclusion, including the Golgi apparatus. While cellular F-actin is important for maintaining inclusion membrane integrity, InaC is not and is furthermore dispensable for cell autonomous IFN responses to *C. trachomatis* infection. Through its cleavage of intermediate filaments surrounding the inclusion, CPAF was considered to be required for inclusion integrity (Jorgensen et al., 2011), however, inclusion membranes appear intact in the absence of CPAF. Indeed, cytoskeletal assembly at the inclusion appears to function more to dynamically redistribute organelles than to play a membrane-supportive role. However, the significance of these organellar redistributions remains unclear and would be a fruitful avenue of future investigations. While Golgi redistribution was previously proposed to facilitate lipid trafficking to the inclusion, sphingolipids traffic to the inclusion via Golgi-dependent and independent pathways at wild-type efficiency in the absence of InaC. Either through Golgi repositioning or F-actin redistribution, InaC could mediate defects in front-end polarity and directional migration

observed in *C. trachomatis*-infected cells (Heymann et al., 2013; Kumar and Valdivia, 2008b), which could affect the success of *in vivo* infections. Lastly, the primary site of infection for *C. trachomatis* genital infections is of columnar epithelial cells in the endocervix. *Chlamydia*-mediated alterations to the specialized cell biology of polarized cells is understudied and likely under-appreciated. For example, *Chlamydia* preferentially intercepts basolaterally-targeted sphingolipids. Polarized cells have distinct apical and basolateral domains, and their subcellular architecture and cytoskeletal and organellar distribution can differ dramatically from unpolarized cells. The functional impact of InaC-mediated changes to subcellular architecture may be more apparent and specific to polarized cell biology.

In closing, the work presented here is an early example of the types of revelations we are likely to see with the implementation of recent genetic tools in *Chlamydia*. From the perspective of cell biology, *Chlamydia* is a fascinating pathogen, yet it has remained historically understudied due to a lack of tools and difficulties inherent to studying obligate intracellular pathogens. I have witnessed remarkable advances in the last several years and look forward to future discoveries and anticipate an exciting expansion of the field of cell biology of *Chlamydia* infections.

5. Appendix I. Differential translocation of host cellular materials into the *Chlamydia trachomatis* inclusion lumen during chemical fixation¹

Chlamydia trachomatis manipulates host cellular pathways to ensure its proliferation and survival. Translocation of host materials into the pathogenic vacuole (termed 'inclusion') may facilitate nutrient acquisition and various organelles have been observed within the inclusion, including lipid droplets, peroxisomes, multivesicular body components, and membranes of the endoplasmic reticulum (ER). However, few of these processes have been documented in living cells. Here, we survey the localization of a broad panel of subcellular elements and find ER, mitochondria, and inclusion membranes within the inclusion lumen of fixed cells. However, we see little evidence of intraluminal localization of these organelles in live inclusions. Using time-lapse video microscopy we document ER marker translocation into the inclusion lumen during chemical fixation. These intra-inclusion ER elements resist a variety of post-fixation manipulations and are detectable via immunofluorescence microscopy. We speculate that the localization of a subset of organelles may be exaggerated during fixation and their detection within the inclusion of fixed cells does not accurately reflect localization prior to manipulation. Finally, we find similar structures within the pathogenic vacuole of *Coxiella burnetii* infected cells, suggesting that fixation-induced translocation of cellular materials may occur into the vacuole of a range of intracellular pathogens.

¹ Chapter 5 has been submitted as a manuscript to PLoS ONE and is under review (with the addition of supplemental figures and videos), and reprint here is permitted under PLoS policy.

5.1 Introduction

Chlamydia trachomatis is a human pathogen of global significance – it is the most common sexually-transmitted bacterial pathogen and the leading cause of preventable blindness worldwide (Schachter J, 1999). During infection of mammalian cells, bacteria remain sequestered within a membrane-bound compartment termed an inclusion. The inclusion is fundamental to the intracellular lifestyle of *C. trachomatis* as it represents a first line of defense against immune surveillance and anti-microbial effectors (Kumar and Valdivia, 2009). In addition, as an obligate intracellular pathogen, *C. trachomatis* requires vital nutrients obtained from its infected host cell (reviewed in (Saka and Valdivia, 2010)) and interactions between the inclusion and host cellular components play an important role in this process (reviewed in (Kokes M and Valdivia RH, 2012)).

Many subcellular organelles reside in close proximity to the inclusion, some of which have been reported to interact intimately with inclusions (reviewed in (Kokes M and Valdivia RH, 2012)). In a well-characterized example, endoplasmic reticulum (ER) tubules closely appose to *C. trachomatis* inclusion membranes (Giles and Wyrick, 2008; Peterson and de la Maza, 1988) to form membrane contact sites that facilitate the transfer of lipids directly between the ER and the pathogenic vacuole (Derré et al., 2011; Elwell et al., 2011). The Golgi apparatus fragments into mini-stacks (Heuer et al., 2009) in an actin and bacterial effector-dependent manner (Kokes et al., 2015) which closely surround the inclusion (Hackstadt et al., 1995, 1996). Lipid droplets are recruited to the inclusion periphery (Kumar et al., 2006) and can translocate into the inclusion lumen (Cocchiaro et al., 2008) while lysosomes closely surround the inclusion to presumably enhance the ability of bacteria to acquire amino acids from degraded proteins (Ouellette

et al., 2011). Multivesicular bodies (MVBs) are enriched at the inclusion periphery and inhibition of MVB biogenesis can disrupt *C. trachomatis* lipid uptake (Beatty, 2006, 2008). Recycling endosomes closely associate with the inclusion (van Ooij et al., 1997; Scidmore et al., 1996b; Taraska et al., 1996) but are thought to interact with the inclusion in a fusion-inhibited state (Scidmore et al., 1996b, 2003). Mitochondria localize around the inclusion of some *Chlamydia* species (Matsumoto et al., 1991; Peterson and de la Maza, 1988), and mitochondrial protein import is important for replication of *C. caviae* (Derré et al., 2007).

In several instances, it has been suggested that interactions with the inclusion may extend beyond recruitment to the periphery and entire organelles translocate into the inclusion lumen. However, many of these observations were made in cells that have undergone chemical fixation. Briefly, sphingolipids (Hackstadt et al., 1995), cholesterol (Carabeo et al., 2003), intact lipid droplets (Cocchiario et al., 2008), and an ER marker (Dumoux et al., 2012) have been reported within the inclusion of living cells. Components of the ER (Dumoux et al., 2012; Majeed et al., 1999), MVBs (Beatty, 2006), and peroxisomes (Boncompain et al., 2014), have been observed within fixed inclusions, as well as Rab14 (Capmany and Damiani, 2010), apoA-1 and phosphatidylcholine (Cox et al., 2012) and proteins that interact with acyl-CoA or each other including ASCL3, ACBD6, and ZNF23 (Soupene et al., 2012). Additionally, some subcellular components and markers such as MVBs (Ouellette and Carabeo, 2010) or phosphatidylcholine (Hackstadt et al., 1996) have been only observed within inclusions of fixed cells and not in living cells.

In this study, we sought to characterize organelle interactions with the inclusion by systematically surveying organelle markers for localization within infected cells. We

found a subset of the many inclusion-proximal subcellular elements within inclusions, including components of the ER, mitochondria, and markers of the inclusion membrane. However, we found no obvious accumulation of ER within live inclusions. We document the striking translocation of ER markers into the inclusion lumen during the process of chemical fixation. These internalized structures persisted through the process of sample processing for indirect immunofluorescence, indicating that the localization of a subset of organelles to the inclusion may be exaggerated by the fixation process rather than accurately reflect organelle localization prior to manipulation. Finally, we observed similar structures within the pathogenic vacuole of *Coxiella burnettii*-infected cells, suggesting that fixation-induced translocation of subcellular elements may constitute a more widespread phenomenon in the study of intracellular pathogens within large vacuoles.

5.2 A subset of inclusion-proximal subcellular organelles localize to the lumen of inclusions

We surveyed interactions between host organelles and mid-to-late cycle inclusions by expressing a panel of fluorescent protein-tagged markers of various subcellular organelles in cells infected for 30 hr (Figure 26A). We fixed cells and quantified the frequency of cells with fluorescent material in the inclusion lumen (Figure 26B). To enhance our ability to accurately define the inclusion edge in three dimensions without interference from light above and below each plane of focus, we used confocal rather than widefield microscopy. Furthermore, since most markers had much lower intensity within the inclusion compared to cellular structures, we used spinning disk rather than laser scanning confocal microscopy for increased sensitivity and to reduce photobleaching while imaging cells in three dimensions.

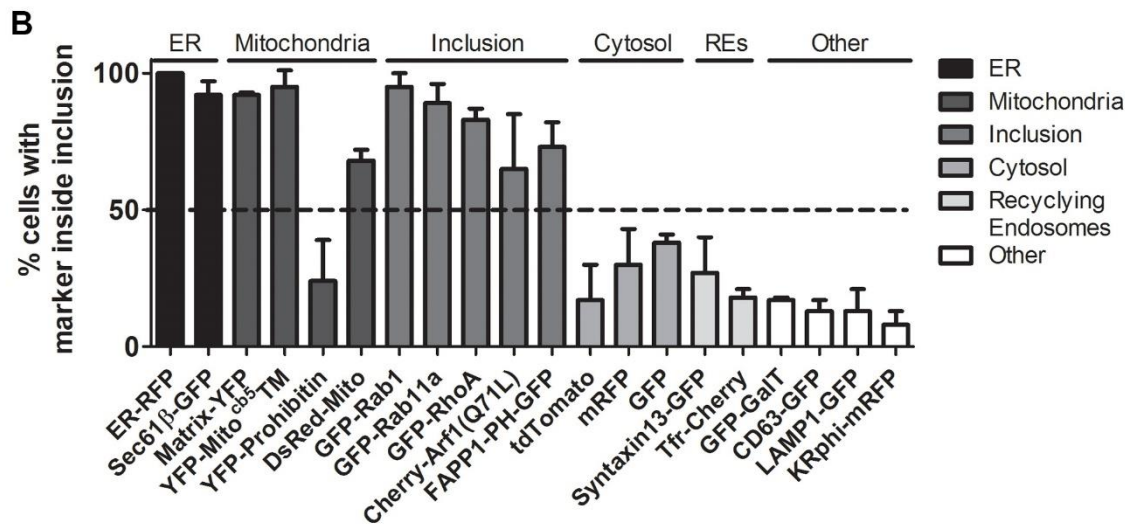
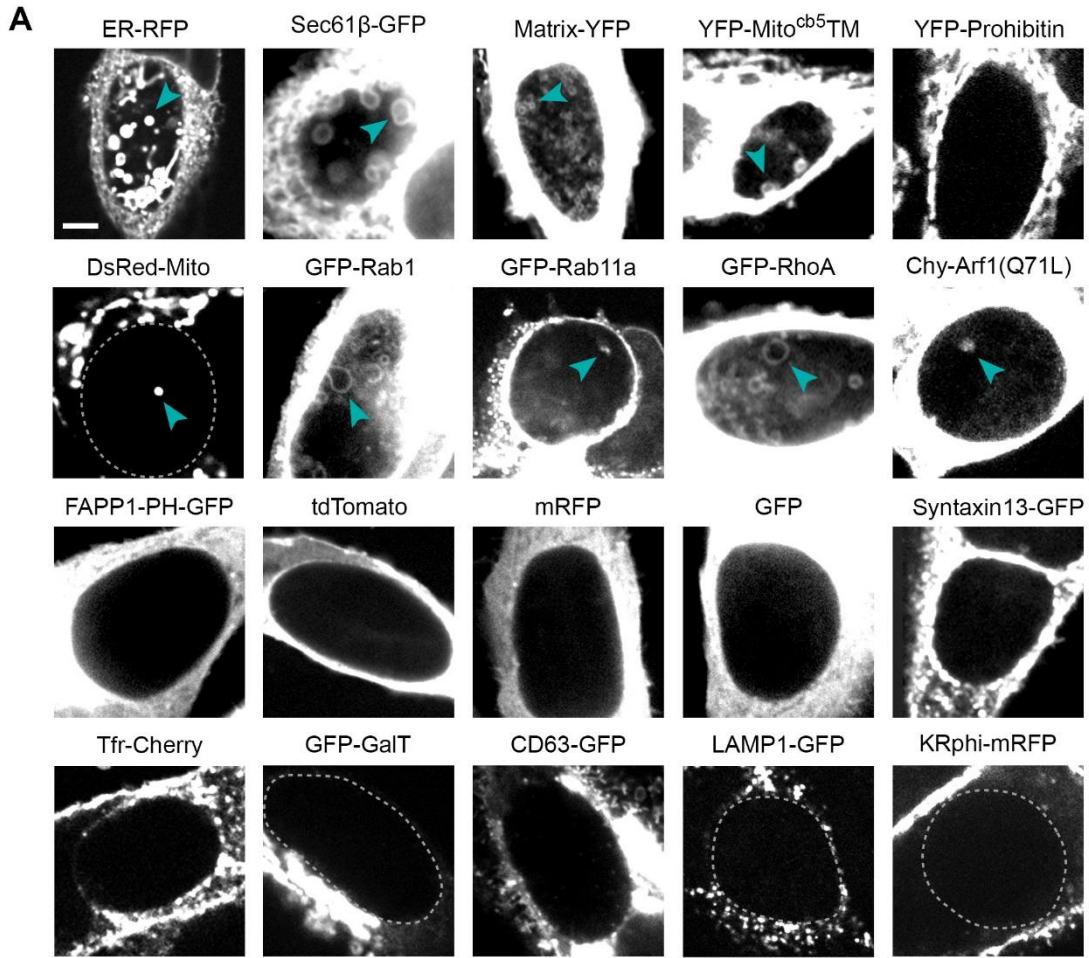


Figure 26. Mitochondria, ER, and inclusion membranes are found within the lumen of *C. trachomatis* inclusions. HeLa cells were infected with *C. trachomatis* LGV L2, transfected with the indicated plasmids, and fixed at 30 hpi for serial spinning disk laser confocal analysis. Note the presence of markers of the ER, mitochondrial matrix and outer membranes, and inclusion membranes within the inclusion lumen (A, cyan arrowheads). Images portray a single z-section from the center of an inclusion, and inclusions are visually identified as large black centered ovals or with a dashed line. Cellular-localized markers appear saturated because material within the inclusion was often significantly dimmer. (B) The frequency of internalized structures within the entire 3D space of each inclusion was assessed. Plasmids are categorized as markers of the ER, mitochondria, inclusion, cytosol, recycling endosomes, or other as indicated. Within the other category, GFP-GalT localizes to the Golgi, CD63-GFP to MVBs, LAMP1-GFP to lysosomes, and KRphi-mRFP to the plasma membrane. A dashed line at 50% distinguishes between high and low frequencies of intraluminal structures within inclusions. 12-20 inclusions were assessed in each experiment, and the mean \pm SEM for three independent experiments is shown. Scale bar represents 5 μ m.

Of all intracellular compartments tested, we found markers of the ER lumen and membrane, mitochondrial matrix and outer membrane (Hailey et al., 2010), and proteins which, in addition to differentially localizing to a range of subcellular compartments, also associate with the inclusion (FAPP1-PH-GFP is a marker of phosphatidylinositol 4-phosphates (Balla et al., 2005) which are enriched on the inclusion (Moorhead et al., 2010)) (Kumar and Valdivia, 2008a; Rzomp et al., 2003) within a significant proportion (over 50%) of inclusions (Figure 26B) appearing as bleb-like structures (Figure 26A, arrowheads). Notably, we found markers of the cytosol and other inclusion-proximal subcellular organelles including recycling endosomes, MVBs, the Golgi apparatus, and lysosomes (Beatty, 2006; Hackstadt et al., 1996; Heuer et al., 2009; van Ooij et al., 1997; Ouellette and Carabeo, 2010; Scidmore et al., 2003) also as bleb-like structures within only approximately one-quarter of inclusions, but did not observe a marker of the more distal plasma membrane (Yeung et al., 2006) within inclusions. These findings reveal a selectivity to which inclusion-proximal subcellular elements are found within inclusions themselves in fixed cells.

5.3 ER components appear as large structures inside the inclusion of fixed but not living cells

The markers we routinely observed within the lumen of inclusions, such as ER-RFP and Sec61 β -GFP, typically formed an expansive network of large blebs and tubules within much of the three-dimensional space of the inclusion lumen (Figure 27, A and B). However, we were unable to detect these structures within living infected cells (Figure 27, A and B, bottom panel) despite extensive imaging. In some instances, the ER initially appeared to be within the inclusion as previously reported (Dumoux et al., 2012), but when compiled and viewed in 3D, the ER was invariably in the host cell cytosol above or below the inclusion and failed to localize within the lumen.

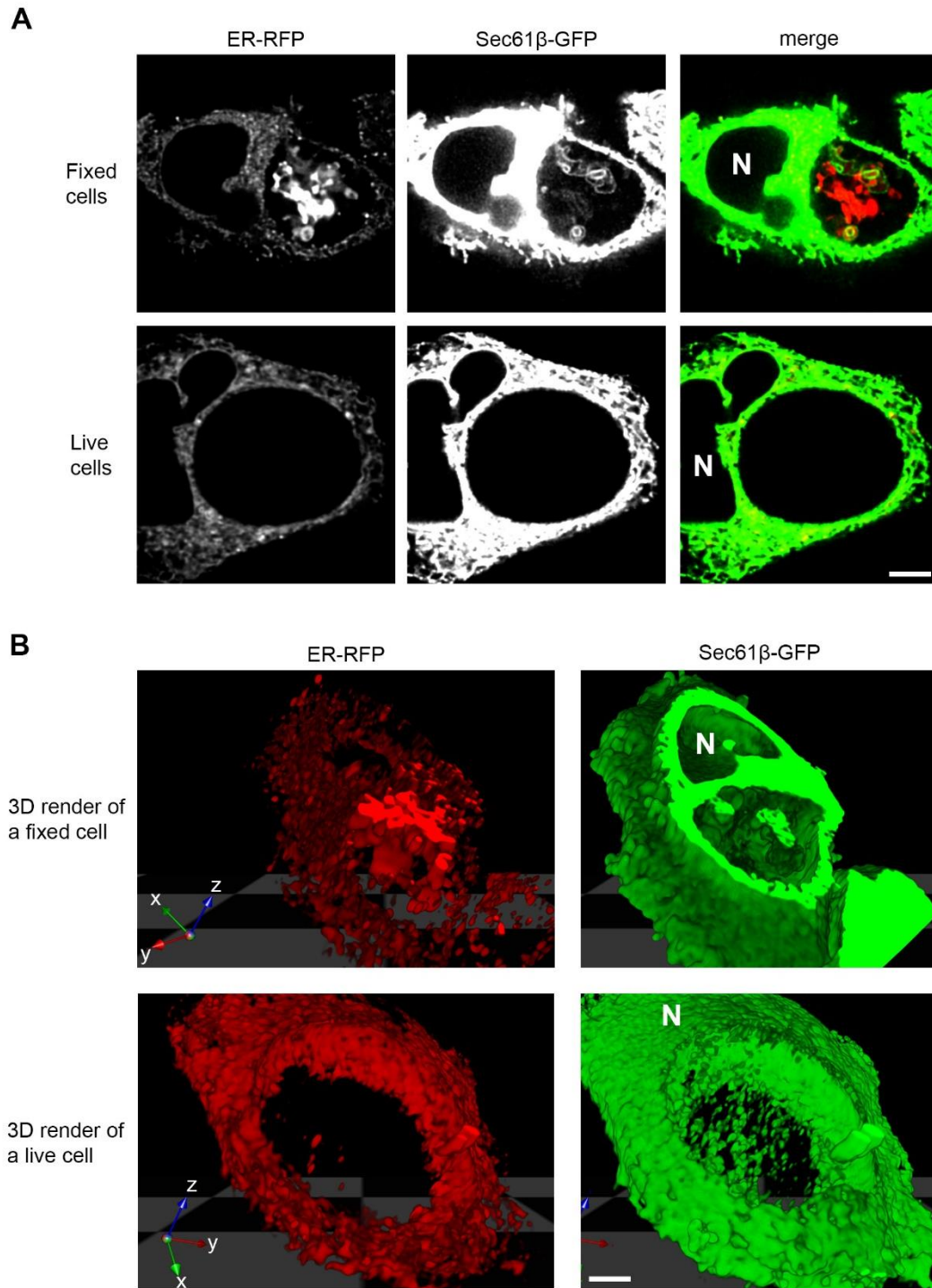


Figure 27. ER markers reveal expansive structures within the inclusion lumen of fixed but not living cells. HeLa cells were infected with *C. trachomatis* LGV L2, co-transfected with ER-RFP (red) and Sec61 β -GFP (green) and at 30 hpi were either fixed

or imaged in three dimensions while living. Images were acquired with a laser scanning confocal microscope. (A) A single xy micrograph towards the center of a cell. (B) Images were used to render volumes in 3D. 3D render of a fixed cell is limited in the z-axis to allow viewing within the inclusion. Note the presence of an expansive network of material within the inclusion lumen of fixed cells but absent within a living inclusion. N marks the nucleus. Scale bars represent 5 μm .

5.4 Chemical fixation induces ER internalization into the inclusion lumen

Because of the drastic differences in ER localization patterns between living and fixed cells, we considered the possibility that the process of fixation exaggerates the degree of translocation of this organelle into the inclusion lumen. To test this, we used laser scanning confocal microscopy on living infected cells to monitor changes to ER-RFP localization during paraformaldehyde fixation (Figure 28). Within minutes of the addition of fixative, we observed the formation of blebs of ER-RFP material expanding into the inclusion lumen. These blebs appeared at random sites along the inclusion periphery and enlarged over time as new sites of inward blebbing (Figure 28, arrowheads) emerged. Many blebs remained attached to the inclusion edge but some appeared to detach into the center of the inclusion. By ten minutes, most new ER blebbing and expansion had stopped and existing structures varied in fluorescence intensity. We also noted the formation of a few smaller and less distinct bleb-like aggregates of ER-RFP in other areas of the cell, mostly at cell edges. These findings demonstrate that chemical fixation can induce a dramatic translocation of ER material into the inclusion lumen.

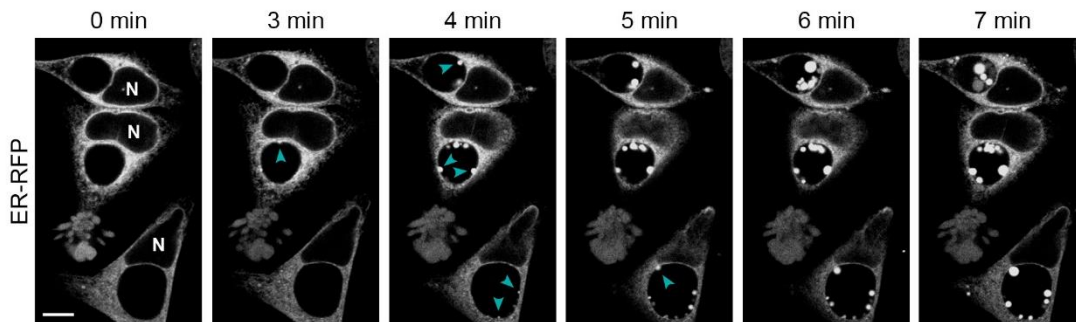


Figure 28. ER-RFP translocates into the inclusion lumen during chemical fixation. HeLa cells were infected with *C. trachomatis* LGV L2 and transfected with ER-RFP. At 30 hpi, living cells were placed in 4% paraformaldehyde and imaged over time with a laser scanning confocal microscope. Note the genesis of ER-RFP blebs into the inclusions lumen (cyan arrowheads) during fixation. N marks the nuclei. Scale bar represents 10 μ m.

5.5 Chemical fixation influences the degree to which organelles are observed within the inclusion

To assess whether the organelle internalization process can occur during various fixation techniques used previously in the study of host cellular material within *Chlamydia* inclusions (Beatty, 2006; Cocchiaro et al., 2008; Cox et al., 2012; Hackstadt et al., 1996; Leiva et al., 2013), we quantified the frequency of ER-RFP structures in inclusions after fixation of infected cells (Figure 29A). Fixation with different concentrations of formaldehyde prepared from either paraformaldehyde or liquid formalin (which contains small amounts of methanol) resulted in similarly high frequencies of inclusions with internal ER-RFP structures, indicating that formaldehyde concentrations and trace levels of methanol in formalin do not affect the frequency of internalization. Since gluteraldehyde fixation as used for electron microscopy causes high levels of autofluorescence across the visible light spectrum (Lee et al., 2013), we could not reliably distinguish any fluorescent marker or dye tested from background fluorescence under these conditions (data not shown). Furthermore, we could not assess the

frequency of ER-RFP structures within inclusions after methanol fixation since mRFP fluorescence was quenched by this treatment.

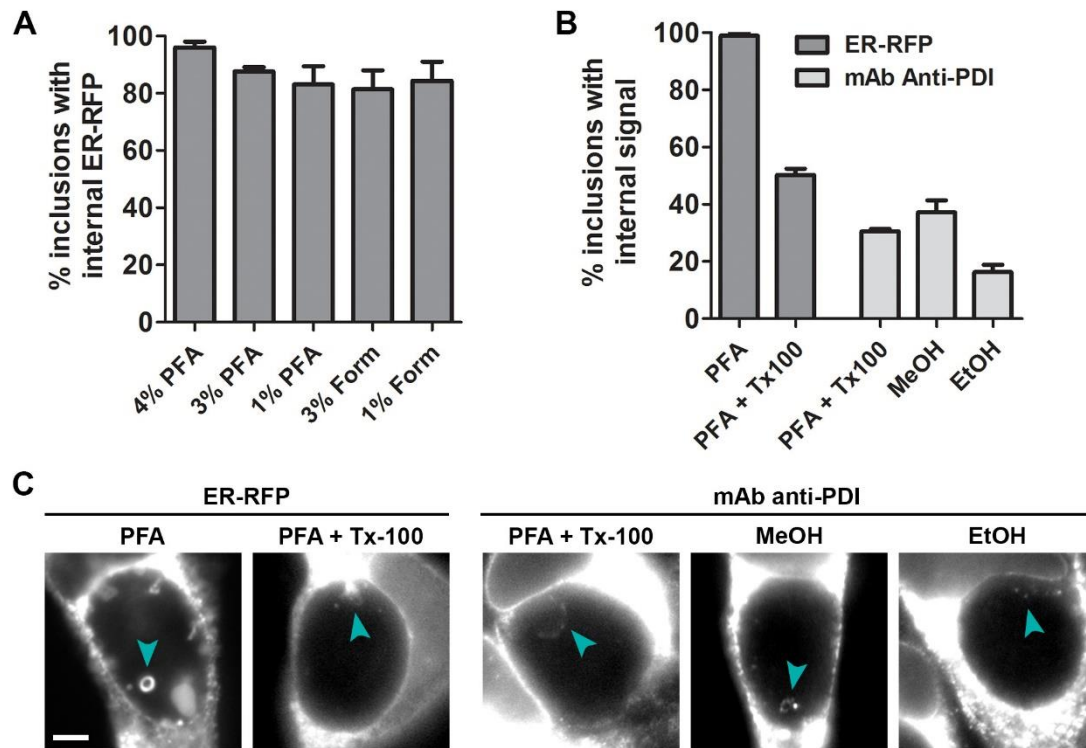


Figure 29. ER structures are detected via immunofluorescence microscopy within inclusions after both formaldehyde and alcohol-based chemical fixation. HeLa cells were infected with *C. trachomatis* LGV L2. (A) Infected cells were transfected with ER-RFP, fixed at 30 hpi with different concentrations of either paraformaldehyde (PFA) or formaldehyde (Form), and assessed for the frequency of ER-RFP within inclusions. (B and C) Infected cells were transfected with ER-RFP as indicated. At 30 hpi, cells were fixed with PFA, methanol, or ethanol, and subsequently permeabilized with Triton X-100 (Tx100) as indicated. Treated cells were processed for immunofluorescence with an antibody to the ER protein PDI and assessed for the frequency of PDI-positive structures within inclusions. Scale bar represents 5 μ m.

To compare the effect of denaturing fixatives such as alcohols to cross-linking fixatives such as aldehydes, we sought to assess ER internalization into the inclusion via immunofluorescence microscopy. Because alcohol fixation simultaneously fixes and permeabilizes membranes, we first assessed how well ER-RFP intra-inclusion structures

resist detergent permeabilization. Using a range of conditions previously employed in the study of host cellular material within inclusions (Beatty, 2006; Cocchiaro et al., 2008; Hackstadt et al., 1996), we found that ER-RFP structures persisted at a reduced number per inclusion (Figure 29C) and typically in only half of all inclusions (Figure 29B and Figure 30). We next performed immunofluorescence on paraformaldehyde-fixed and detergent-permeabilized cells and compared it to methanol or ethanol fixed/permeabilized cells using an antibody to the ER-resident protein PDI (Figure 29, B and C). Notably, we observed PDI-positive structures under all conditions within one-quarter to one-half of inclusions. These findings suggest that both formaldehyde and alcohol-based chemical fixation result in the translocation of endogenous ER materials into the inclusion lumen.

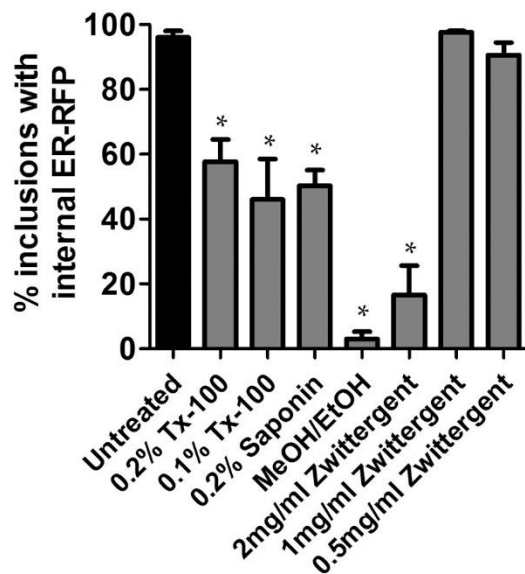


Figure 30. Fixation-induced intraluminal ER-RFP structures within inclusions persist through many post-fixation manipulations. HeLa cells were infected with *C. trachomatis* LGV L2 and transfected with ER-RFP for 30 hr, fixed with 4% paraformaldehyde, treated with the indicated permeabilization solutions, and assessed for the frequency of ER-RFP within inclusions. Treatments included the nonionic detergent Triton X-100 (Tx-100), Saponin, an amphipathic glucoside, a 1:1 mix of

methanol and ethanol, or Zwittergent 3-12, a dipolar ionic detergent for various times. 50-100 inclusions were enumerated in each experiment, and the mean \pm SEM for three independent experiments is shown. * indicates $P < 0.05$ by one-way ANOVA and Dunnett's Multiple Comparison *post hoc* analysis comparing each condition (gray bars) to the control (black bars).

5.6 ER material is internalized into the vacuole of another intracellular pathogen

The *Chlamydia* inclusion is an unusually spacious organelle and the luminal space is largely devoid of electron-dense material compared to the host cytoplasm as assessed by transmission electron microscopy (Stokes, 1980). We speculated that this spacious nature may be conducive to fixation-induced translocation of materials that might otherwise not occur elsewhere in the cell. To assess this, we asked whether another similarly spacious pathogenic vacuole occupied by *Coxiella burnettii* (reviewed in (Voth and Heinzen, 2007)) would display similar internalized structures. When we transfected *Coxiella burnettii*-infected cells with ER-RFP and fixed after 52 hr of infection, we found ER-RFP structures within the lumen of the pathogenic vacuole with similar appearance and frequency (90%) as those found within *Chlamydia* inclusions (Figure 31).

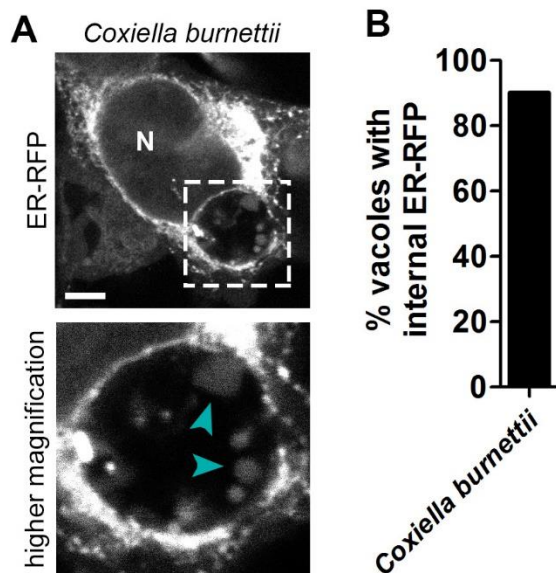


Figure 31. ER-RFP within the pathogenic vacuole of *Coxiella burnetii*. HeLa cells were infected with *Coxiella burnetii*, transfected with ER-RFP, and fixed at 52 hpi. Note the presence of ER-RFP structures within the lumen of the pathogenic vacuole (cyan arrowheads) similar to those within *Chlamydia trachomatis* inclusions. N indicates the nucleus and a dashed line outlines a region of higher magnification. Scale bar represents 5 μ m.

5.7 Discussion

In this study, we report that fluorescently tagged markers of the ER, mitochondria, and inclusion membranes are readily observed within the lumen of fixed *Chlamydia trachomatis* inclusions. However this is not a true reflection of *in vivo* processes as we determined that chemical fixation can induce the translocation of ER components into the inclusion. These internalized structures resist many common immunostaining procedures and were detected by immunofluorescence microscopy, indicating that select cellular materials detected within the inclusions of fixed cells may not reflect the true localization in living cells.

Our findings indicate that fixation-induced internalization into the inclusion lumen is selective amongst subcellular components that reside in close proximity to the

inclusion. We routinely found markers of the inclusion membrane, ER lumen, ER membrane, mitochondrial matrix and mitochondrial outer membrane within inclusion lumen of fixed cells – organelles which all closely associate with the inclusion. However, we failed to observe a high frequency of markers of other inclusion-proximal subcellular elements, including the Golgi, recycling endosomes, lysosomes, and the cytosol. Similarly, we did not observe a marker of the more distal plasma membrane within inclusions. As lipids are directly transferred between the ER and inclusion at membrane-contact sites between the two (Derré et al., 2011; Elwell et al., 2011), we speculate that fixation-induced internalization may occur specifically at inclusion-organelle interaction areas of direct material transfer. Indeed, we infrequently observed what appeared to be the translocation of ER markers across the plasma membrane outward from cells during fixation, and membrane-contact sites between the ER and the plasma membrane have been reported (reviewed in (Rowland and Voeltz, 2012)). However, while mitochondrial protein import plays a role in *Chlamydia caviae* infections (Derré et al., 2007), functional interactions between mitochondria and *C. trachomatis* inclusions have yet to be identified. Some organelles have been suggested to directly transfer in their entirety into the inclusion, including lipid droplets (Cocchiari et al., 2008) and peroxisomes (Boncompain et al., 2014), the former of which has been confirmed in living cells. While we did not assess the internalization of these particular organelles in this study, it remains possible that fixation-induced translocation increases the frequency of *bona fide* interaction or translocation events by internalizing organelles that are interacting with the inclusion or in an early state of translocation at the moment of fixation.

Methanol and ethanol disrupt hydrophobic and hydrogen bonding acting to denature proteins, and are sometimes used to fix samples for immunofluorescence

microscopy due to ease of use, but can shrink and distort tissues and cells (Fox et al., 1985). Formaldehyde reacts with and crosslinks various reactive groups of biological molecules, including proteins, DNA, and sugars. It is routinely used to preserve cellular architecture and the spatial relationships of proteins in cell and tissues (reviewed in (Fox et al., 1985; Thavarajah et al., 2012)). However, there are clear cases in which chemical or aldehyde fixation alters rather than preserves cellular structures. A prominent example is the mesosome, which was thought to be a separate intracellular organelle in bacteria until it was shown to be an artifact of chemical fixation (Nanninga, 1971) of exaggerated invaginations from the cell membrane (Higgins et al., 1976). There is also precedence for fixation-induced membrane blebbing in mammalian cells. Exposing cell monolayers to low concentrations of paraformaldehyde causes the release of vesicles from the plasma membrane (Scott, 1976). These vesicles range in size from 0.5 μm to 15 μm and appear at cell edges similarly to the infrequent blebbing of ER-RFP that we observed during fixation. The kinetics of large membrane blebs forming outwardly from cells fixed under standard paraformaldehyde concentrations (Fox et al., 1985) are similar to that of structures we observed forming within inclusion lumens and may share the same mechanism of genesis.

By transmission electron microscopy, the inclusion lumen appears spacious with large distances between bacteria particularly in the center, and except for glycogen, is largely devoid of electron-dense material (Matsumoto et al., 1991; Stokes, 1980). We speculate that a space largely devoid of non-reactive material is needed to accommodate the blebs that formaldehyde can induce, like the inclusion lumen or extracellular milieu. Consistent with this model, we also observed ER-RFP structures within fixed pathogenic vacuoles of *Coxiella burnetii* at 52 hpi – a time when this

vacuole appears similarly spacious by electron microscopy (reviewed in (Voth and Heinzen, 2007)).

Our findings indicate that the process of chemical fixation can exaggerate the translocation of subcellular components into the lumen of the pathogenic vacuole from two intracellular pathogens – *Chlamydia trachomatis* and *Coxiella burnettii*. The discrepancy between the relative efficiency with which ER membranes are found in the lumen of inclusions between fixed and live cells suggest that caution should be exercised when interpreting events observed in fixed cells. As imaging technologies begin to surpass the diffraction-limit of light and capture images at super-resolution, sub-micron level differences in protein localization and aggregation are becoming apparent between chemically fixed and living cells (Ji et al., 2008). Chemical fixation cannot perfectly preserve the internal architecture of cells and thus observing subcellular components in living, intact cells should remain the gold standard when assessing the significance of any observed interactions. Alternative fixation techniques that better preserve structures, such cryofixation should also reduce subcellular distortions (Pearse, 1980). These methods are becoming more common in the study of intracellular vacuolar pathogens like *Chlamydia*, with the detection of ER components by immunogold labeling within high pressure frozen and freeze-substituted inclusions (Dumoux et al., 2012). Ideally, by assessing the interaction between the inclusion and host organelles by a combination of multiple techniques, a more accurate picture of what occurs in unperturbed, living *C. trachomatis*-infected cells will emerge.

5.8 Materials and Methods

5.8.1 Cell culture, *Chlamydia* infections, transfection, antibodies and plasmids

HeLa cells (ATCC CCL-2) were grown in high glucose DMEM supplemented with L-glutamine, sodium pyruvate (Gibco, Life Technologies) and 10% FBS (Mediatech, CellGro), at 37 °C in a 5% CO₂ humidified incubator. *C. trachomatis* LGV biovar L2 434/Bu (Kumar et al., 2006) was propagated in Vero cells (ATCC CCL-81) and purified as previously described (Caldwell et al., 1981). EB titers were determined by infecting Vero cell monolayers seeded in a 96 well plate. At 24 hpi cells were fixed and stained with anti-MOMP antibodies. Inclusion forming units (IFUs) were counted using a Cellomics ArrayScan automated fluorescence imaging system (Thermo Scientific). Cells were infected at an MOI of 1, synchronized by centrifugation (2,500 x g for 30 min at 10 °C) onto HeLa cell monolayers, and incubated for 30 hr. As indicated, cells were transfected at the time of infection with jetPRIME (Polyplus transfection) according to manufacturer directions with a fresh media exchange after 4 hr. Antibody and plasmid sources: rabbit anti-*Chlamydia* MOMP (Kenneth Fields, University of Kentucky), mouse anti-PDI (Abcam ab2792) ER-RFP and DsRed-Mito (Richard Youle, NIH), Sec61β-GFP (Addgene 15108, Tom Rapoport, Harvard Medical School), GFP-GaIT (Addgene 11929), Matrix-YFP, YFP-Mito^{cb5}TM and YFP-Prohibitin (Jennifer Lippincott-Schwartz, Eunice Kennedy Shriver NICHD), GFP-Rab1 (Craig Roy, Yale), GFP-RhoA, CD63-GFP, and LAMP1-GFP (Soman Abraham, Duke University), Chy-Arf1(Q71L) and mRFP (Micheal Ehlers, Pfizer Neuroscience, formerly Duke University), FAPP1-PH-GFP (Tamas Balla, Eunice Kennedy Shriver NICHD), tdTomato (Marc Caron, Duke University), KRphi-

mRFP (Addgene 17276, Sergio Grinstein, University of Toronto), GFP (pcDNA3.1-CT, Invitrogen, Life Technologies), Syntaxin13-GFP (William Trimble, University of Toronto).

5.8.2 Imaging of subcellular organelles and quantitation of intraluminal structures in fixed inclusions

HeLa cells grown on glass coverslips to 50% confluence were infected with *C. trachomatis* LGV L2 and transfected with the indicated (Figure 26) plasmids. At 30 hpi, cells were fixed with 4% paraformaldehyde (PFA) in PBS at pH 7.4 for 20 minutes at RT, incubated with 1 µg/mL Hoechst 33258 (Life Technologies) in PBS for 20 minutes at RT, mounted to slides in 5 µl SlowFade Gold (Life Technologies), and sealed with nail polish. Images were acquired using a Marianas system (Intelligent Imaging Innovations) equipped with an inverted microscope (Zeiss, Axio-Observer using a 100x 1.4 NA oil objective) and a Yokogawa spinning disk confocal unit (model CSU-22). All the hardware was controlled by SlideBook version 4.2 (Intelligent Imaging Innovations). Z-sections were acquired from above to below each cell, with optimal spacing between z-sections to meet the Nyquist resolution criterion. To assess the frequency of fluorescent blebs within inclusions, both the DNA staining signal (to define the inclusion and nucleus) and fluorescent protein signal in each individual z-section (approximately 30 per cell) from a z-stack of images of each inclusion were viewed with Slidebook version 4.2 or 5.5 (Intelligent Imaging Innovations). At least 12 inclusions for each marker in each independent experiment were assessed. Values from three independent experiments were averaged and standard errors were calculated. Calculations and graphs were prepared with Prism (GraphPad Software) and images were processed for display with Photoshop CS6 (Adobe).

5.8.3 Comparison of intraluminal structures in living and fixed cells

For fixed cells, HeLa cells were prepared as above. For living cells, HeLa cells grown on 35 mm #1.5 glass-bottom dishes (MatTek) to 50% confluence were infected with *C. trachomatis* LGV L2 and cotransfected with ER-RFP and Sec61 β -GFP. At 30 hpi, cells were imaged in a phenol red-free DMEM HG (Gibco, Life Technologies) media supplemented with 10% FBS and 10 μ M HEPES (Gibco, Life Technologies) in a humidified chamber maintaining 37 °C and 5% CO₂. Images were captured on a Leica SP5 laser scanning confocal inverted microscope equipped with a 100x 1.4 NA oil objective. Z-sections were acquired at optimal spacing to meet the Nyquist resolution criterion. Images were deconvolved using Huygens Essential (SVI) and processed with ImageJ (NIH) to create video .AVI files and Photoshop CS6 (Adobe) for presentation. To create 3D-rendered volumes, deconvolved images were further processed with Volocity (PerkinElmer), with the z-axis expanded three-fold to reduce flatness. 3D volumes of each channel acquired of living and fixed cells were exported into the QuickTime (Apple Inc.) Virtual Reality format for viewing (Movie S3-S6).

5.8.4 Time-lapse imaging of ER-RFP translocation during chemical fixation

HeLa cells grown on 35 mm # 1.5 glass-bottom dishes (MatTek) to 50% confluence were infected with *C. trachomatis* LGV L2 and cotransfected with ER-RFP and Sec61 β -GFP. At 30 hpi, cells were bathed in a phenol red-free DMEM HG (Gibco, Life Technologies) media supplemented with 10% FBS and 10 μ M HEPES in a humidified chamber maintaining 37 °C and 5% CO₂, and 8% paraformaldehyde in PBS was added to a final concentration of 4%. Images were captured on a Leica SP5 laser scanning confocal inverted microscope equipped with a 63x 1.2 NA water objective.

Images were acquired every 3.4 sec and the z-position was adjusted manually as needed to offset focal drift due to thermal changes. Images were compiled for display with ImageJ (NIH) and Photoshop CS6 (Adobe).

5.8.5 Quantitation of ER-RFP intraluminal structures in inclusions after various fixation and permeabilization conditions

HeLa cells grown on glass coverslips to 50% confluence were infected with *C. trachomatis* LGV L2 and transfected with ER-RFP as indicated. At 30 hpi, cells were processed in one of three major ways.

Fixatives: Cells were fixed with either 4%, 3%, 1% PFA, 3%, or 1% formaldehyde in PBS pH 7.4 (the latter prepared from a formalin stock containing trace methanol) for 20 min at RT, or pre-chilled 100% methanol or ethanol for 20 min, mounted to slides in 5 μ l SlowFade Gold (Life Technologies), and sealed with nail polish.

Permeabilization methods: As indicated, cells were first fixed with 4% PFA for 20 min at RT, then incubated with just PBS (untreated) or pre-chilled 0.2% (Figure 29 and Figure 30), 0.1% Tx-100, 0.2% Saponin on ice for 10 min, ice-cold 1:1 mix of methanol and ethanol for 5 min on ice, or 2 mg/mL, 1 mg/mL, or 0.5 mg/mL of Zwittergent 3-12 (all detergents in PBS) for 1 min on ice, mounted to slides in 5 μ l SlowFade Gold (Life Technologies), and sealed with nail polish.

Samples were double-blinded and viewed on an Axioskop 2 (Zeiss) inverted widefield fluorescence microscope or an Axio Observer Z1 (Zeiss) (Figure 29 and Figure 30) with a 63X 1.4 NA oil objective (Zeiss) and the frequency of inclusions containing ER-RFP intraluminal structures was quantified in 50-100 cells for each experiment. Values from three independent experiments were averaged and standard errors were calculated. Statistically significant differences were assessed by a one-way ANOVA

followed by Dunnett's Multiple Comparison *post hoc* analysis comparing each condition to untreated with a p-value < 0.05 considered significant. Statistics and graphs were prepared with Prism (GraphPad Software) and Photoshop CS6 (Adobe).

5.8.6 Imaging and quantitation of ER-RFP structures within fixed *Coxiella burnettii* pathogenic vacuoles

HeLa cells grown on glass coverslips to 50% confluence were infected with *Coxiella burnettii* Nine Mile RSA439 (phase II, clone 4) and synchronized by centrifugation (3,000 rpm for 30 min at 10 °C). At 24 hpi, cells were transfected with ER-RFP. At 52 hpi, cells were fixed with 4% paraformaldehyde (PFA) in PBS for 20 minutes at RT, incubated with 1 µg/mL Hoechst 33258 (Life Technologies) in PBS for 20 minutes at RT, mounted to slides in 5 µl SlowFade Gold (Life Technologies), and sealed with nail polish. Images were captured on a Leica SP5 laser scanning confocal inverted microscope equipped with a 100x 1.4 NA oil objective and over 50 infected cells were assessed for the frequency of ER-RFP structures within the pathogenic vacuole. Images were minimally processed with Photoshop CS6 (Adobe) for presentation.

Works Cited

- A Conrad, T., Yang, Z., Ojcius, D., and Zhong, G. (2013). A path forward for the chlamydial virulence factor CPAF. *Microbes Infect. Inst. Pasteur* *15*, 1026–1032.
- Aeberhard, L., Banhart, S., Fischer, M., Jehmlich, N., Rose, L., Koch, S., Laue, M., Renard, B.Y., Schmidt, F., and Heuer, D. (2015). The Proteome of the Isolated Chlamydia trachomatis Containing Vacuole Reveals a Complex Trafficking Platform Enriched for Retromer Components. *PLoS Pathog.* *11*, e1004883.
- Agaisse, H., and Derré, I. (2015). STIM1 Is a Novel Component of ER-Chlamydia trachomatis Inclusion Membrane Contact Sites. *PloS One* *10*, e0125671.
- Balla, A., Tuymetova, G., Tsiomenko, A., Varnai, P., and Balla, T. (2005). A Plasma Membrane Pool of Phosphatidylinositol 4-Phosphate Is Generated by Phosphatidylinositol 4-Kinase Type-III Alpha: Studies with the PH Domains of the Oxysterol Binding Protein and FAPP1. *Mol Biol Cell* *16*, 1282–1295.

- Balsara, Z.R., Misaghi, S., Lafave, J.N., and Starnbach, M.N. (2006). Chlamydia trachomatis infection induces cleavage of the mitotic cyclin B1. *Infect. Immun.* 74, 5602–5608.
- Barker, J.R., Koestler, B.J., Carpenter, V.K., Burdette, D.L., Waters, C.M., Vance, R.E., and Valdivia, R.H. (2013). STING-dependent recognition of cyclic di-AMP mediates type I interferon responses during Chlamydia trachomatis infection. *mBio* 4, e00018–00013.
- Beatty, W.L. (2006). Trafficking from CD63-positive late endocytic multivesicular bodies is essential for intracellular development of Chlamydia trachomatis. *J. Cell Sci.* 119, 350–359.
- Beatty, W.L. (2007). Lysosome repair enables host cell survival and bacterial persistence following Chlamydia trachomatis infection. *Cell. Microbiol.* 9, 2141–2152.
- Beatty, W.L. (2008). Late endocytic multivesicular bodies intersect the chlamydial inclusion in the absence of CD63. *Infect. Immun.* 76, 2872–2881.
- Bednar, M.M., Jorgensen, I., Valdivia, R.H., and McCafferty, D.G. (2011). Chlamydia protease-like activity factor (CPAF): characterization of proteolysis activity in vitro and development of a nanomolar affinity CPAF zymogen-derived inhibitor. *Biochemistry (Mosc.)* 50, 7441–7443.
- Behnia, R., and Munro, S. (2005). Organelle identity and the signposts for membrane traffic. *Nature* 438, 597–604.
- Belland, R., Ojcius, D.M., and Byrne, G.I. (2004). Chlamydia. *Nat. Rev. Microbiol.* 2, 530–531.
- Belland, R.J., Zhong, G., Crane, D.D., Hogan, D., Sturdevant, D., Sharma, J., Beatty, W.L., and Caldwell, H.D. (2003). Genomic transcriptional profiling of the developmental cycle of Chlamydia trachomatis. *Proc. Natl. Acad. Sci. U. S. A.* 100, 8478–8483.
- Betts, H.J., Wolf, K., and Fields, K.A. (2009). Effector protein modulation of host cells: examples in the Chlamydia spp. arsenal. *Curr. Opin. Microbiol.* 12, 81–87.
- Boncompain, G., Müller, C., Meas-Yedid, V., Schmitt-Kopplin, P., Lazarow, P.B., and Subtil, A. (2014). The intracellular bacteria Chlamydia hijack peroxisomes and utilize their enzymatic capacity to produce bacteria-specific phospholipids. *PloS One* 9, e86196.
- Brown, H.M., Knowlton, A.E., and Grieshaber, S.S. (2012). Chlamydial infection induces host cytokinesis failure at abscission. *Cell. Microbiol.* 14, 1554–1567.
- Brown, H.M., Knowlton, A.E., Snaveley, E., Nguyen, B.D., Richards, T.S., and Grieshaber, S.S. (2014). Multinucleation during C. trachomatis infections is caused by the contribution of two effector pathways. *PloS One* 9, e100763.

Buckner, L.R., Schust, D.J., Ding, J., Nagamatsu, T., Beatty, W., Chang, T.L., Greene, S.J., Lewis, M.E., Ruiz, B., Holman, S.L., et al. (2011). Innate immune mediator profiles and their regulation in a novel polarized immortalized epithelial cell model derived from human endocervix. *J. Reprod. Immunol.* 92, 8–20.

Burnaevskiy, N., Fox, T.G., Plymire, D.A., Ertelt, J.M., Weigele, B.A., Selyunin, A.S., Way, S.S., Patrie, S.M., and Alto, N.M. (2013). Proteolytic elimination of N-myristoyl modifications by the *Shigella* virulence factor IpaJ. *Nature* 496, 106–109.

Byers, B., and Goetsch, L. (1976). A highly ordered ring of membrane-associated filaments in budding yeast. *J. Cell Biol.* 69, 717–721.

Caldwell, H.D., Kromhout, J., and Schachter, J. (1981). Purification and partial characterization of the major outer membrane protein of *Chlamydia trachomatis*. *Infect. Immun.* 31, 1161–1176.

Capmany, A., and Damiani, M.T. (2010). *Chlamydia trachomatis* intercepts Golgi-derived sphingolipids through a Rab14-mediated transport required for bacterial development and replication. *PLoS One* 5, e14084.

Carabeo, R.A., Mead, D.J., and Hackstadt, T. (2003). Golgi-dependent transport of cholesterol to the *Chlamydia trachomatis* inclusion. *Proc. Natl. Acad. Sci. U. S. A.* 100, 6771–6776.

Chellas-Géry, B., Linton, C.N., and Fields, K.A. (2007). Human GCIP interacts with CT847, a novel *Chlamydia trachomatis* type III secretion substrate, and is degraded in a tissue-culture infection model. *Cell. Microbiol.* 9, 2417–2430.

Chen, Y.A., and Scheller, R.H. (2001). SNARE-mediated membrane fusion. *Nat. Rev. Mol. Cell Biol.* 2, 98–106.

Chen, A.L., Johnson, K.A., Lee, J.K., Sütterlin, C., and Tan, M. (2012). CPAF: A Chlamydial Protease in Search of an Authentic Substrate. *PLoS Pathog.* 8, e1002842.

Chen, C., Chen, D., Sharma, J., Cheng, W., Zhong, Y., Liu, K., Jensen, J., Shain, R., Arulanandam, B., and Zhong, G. (2006). The Hypothetical Protein CT813 Is Localized in the *Chlamydia trachomatis* Inclusion Membrane and Is Immunogenic in Women Urogenitally Infected with *C. trachomatis*. *Infect. Immun.* 74, 4826–4840.

Chen, D., Lei, L., Lu, C., Flores, R., DeLisa, M.P., Roberts, T.C., Romesberg, F.E., and Zhong, G. (2010). Secretion of the chlamydial virulence factor CPAF requires the Sec-dependent pathway. *Microbiol. Read. Engl.* 156, 3031–3040.

Chhabra, E.S., and Higgs, H.N. (2007). The many faces of actin: matching assembly factors with cellular structures. *Nat. Cell Biol.* 9, 1110–1121.

Chin, E., Kirker, K., Zuck, M., James, G., and Hybiske, K. (2012). Actin recruitment to the Chlamydia inclusion is spatiotemporally regulated by a mechanism that requires host and bacterial factors. *PLoS One* 7, e46949.

Christian, J., Vier, J., Paschen, S.A., and Häcker, G. (2010). Cleavage of the NF- κ B family protein p65/RelA by the chlamydial protease-like activity factor (CPAF) impairs proinflammatory signaling in cells infected with Chlamydiae. *J. Biol. Chem.* 285, 41320–41327.

Christian, J.G., Heymann, J., Paschen, S.A., Vier, J., Schauenburg, L., Rupp, J., Meyer, T.F., Häcker, G., and Heuer, D. (2011). Targeting of a chlamydial protease impedes intracellular bacterial growth. *PLoS Pathog.* 7, e1002283.

Claude, A., Zhao, B.P., Kuziemy, C.E., Dahan, S., Berger, S.J., Yan, J.P., Arnold, A.D., Sullivan, E.M., and Melançon, P. (1999). GBF1: A novel Golgi-associated BFA-resistant guanine nucleotide exchange factor that displays specificity for ADP-ribosylation factor 5. *J. Cell Biol.* 146, 71–84.

Clausen, J.D., Christiansen, G., Holst, H.U., and Birkelund, S. (1997). Chlamydia trachomatis utilizes the host cell microtubule network during early events of infection. *Mol. Microbiol.* 25, 441–449.

Clifton, D.R., Fields, K.A., Grieshaber, S.S., Dooley, C.A., Fischer, E.R., Mead, D.J., Carabeo, R.A., and Hackstadt, T. (2004). A chlamydial type III translocated protein is tyrosine-phosphorylated at the site of entry and associated with recruitment of actin. *Proc. Natl. Acad. Sci. U. S. A.* 101, 10166–10171.

Cocchiari, J.L., and Valdivia, R.H. (2009). New insights into Chlamydia intracellular survival mechanisms. *Cell. Microbiol.* 11, 1571–1578.

Cocchiari, J.L., Kumar, Y., Fischer, E.R., Hackstadt, T., and Valdivia, R.H. (2008). Cytoplasmic lipid droplets are translocated into the lumen of the Chlamydia trachomatis parasitophorous vacuole. *Proc. Natl. Acad. Sci. U. S. A.* 105, 9379–9384.

Cortes, C., Rzomp, K.A., Tvinnereim, A., Scidmore, M.A., and Wizel, B. (2007). Chlamydia pneumoniae inclusion membrane protein Cpn0585 interacts with multiple Rab GTPases. *Infect. Immun.* 75, 5586–5596.

Cossart, P., Boquet, P., Normark, Staffan, and Rappuoli, Rino (2005). Cellular microbiology (ASM Press).

Cox, J.V., Naher, N., Abdelrahman, Y.M., and Belland, R.J. (2012). Host HDL biogenesis machinery is recruited to the inclusion of Chlamydia trachomatis-infected cells and regulates chlamydial growth. *Cell. Microbiol.* 14, 1497–1512.

Darville, T., and Hiltke, T.J. (2010). Pathogenesis of genital tract disease due to Chlamydia trachomatis. *J. Infect. Dis.* 201 Suppl 2, S114–S125.

- Delevoeye, C., Nilges, M., Dautry-Varsat, A., and Subtil, A. (2004). Conservation of the biochemical properties of IncA from *Chlamydia trachomatis* and *Chlamydia caviae*: oligomerization of IncA mediates interaction between facing membranes. *J. Biol. Chem.* *279*, 46896–46906.
- Delevoeye, C., Nilges, M., Dehoux, P., Paumet, F., Perrinet, S., Dautry-Varsat, A., and Subtil, A. (2008). SNARE protein mimicry by an intracellular bacterium. *PLoS Pathog.* *4*, e1000022.
- Delorenzi, M., and Speed, T. (2002). An HMM model for coiled-coil domains and a comparison with PSSM-based predictions. *Bioinforma. Oxf. Engl.* *18*, 617–625.
- Derré, I., Pypaert, M., Dautry-Varsat, A., and Agaisse, H. (2007). RNAi Screen in *Drosophila* Cells Reveals the Involvement of the Tom Complex in *Chlamydia* Infection. *PLoS Pathog* *3*, e155.
- Derré, I., Swiss, R., and Agaisse, H. (2011). The Lipid Transfer Protein CERT Interacts with the *Chlamydia* Inclusion Protein IncD and Participates to ER-*Chlamydia* Inclusion Membrane Contact Sites. *PLoS Pathog.* *7*, e1002092.
- Donaldson, J.G., and Jackson, C.L. (2011). ARF family G proteins and their regulators: roles in membrane transport, development and disease. *Nat. Rev. Mol. Cell Biol.* *12*, 362–375.
- Dong, F., Su, H., Huang, Y., Zhong, Y., and Zhong, G. (2004a). Cleavage of host keratin 8 by a *Chlamydia*-secreted protease. *Infect. Immun.* *72*, 3863–3868.
- Dong, F., Pirbhai, M., Zhong, Y., and Zhong, G. (2004b). Cleavage-dependent activation of a *chlamydia*-secreted protease. *Mol. Microbiol.* *52*, 1487–1494.
- D'Souza-Schorey, C., and Chavrier, P. (2006). ARF proteins: roles in membrane traffic and beyond. *Nat Rev Mol Cell Biol* *7*, 347–358.
- Dumoux, M., Clare, D.K., Saibil, H.R., and Hayward, R.D. (2012). *Chlamydiae* assemble a pathogen synapse to hijack the host endoplasmic reticulum. *Traffic Cph. Den.*
- Egea, G., Lázaro-Diéguéz, F., and Vilella, M. (2006). Actin dynamics at the Golgi complex in mammalian cells. *Curr. Opin. Cell Biol.* *18*, 168–178.
- Elwell, C.A., Ceesay, A., Kim, J.H., Kalman, D., and Engel, J.N. (2008). RNA Interference Screen Identifies Abl Kinase and PDGFR Signaling in *Chlamydia trachomatis* Entry. *PLoS Pathog* *4*, e1000021.
- Elwell, C.A., Jiang, S., Kim, J.H., Lee, A., Wittmann, T., Hanada, K., Melancon, P., and Engel, J.N. (2011). *Chlamydia trachomatis* co-opts GBF1 and CERT to acquire host sphingomyelin for distinct roles during intracellular development. *PLoS Pathog.* *7*, e1002198.

- Etienne-Manneville, S., and Hall, A. (2002). Rho GTPases in cell biology. *Nature* 420, 629–635.
- Farese Jr., R.V., and Walther, T.C. (2009). Lipid Droplets Finally Get a Little R-E-S-P-E-C-T. *Cell* 139, 855–860.
- Fields, K.A., and Hackstadt, T. (2002). The Chlamydial Inclusion: Escape from the Endocytic Pathway. *Annu. Rev. Cell Dev. Biol.* 18, 221–245.
- Fields, K.A., Fischer, E., and Hackstadt, T. (2002). Inhibition of fusion of *Chlamydia trachomatis* inclusions at 32 degrees C correlates with restricted export of InCA. *Infect. Immun.* 70, 3816–3823.
- Fox, C.H., Johnson, F.B., Whiting, J., and Roller, P.P. (1985). Formaldehyde fixation. *J. Histochem. Cytochem. Off. J. Histochem. Soc.* 33, 845–853.
- Gauliard, E., Ouellette, S.P., Rueden, K.J., and Ladant, D. (2015). Characterization of interactions between inclusion membrane proteins from *Chlamydia trachomatis*. *Front. Cell. Infect. Microbiol.* 5, 13.
- Giles, D.K., and Wyrick, P.B. (2008). Trafficking of chlamydial antigens to the endoplasmic reticulum of infected epithelial cells. *Microbes Infect. Inst. Pasteur* 10, 1494–1503.
- Giles, D.K., Whittimore, J.D., LaRue, R.W., Raulston, J.E., and Wyrick, P.B. (2006). Ultrastructural analysis of chlamydial antigen-containing vesicles everting from the *Chlamydia trachomatis* inclusion. *Microbes Infect. Inst. Pasteur* 8, 1579–1591.
- Gondek, D.C., Olive, A.J., Stary, G., and Starnbach, M.N. (2012). CD4+ T cells are necessary and sufficient to confer protection against *Chlamydia trachomatis* infection in the murine upper genital tract. *J. Immunol. Baltim. Md 1950* 189, 2441–2449.
- Goodchild, R.E., and Dauer, W.T. (2005). The AAA+ protein torsinA interacts with a conserved domain present in LAP1 and a novel ER protein. *J. Cell Biol.* 168, 855–862.
- Grieshaber, S.S., Grieshaber, N.A., and Hackstadt, T. (2003). *Chlamydia trachomatis* uses host cell dynein to traffic to the microtubule-organizing center in a p50 dynamitin-independent process. *J. Cell Sci.* 116, 3793–3802.
- Grieshaber, S.S., Grieshaber, N.A., Miller, N., and Hackstadt, T. (2006). *Chlamydia trachomatis* causes centrosomal defects resulting in chromosomal segregation abnormalities. *Traffic Cph. Den.* 7, 940–949.
- Guo, Y., Cordes, K.R., Farese, R.V., and Walther, T.C. (2009). Lipid droplets at a glance. *J Cell Sci* 122, 749–752.
- Gurumurthy, R.K., Mäurer, A.P., Machuy, N., Hess, S., Pleissner, K.P., Schuchhardt, J., Rudel, T., and Meyer, T.F. (2010). A loss-of-function screen reveals Ras- and Raf-

independent MEK-ERK signaling during *Chlamydia trachomatis* infection. *Sci. Signal.* 3, ra21.

Haarer, B.K., and Pringle, J.R. (1987). Immunofluorescence localization of the *Saccharomyces cerevisiae* CDC12 gene product to the vicinity of the 10-nm filaments in the mother-bud neck. *Mol. Cell. Biol.* 7, 3678–3687.

Hackstadt, T., Scidmore, M.A., and Rockey, D.D. (1995). Lipid metabolism in *Chlamydia trachomatis*-infected cells: directed trafficking of Golgi-derived sphingolipids to the chlamydial inclusion. *Proc. Natl. Acad. Sci. U. S. A.* 92, 4877–4881.

Hackstadt, T., Rockey, D.D., Heinzen, R.A., and Scidmore, M.A. (1996). *Chlamydia trachomatis* interrupts an exocytic pathway to acquire endogenously synthesized sphingomyelin in transit from the Golgi apparatus to the plasma membrane. *EMBO J.* 15, 964–977.

Hackstadt, T., Scidmore-Carlson, M.A., Shaw, E.I., and Fischer, E.R. (1999). The *Chlamydia trachomatis* IncA protein is required for homotypic vesicle fusion. *Cell. Microbiol.* 1, 119–130.

Haglund, C.M., and Welch, M.D. (2011). Pathogens and polymers: microbe-host interactions illuminate the cytoskeleton. *J. Cell Biol.* 195, 7–17.

Hailey, D.W., Rambold, A.S., Satpute-Krishnan, P., Mitra, K., Sougrat, R., Kim, P.K., and Lippincott-Schwartz, J. (2010). Mitochondria Supply Membranes for Autophagosome Biogenesis during Starvation. *Cell* 141, 656–667.

Hanada, K., Kumagai, K., Yasuda, S., Miura, Y., Kawano, M., Fukasawa, M., and Nishijima, M. (2003). Molecular machinery for non-vesicular trafficking of ceramide. *Nature* 426, 803–809.

Hartwell, L.H. (1971). Genetic control of the cell division cycle in yeast. IV. Genes controlling bud emergence and cytokinesis. *Exp. Cell Res.* 69, 265–276.

Hatch, G.M., and McClarty, G. (1998a). Phospholipid composition of purified *Chlamydia trachomatis* mimics that of the eucaryotic host cell. *Infect. Immun.* 66, 3727–3735.

Hatch, G.M., and McClarty, G. (1998b). Cardiolipin remodeling in eukaryotic cells infected with *Chlamydia trachomatis* is linked to elevated mitochondrial metabolism. *Biochem. Biophys. Res. Commun.* 243, 356–360.

Heuer, D., Rejman Lipinski, A., Machuy, N., Karlas, A., Wehrens, A., Siedler, F., Brinkmann, V., and Meyer, T.F. (2009). *Chlamydia* causes fragmentation of the Golgi compartment to ensure reproduction. *Nature* 457, 731–735.

Heymann, J., Rejman Lipinski, A., Bauer, B., Meyer, T.F., and Heuer, D. (2013). *Chlamydia trachomatis* infection prevents front-rear polarity of migrating HeLa cells. *Cell. Microbiol.*

- Higgins, M.L., Tsien, H.C., and Daneo-Moore, L. (1976). Organization of mesosomes in fixed and unfixed cells. *J. Bacteriol.* *127*, 1519–1523.
- Ho, T.D., and Starnbach, M.N. (2005). The *Salmonella enterica* serovar typhimurium-encoded type III secretion systems can translocate *Chlamydia trachomatis* proteins into the cytosol of host cells. *Infect. Immun.* *73*, 905–911.
- Horn, M. (2008). Chlamydiae as symbionts in eukaryotes. *Annu. Rev. Microbiol.* *62*, 113–131.
- Hotulainen, P., and Lappalainen, P. (2006). Stress fibers are generated by two distinct actin assembly mechanisms in motile cells. *J. Cell Biol.* *173*, 383–394.
- Hou, S., Lei, L., Yang, Z., Qi, M., Liu, Q., and Zhong, G. (2013). *Chlamydia trachomatis* Outer Membrane Complex Protein B (OmcB) Is Processed by the Protease CPAF. *J. Bacteriol.* *195*, 951–957.
- Hu, V.H., Harding-Esch, E.M., Burton, M.J., Bailey, R.L., Kadimpeul, J., and Mabey, D.C.W. (2010). Epidemiology and control of trachoma: systematic review. *Trop. Med. Int. Health* *15*, 673–691.
- Hybiske, K., and Stephens, R.S. (2007). Mechanisms of host cell exit by the intracellular bacterium *Chlamydia*. *Proc. Natl. Acad. Sci.* *104*, 11430–11435.
- Igal, R.A., Wang, P., and Coleman, R.A. (1997). Triacsin C blocks de novo synthesis of glycerolipids and cholesterol esters but not recycling of fatty acid into phospholipid: evidence for functionally separate pools of acyl-CoA. *Biochem. J.* *324* (Pt 2), 529–534.
- Janke, C., and Bulinski, J.C. (2011). Post-translational regulation of the microtubule cytoskeleton: mechanisms and functions. *Nat. Rev. Mol. Cell Biol.* *12*, 773–786.
- Jewett, T.J., Fischer, E.R., Mead, D.J., and Hackstadt, T. (2006). Chlamydial TARP is a bacterial nucleator of actin. *Proc. Natl. Acad. Sci. U. S. A.* *103*, 15599–15604.
- Ji, N., Shroff, H., Zhong, H., and Betzig, E. (2008). Advances in the speed and resolution of light microscopy. *Curr. Opin. Neurobiol.* *18*, 605–616.
- Johnson, C.M., and Fisher, D.J. (2013). Site-specific, insertional inactivation of *incA* in *Chlamydia trachomatis* using a group II intron. *PLoS One* *8*, e83989.
- Jorgensen, I., Bednar, M.M., Amin, V., Davis, B.K., Ting, J.P.Y., McCafferty, D.G., and Valdivia, R.H. (2011). The *Chlamydia* Protease CPAF Regulates Host and Bacterial Proteins to Maintain Pathogen Vacuole Integrity and Promote Virulence. *Cell Host Microbe* *10*, 21–32.
- Kabeiseman, E.J., Cichos, K., Hackstadt, T., Lucas, A., and Moore, E.R. (2013). Vesicle-associated membrane protein 4 and syntaxin 6 interactions at the chlamydial inclusion. *Infect. Immun.* *81*, 3326–3337.

- Kabeiseman, E.J., Cichos, K.H., and Moore, E.R. (2014). The eukaryotic signal sequence, YGRL, targets the chlamydial inclusion. *Front. Cell. Infect. Microbiol.* *4*, 129.
- Kari, L., Goheen, M.M., Randall, L.B., Taylor, L.D., Carlson, J.H., Whitmire, W.M., Virok, D., Rajaram, K., Endresz, V., McClarty, G., et al. (2011). Generation of targeted *Chlamydia trachomatis* null mutants. *Proc. Natl. Acad. Sci. U. S. A.* *108*, 7189–7193.
- Kawana, K., Quayle, A.J., Ficarra, M., Ibane, J.A., Shen, L., Kawana, Y., Yang, H., Marrero, L., Yavagal, S., Greene, S.J., et al. (2007). CD1d degradation in *Chlamydia trachomatis*-infected epithelial cells is the result of both cellular and chlamydial proteasomal activity. *J. Biol. Chem.* *282*, 7368–7375.
- Kawano, M., Kumagai, K., Nishijima, M., and Hanada, K. (2006). Efficient trafficking of ceramide from the endoplasmic reticulum to the Golgi apparatus requires a VAMP-associated protein-interacting FFAT motif of CERT. *J. Biol. Chem.* *281*, 30279–30288.
- Kim, H.B., Haarer, B.K., and Pringle, J.R. (1991). Cellular morphogenesis in the *Saccharomyces cerevisiae* cell cycle: localization of the CDC3 gene product and the timing of events at the budding site. *J. Cell Biol.* *112*, 535–544.
- Kokes, M., Dunn, J.D., Granek, J.A., Nguyen, B.D., Barker, J.R., Valdivia, R.H., and Bastidas, R.J. (2015). Integrating Chemical Mutagenesis and Whole-Genome Sequencing as a Platform for Forward and Reverse Genetic Analysis of *Chlamydia*. *Cell Host Microbe* *17*, 716–725.
- Kokes M, and Valdivia RH (2012). Cell Biology of the Chlamydial Inclusion. In *Intracellular Pathogens I: Chlamydiales*, Tan M, and Bavoil PM, eds. (Washington, DC: ASM Press), pp. 170–191.
- Kumar, Y., and Valdivia, R.H. (2008a). Actin and Intermediate Filaments Stabilize the *Chlamydia trachomatis* Vacuole by Forming Dynamic Structural Scaffolds. *Cell Host Microbe* *4*, 159–169.
- Kumar, Y., and Valdivia, R.H. (2008b). Reorganization of the host cytoskeleton by the intracellular pathogen *Chlamydia trachomatis*. *Commun Integr Biol* *1*, 175–177.
- Kumar, Y., and Valdivia, R.H. (2009). Leading a sheltered life: intracellular pathogens and maintenance of vacuolar compartments. *Cell Host Microbe* *5*, 593–601.
- Kumar, Y., Cocchiaro, J., and Valdivia, R.H. (2006). The obligate intracellular pathogen *Chlamydia trachomatis* targets host lipid droplets. *Curr. Biol. CB* *16*, 1646–1651.
- Lane, B.J., Mutchler, C., Al Khodor, S., Grieshaber, S.S., and Carabeo, R.A. (2008). Chlamydial entry involves TARP binding of guanine nucleotide exchange factors. *PLoS Pathog.* *4*, e1000014.

- Lee, K., Choi, S., Yang, C., Wu, H.-C., and Yu, J. (2013). Autofluorescence generation and elimination: a lesson from glutaraldehyde. *Chem. Commun. Camb. Engl.* 49, 3028–3030.
- Leiva, N., Capmany, A., and Damiani, M.T. (2013). Rab11-family of interacting protein 2 associates with chlamydial inclusions through its Rab-binding domain and promotes bacterial multiplication. *Cell. Microbiol.* 15, 114–129.
- Levine, T., and Loewen, C. (2006). Inter-organelle membrane contact sites: through a glass, darkly. *Curr. Opin. Cell Biol.* 18, 371–378.
- Li, Z., Chen, C., Chen, D., Wu, Y., Zhong, Y., and Zhong, G. (2008). Characterization of fifty putative inclusion membrane proteins encoded in the *Chlamydia trachomatis* genome. *Infect. Immun.* 76, 2746–2757.
- Lippincott-Schwartz, J., and Phair, R.D. (2010). Lipids and cholesterol as regulators of traffic in the endomembrane system. *Annu. Rev. Biophys.* 39, 559–578.
- Lippincott-Schwartz, J., Yuan, L.C., Bonifacino, J.S., and Klausner, R.D. (1989). Rapid redistribution of Golgi proteins into the ER in cells treated with brefeldin A: evidence for membrane cycling from Golgi to ER. *Cell* 56, 801–813.
- Lippincott-Schwartz, J., Cole, N.B., and Donaldson, J.G. (1998). Building a secretory apparatus: role of ARF1/COPI in Golgi biogenesis and maintenance. *Histochem. Cell Biol.* 109, 449–462.
- Lutter, E.I., Martens, C., and Hackstadt, T. (2012). Evolution and conservation of predicted inclusion membrane proteins in chlamydiae. *Comp. Funct. Genomics* 2012, 362104.
- Lutter, E.I., Barger, A.C., Nair, V., and Hackstadt, T. (2013). *Chlamydia trachomatis* Inclusion Membrane Protein CT228 Recruits Elements of the Myosin Phosphatase Pathway to Regulate Release Mechanisms. *Cell Rep.*
- Majeed, M., Krause, K.H., Clark, R.A., Kihlström, E., and Stendahl, O. (1999). Localization of intracellular Ca²⁺ stores in HeLa cells during infection with *Chlamydia trachomatis*. *J. Cell Sci.* 112 (Pt 1), 35–44.
- Manolea, F., Claude, A., Chun, J., Rosas, J., and Melançon, P. (2008). Distinct functions for Arf guanine nucleotide exchange factors at the Golgi complex: GBF1 and BIGs are required for assembly and maintenance of the Golgi stack and trans-Golgi network, respectively. *Mol. Biol. Cell* 19, 523–535.
- Mansour, S.J., Skaug, J., Zhao, X.H., Giordano, J., Scherer, S.W., and Melançon, P. (1999). p200 ARF-GEP1: a Golgi-localized guanine nucleotide exchange protein whose Sec7 domain is targeted by the drug brefeldin A. *Proc. Natl. Acad. Sci. U. S. A.* 96, 7968–7973.

- Martens, S., and McMahon, H.T. (2008). Mechanisms of membrane fusion: disparate players and common principles. *Nat. Rev. Mol. Cell Biol.* 9, 543–556.
- Mason, J.M., and Arndt, K.M. (2004). Coiled Coil Domains: Stability, Specificity, and Biological Implications. *ChemBioChem* 5, 170–176.
- Matanis, T., Akhmanova, A., Wulf, P., Del Nery, E., Weide, T., Stepanova, T., Galjart, N., Grosveld, F., Goud, B., De Zeeuw, C.I., et al. (2002). Bicaudal-D regulates COPI-independent Golgi-ER transport by recruiting the dynein-dynactin motor complex. *Nat. Cell Biol.* 4, 986–992.
- Matsumoto, A., Bessho, H., Uehira, K., and Suda, T. (1991). Morphological studies of the association of mitochondria with chlamydial inclusions and the fusion of chlamydial inclusions. *J. Electron Microsc. (Tokyo)* 40, 356–363.
- Medzhitov, R. (2001). Toll-like receptors and innate immunity. *Nat. Rev. Immunol.* 1, 135–145.
- Mirrashidi, K.M., Elwell, C.A., Verschueren, E., Johnson, J.R., Frando, A., Von Dollen, J., Rosenberg, O., Gulbahce, N., Jang, G., Johnson, T., et al. (2015). Global Mapping of the Inc-Human Interactome Reveals that Retromer Restricts Chlamydia Infection. *Cell Host Microbe*.
- Misaghi, S., Balsara, Z.R., Catic, A., Spooner, E., Ploegh, H.L., and Starnbach, M.N. (2006). Chlamydia trachomatis-derived deubiquitinating enzymes in mammalian cells during infection. *Mol. Microbiol.* 61, 142–150.
- Mital, J., Miller, N.J., Fischer, E.R., and Hackstadt, T. (2010). Specific chlamydial inclusion membrane proteins associate with active Src family kinases in microdomains that interact with the host microtubule network. *Cell. Microbiol.* 12, 1235–1249.
- Mital, J., Miller, N.J., Dorward, D.W., Dooley, C.A., and Hackstadt, T. (2013). Role for chlamydial inclusion membrane proteins in inclusion membrane structure and biogenesis. *PLoS One* 8, e63426.
- Mital, J., Lutter, E.I., Barger, A.C., Dooley, C.A., and Hackstadt, T. (2015). Chlamydia trachomatis inclusion membrane protein CT850 interacts with the dynein light chain DYNLT1 (Tctex1). *Biochem. Biophys. Res. Commun.* 462, 165–170.
- Moore, E.R., Fischer, E.R., Mead, D.J., and Hackstadt, T. (2008). The chlamydial inclusion preferentially intercepts basolaterally directed sphingomyelin-containing exocytic vacuoles. *Traffic Cph. Den.* 9, 2130–2140.
- Moore, L., Mead, D., Dooley, C., Sager, J., and Hackstadt, T. (2010). The trans-Golgi SNARE syntaxin 6 is recruited to the chlamydial inclusion membrane. *Microbiol. Read. Engl.*

- Moorhead, A.M., Jung, J.-Y., Smirnov, A., Kaufer, S., and Scidmore, M.A. (2010). Multiple Host Proteins That Function in Phosphatidylinositol-4-Phosphate Metabolism Are Recruited to the Chlamydial Inclusion. *Infect Immun* 78, 1990–2007.
- Moorhead, A.R., Rzomp, K.A., and Scidmore, M.A. (2007). The Rab6 effector Bicaudal D1 associates with *Chlamydia trachomatis* inclusions in a biovar-specific manner. *Infect. Immun.* 75, 781–791.
- Morrison, D.K. (2009). The 14-3-3 proteins: integrators of diverse signaling cues that impact cell fate and cancer development. *Trends Cell Biol.* 19, 16–23.
- Mostowy, S., and Cossart, P. (2011). Septins as key regulators of actin based processes in bacterial infection. *Biol. Chem.* 392, 831–835.
- Mostowy, S., and Cossart, P. (2012). Septins: the fourth component of the cytoskeleton. *Nat. Rev. Mol. Cell Biol.* 13, 183–194.
- Murthy, A.K., Guentzel, M.N., Zhong, G., and Arulanandam, B.P. (2009). Chlamydial protease-like activity factor--insights into immunity and vaccine development. *J. Reprod. Immunol.* 83, 179–184.
- Murthy, A.K., Li, W., Guentzel, M.N., Zhong, G., and Arulanandam, B.P. (2011). Vaccination with the defined chlamydial secreted protein CPAF induces robust protection against female infertility following repeated genital chlamydial challenge. *Vaccine* 29, 2519–2522.
- Myers, K.R., and Casanova, J.E. (2008). Regulation of actin cytoskeleton dynamics by Arf-family GTPases. *Trends Cell Biol.* 18, 184–192.
- Nagai, T., Abe, A., and Sasakawa, C. (2005). Targeting of enteropathogenic *Escherichia coli* EspF to host mitochondria is essential for bacterial pathogenesis: critical role of the 16th leucine residue in EspF. *J. Biol. Chem.* 280, 2998–3011.
- Nanninga, N. (1971). The mesosome of *Bacillus subtilis* as affected by chemical and physical fixation. *J. Cell Biol.* 48, 219–224.
- Naumanen, P., Lappalainen, P., and Hotulainen, P. (2008). Mechanisms of actin stress fibre assembly. *J. Microsc.* 231, 446–454.
- Le Negrate, G., Krieg, A., Faustin, B., Loeffler, M., Godzik, A., Krajewski, S., and Reed, J.C. (2008). ChlaDub1 of *Chlamydia trachomatis* suppresses NF-kappaB activation and inhibits I-kappaBalpha ubiquitination and degradation. *Cell. Microbiol.* 10, 1879–1892.
- Nguyen, B.D., and Valdivia, R.H. (2012). Virulence determinants in the obligate intracellular pathogen *Chlamydia trachomatis* revealed by forward genetic approaches. *Proc. Natl. Acad. Sci. U. S. A.* 109, 1263–1268.

- Nguyen, B.D., and Valdivia, R.H. (2013). Forward genetic approaches in *Chlamydia trachomatis*. *J. Vis. Exp. JoVE* e50636.
- Van Niel, G., Porto-Carreiro, I., Simoes, S., and Raposo, G. (2006). Exosomes: a common pathway for a specialized function. *J. Biochem. (Tokyo)* *140*, 13–21.
- Ojcius, D.M., Degani, H., Mispelter, J., and Dautry-Varsat, A. (1998). Enhancement of ATP levels and glucose metabolism during an infection by *Chlamydia*. NMR studies of living cells. *J. Biol. Chem.* *273*, 7052–7058.
- Van Ooij, C., Apodaca, G., and Engel, J. (1997). Characterization of the *Chlamydia trachomatis* vacuole and its interaction with the host endocytic pathway in HeLa cells. *Infect. Immun.* *65*, 758–766.
- Van Ooij, C., Homola, E., Kincaid, E., and Engel, J. (1998). Fusion of *Chlamydia trachomatis*-containing inclusions is inhibited at low temperatures and requires bacterial protein synthesis. *Infect. Immun.* *66*, 5364–5371.
- Van Ooij, C., Kalman, L., van Ijzendoorn, S., Nishijima, M., Hanada, K., Mostov, K., and Engel, J.N. (2000). Host cell-derived sphingolipids are required for the intracellular growth of *Chlamydia trachomatis*. *Cell. Microbiol.* *2*, 627–637.
- Ouellette, S., and Carabeo, R.A. (2010). A Functional Slow Recycling Pathway of Transferrin is Required for Growth of *Chlamydia*. *Front. Cell. Infect. Microbiol.* *1*.
- Ouellette, S.P., Dorsey, F.C., Moshiaich, S., Cleveland, J.L., and Carabeo, R.A. (2011). *Chlamydia* species-dependent differences in the growth requirement for lysosomes. *PLoS One* *6*, e16783.
- Papatheodorou, P., Domańska, G., Oxle, M., Mathieu, J., Selchow, O., Kenny, B., and Rassow, J. (2006). The enteropathogenic *Escherichia coli* (EPEC) Map effector is imported into the mitochondrial matrix by the TOM/Hsp70 system and alters organelle morphology. *Cell. Microbiol.* *8*, 677–689.
- Parsons, J.T., Horwitz, A.R., and Schwartz, M.A. (2010). Cell adhesion: integrating cytoskeletal dynamics and cellular tension. *Nat. Rev. Mol. Cell Biol.* *11*, 633–643.
- Paschen, S.A., Christian, J.G., Vier, J., Schmidt, F., Walch, A., Ojcius, D.M., and Häcker, G. (2008). Cytotoxicity of *Chlamydia* is largely reproduced by expression of a single chlamydial protease. *J. Cell Biol.* *182*, 117–127.
- Paumet, F., Wesolowski, J., Garcia-Diaz, A., Delevoye, C., Aulner, N., Shuman, H.A., Subtil, A., and Rothman, J.E. (2009). Intracellular bacteria encode inhibitory SNARE-like proteins. *PLoS One* *4*, e7375.
- Pearse, A.G.E. (1980). *Histochemistry: Theoretical and Applied* (Churchill Livingstone).

- Pennini, M.E., Perrinet, S., Dautry-Varsat, A., and Subtil, A. (2010). Histone Methylation by NUE, a Novel Nuclear Effector of the Intracellular Pathogen *Chlamydia trachomatis*. *PLoS Pathog* 6, e1000995.
- Perry, R.J., and Ridgway, N.D. (2005). Molecular mechanisms and regulation of ceramide transport. *Biochim. Biophys. Acta* 1734, 220–234.
- Peterson, E.M., and de la Maza, L.M. (1988). *Chlamydia* parasitism: ultrastructural characterization of the interaction between the chlamydial cell envelope and the host cell. *J. Bacteriol.* 170, 1389–1392.
- Piekny, A., Werner, M., and Glotzer, M. (2005). Cytokinesis: welcome to the Rho zone. *Trends Cell Biol.* 15, 651–658.
- Piper, R.C., and Katzmann, D.J. (2007). Biogenesis and function of multivesicular bodies. *Annu. Rev. Cell Dev. Biol.* 23, 519–547.
- Pirbhai, M., Dong, F., Zhong, Y., Pan, K.Z., and Zhong, G. (2006). The Secreted Protease Factor CPAF Is Responsible for Degrading Pro-apoptotic BH3-only Proteins in *Chlamydia trachomatis*-infected Cells. *J. Biol. Chem.* 281, 31495–31501.
- Poh, J., Odendall, C., Spanos, A., Boyle, C., Mei Liu, Freemont, P., and Holden, D.W. (2008). SteC is a *Salmonella* kinase required for SPI-2-dependent F-actin remodelling. *Cell. Microbiol.* 10, 20–30.
- Prantner, D., Darville, T., and Nagarajan, U.M. (2010). Stimulator of IFN gene is critical for induction of IFN-beta during *Chlamydia muridarum* infection. *J. Immunol. Baltim. Md* 1950 184, 2551–2560.
- Qi, M., Gong, S., Lei, L., Liu, Q., and Zhong, G. (2011). A *Chlamydia trachomatis* OmcB C-terminal fragment is released into the host cell cytoplasm and is immunogenic in humans. *Infect. Immun.* 79, 2193–2203.
- Rank, R.G., Whittimore, J., Bowlin, A.K., and Wyrick, P.B. (2011). In Vivo Ultrastructural Analysis of the Intimate Relationship between Polymorphonuclear Leukocytes and the Chlamydial Developmental Cycle. *Infect. Immun.* 79, 3291–3301.
- Razinia, Z., Mäkelä, T., Yläne, J., and Calderwood, D.A. (2012). Filamins in mechanosensing and signaling. *Annu. Rev. Biophys.* 41, 227–246.
- Rejman Lipinski, A., Heymann, J., Meissner, C., Karlas, A., Brinkmann, V., Meyer, T.F., and Heuer, D. (2009). Rab6 and Rab11 regulate *Chlamydia trachomatis* development and golgin-84-dependent Golgi fragmentation. *PLoS Pathog.* 5, e1000615.
- Richardson, D.R., and Ponka, P. (1997). The molecular mechanisms of the metabolism and transport of iron in normal and neoplastic cells. *Biochim. Biophys. Acta* 1331, 1–40.

- Roan, N.R., and Starnbach, M.N. (2008). Immune-mediated control of Chlamydia infection. *Cell. Microbiol.* *10*, 9–19.
- Robertson, D.K., Gu, L., Rowe, R.K., and Beatty, W.L. (2009). Inclusion biogenesis and reactivation of persistent Chlamydia trachomatis requires host cell sphingolipid biosynthesis. *PLoS Pathog.* *5*, e1000664.
- Rockey, D.D., Fischer, E.R., and Hackstadt, T. (1996). Temporal analysis of the developing Chlamydia psittaci inclusion by use of fluorescence and electron microscopy. *Infect. Immun.* *64*, 4269–4278.
- Rockey, D.D., Scidmore, M.A., Bannantine, J.P., and Brown, W.J. (2002). Proteins in the chlamydial inclusion membrane. *Microbes Infect. Inst. Pasteur* *4*, 333–340.
- Rowland, A.A., and Voeltz, G.K. (2012). Endoplasmic reticulum-mitochondria contacts: function of the junction. *Nat. Rev. Mol. Cell Biol.* *13*, 607–625.
- Rzomp, K.A., Scholtes, L.D., Briggs, B.J., Whittaker, G.R., and Scidmore, M.A. (2003). Rab GTPases are recruited to chlamydial inclusions in both a species-dependent and species-independent manner. *Infect. Immun.* *71*, 5855–5870.
- Rzomp, K.A., Moorhead, A.R., and Scidmore, M.A. (2006). The GTPase Rab4 interacts with Chlamydia trachomatis inclusion membrane protein CT229. *Infect. Immun.* *74*, 5362–5373.
- Saitoh, T., Fujita, N., Hayashi, T., Takahara, K., Satoh, T., Lee, H., Matsunaga, K., Kageyama, S., Omori, H., Noda, T., et al. (2009). Atg9a controls dsDNA-driven dynamic translocation of STING and the innate immune response. *Proc. Natl. Acad. Sci. U. S. A.* *106*, 20842–20846.
- Saka, H.A., and Valdivia, R.H. (2010). Acquisition of nutrients by Chlamydiae: unique challenges of living in an intracellular compartment. *Curr. Opin. Microbiol.* *13*, 4–10.
- Saka, H.A., Thompson, J.W., Chen, Y.-S., Kumar, Y., Dubois, L.G., Moseley, M.A., and Valdivia, R.H. (2011). Quantitative proteomics reveals metabolic and pathogenic properties of Chlamydia trachomatis developmental forms. *Mol. Microbiol.* *82*, 1185–1203.
- Sandkvist, M. (2001). Type II secretion and pathogenesis. *Infect. Immun.* *69*, 3523–3535.
- Schachter J (1999). Infection and Disease Epidemiology. In *Chlamydia: Intracellular Biology, Pathogenesis, and Immunity*, Stephens RS, ed. (Washington, DC: ASM Press), pp. 139–169.
- Schramm, N., and Wyrick, P.B. (1995). Cytoskeletal requirements in Chlamydia trachomatis infection of host cells. *Infect. Immun.* *63*, 324–332.

Scidmore, M.A., and Hackstadt, T. (2001). Mammalian 14-3-3beta associates with the Chlamydia trachomatis inclusion membrane via its interaction with IncG. *Mol. Microbiol.* *39*, 1638–1650.

Scidmore, M.A., Rockey, D.D., Fischer, E.R., Heinzen, R.A., and Hackstadt, T. (1996a). Vesicular interactions of the Chlamydia trachomatis inclusion are determined by chlamydial early protein synthesis rather than route of entry. *Infect. Immun.* *64*, 5366–5372.

Scidmore, M.A., Fischer, E.R., and Hackstadt, T. (1996b). Sphingolipids and glycoproteins are differentially trafficked to the Chlamydia trachomatis inclusion. *J. Cell Biol.* *134*, 363–374.

Scidmore, M.A., Fischer, E.R., and Hackstadt, T. (2003). Restricted Fusion of Chlamydia trachomatis Vesicles with Endocytic Compartments during the Initial Stages of Infection. *Infect Immun* *71*, 973–984.

Scott, R.E. (1976). Plasma membrane vesiculation: a new technique for isolation of plasma membranes. *Science* *194*, 743–745.

Selyunin, A.S., Reddick, L.E., Weigele, B.A., and Alto, N.M. (2014). Selective protection of an ARF1-GTP signaling axis by a bacterial scaffold induces bidirectional trafficking arrest. *Cell Rep.* *6*, 878–891.

Shaw, A.C., Vandahl, B.B., Larsen, M.R., Roepstorff, P., Gevaert, K., Vandekerckhove, J., Christiansen, G., and Birkelund, S. (2002). Characterization of a secreted Chlamydia protease. *Cell. Microbiol.* *4*, 411–424.

Shaw, E.I., Dooley, C.A., Fischer, E.R., Scidmore, M.A., Fields, K.A., and Hackstadt, T. (2000). Three temporal classes of gene expression during the Chlamydia trachomatis developmental cycle. *Mol. Microbiol.* *37*, 913–925.

Sisko, J.L., Spaeth, K., Kumar, Y., and Valdivia, R.H. (2006). Multifunctional analysis of Chlamydia-specific genes in a yeast expression system. *Mol. Microbiol.* *60*, 51–66.

Snavely, E.A., Kokes, M., Dunn, J.D., Saka, H.A., Nguyen, B.D., Bastidas, R.J., McCafferty, D.G., and Valdivia, R.H. (2014). Reassessing the role of the secreted protease CPAF in Chlamydia trachomatis infection through genetic approaches. *Pathog. Dis.*

Soupene, E., Rothschild, J., Kuypers, F.A., and Dean, D. (2012). Eukaryotic protein recruitment into the Chlamydia inclusion: implications for survival and growth. *PLoS One* *7*, e36843.

Stenmark, H. (2009). Rab GTPases as coordinators of vesicle traffic. *Nat. Rev. Mol. Cell Biol.* *10*, 513–525.

- Stephens, R.S., Myers, G., Eppinger, M., and Bavoil, P.M. (2009). Divergence without difference: phylogenetics and taxonomy of *Chlamydia* resolved. *FEMS Immunol. Med. Microbiol.* *55*, 115–119.
- Stokes, G.V. (1973). Formation and destruction of internal membranes in L cells infected with *Chlamydia psittaci*. *Infect. Immun.* *7*, 173–177.
- Stokes, G.V. (1980). *Chlamydia psittaci*: inclusion vacuole ultrastructure. *Can. J. Microbiol.* *26*, 396–401.
- Su, H., McClarty, G., Dong, F., Hatch, G.M., Pan, Z.K., and Zhong, G. (2004). Activation of Raf/MEK/ERK/cPLA2 signaling pathway is essential for chlamydial acquisition of host glycerophospholipids. *J. Biol. Chem.* *279*, 9409–9416.
- Subtil, A., Delevoye, C., Balañá, M.-E., Tastevin, L., Perrinet, S., and Dautry-Varsat, A. (2005). A directed screen for chlamydial proteins secreted by a type III mechanism identifies a translocated protein and numerous other new candidates. *Mol. Microbiol.* *56*, 1636–1647.
- Suchland, R.J., Rockey, D.D., Bannantine, J.P., and Stamm, W.E. (2000). Isolates of *Chlamydia trachomatis* that occupy nonfusogenic inclusions lack IncA, a protein localized to the inclusion membrane. *Infect. Immun.* *68*, 360–367.
- Sun, J., and Schoborg, R.V. (2009). The host adherens junction molecule nectin-1 is degraded by chlamydial protease-like activity factor (CPAF) in *Chlamydia trachomatis*-infected genital epithelial cells. *Microbes Infect. Inst. Pasteur* *11*, 12–19.
- Sütterlin, C., and Colanzi, A. (2010). The Golgi and the centrosome: building a functional partnership. *J. Cell Biol.* *188*, 621–628.
- Tafesse, F.G., Huitema, K., Hermansson, M., van der Poel, S., van den Dikkenberg, J., Uphoff, A., Somerharju, P., and Holthuis, J.C.M. (2007). Both sphingomyelin synthases SMS1 and SMS2 are required for sphingomyelin homeostasis and growth in human HeLa cells. *J. Biol. Chem.* *282*, 17537–17547.
- Takala, H., Nurminen, E., Nurmi, S.M., Aatonen, M., Strandin, T., Takatalo, M., Kiema, T., Gahmberg, C.G., Yläne, J., and Fagerholm, S.C. (2008). Beta2 integrin phosphorylation on Thr758 acts as a molecular switch to regulate 14-3-3 and filamin binding. *Blood* *112*, 1853–1862.
- Tang, L., Chen, J., Zhou, Z., Yu, P., Yang, Z., and Zhong, G. (2015). Chlamydia-secreted protease CPAF degrades host antimicrobial peptides. *Microbes Infect. Inst. Pasteur*.
- Taraska, T., Ward, D.M., Ajioka, R.S., Wyrick, P.B., Davis-Kaplan, S.R., Davis, C.H., and Kaplan, J. (1996). The late chlamydial inclusion membrane is not derived from the endocytic pathway and is relatively deficient in host proteins. *Infect. Immun.* *64*, 3713–3727.

- Taylor, L.D., Nelson, D.E., Dorward, D.W., Whitmire, W.M., and Caldwell, H.D. (2010). Biological characterization of *Chlamydia trachomatis* plasticity zone MACPF domain family protein CT153. *Infect. Immun.* 78, 2691–2699.
- Thavarajah, R., Mudimbaimannar, V.K., Elizabeth, J., Rao, U.K., and Ranganathan, K. (2012). Chemical and physical basics of routine formaldehyde fixation. *J. Oral Maxillofac. Pathol. JOMFP* 16, 400–405.
- Thompson, C.C., and Carabeo, R.A. (2011). An Optimal Method of Iron Starvation of the Obligate Intracellular Pathogen, *Chlamydia Trachomatis*. *Front. Microbiol.* 2.
- Tse, S.M.L., Mason, D., Botelho, R.J., Chiu, B., Reyland, M., Hanada, K., Inman, R.D., and Grinstein, S. (2005). Accumulation of diacylglycerol in the *Chlamydia* inclusion vacuole: possible role in the inhibition of host cell apoptosis. *J. Biol. Chem.* 280, 25210–25215.
- Ullrich, O., Reinsch, S., Urbé, S., Zerial, M., and Parton, R.G. (1996). Rab11 regulates recycling through the pericentriolar recycling endosome. *J. Cell Biol.* 135, 913–924.
- Valdivia, R.H. (2008). *Chlamydia* effector proteins and new insights into chlamydial cellular microbiology. *Curr. Opin. Microbiol.* 11, 53–59.
- Verbeke, P., Welter-Stahl, L., Ying, S., Hansen, J., Häcker, G., Darville, T., and Ojcius, D.M. (2006). Recruitment of BAD by the *Chlamydia trachomatis* vacuole correlates with host-cell survival. *PLoS Pathog.* 2, e45.
- Volceanov, L., Herbst, K., Biniossek, M., Schilling, O., Haller, D., Nölke, T., Subbarayal, P., Rudel, T., Zieger, B., and Häcker, G. (2014). Septins Arrange F-Actin-Containing Fibers on the *Chlamydia trachomatis* Inclusion and Are Required for Normal Release of the Inclusion by Extrusion. *mBio* 5, e01802–e01814.
- Volpicelli-Daley, L.A., Li, Y., Zhang, C.-J., and Kahn, R.A. (2005). Isoform-selective effects of the depletion of ADP-ribosylation factors 1-5 on membrane traffic. *Mol. Biol. Cell* 16, 4495–4508.
- Voth, D.E., and Heinzen, R.A. (2007). Lounging in a lysosome: the intracellular lifestyle of *Coxiella burnetii*. *Cell. Microbiol.* 9, 829–840.
- Walther, T.C., and Farese Jr., R.V. (2009). The life of lipid droplets. *Biochim. Biophys. Acta BBA - Mol. Cell Biol. Lipids* 1791, 459–466.
- Wanders, R.J.A., and Waterham, H.R. (2006). Biochemistry of mammalian peroxisomes revisited. *Annu. Rev. Biochem.* 75, 295–332.
- Wang, Y., Kahane, S., Cutcliffe, L.T., Skilton, R.J., Lambden, P.R., and Clarke, I.N. (2011). Development of a transformation system for *Chlamydia trachomatis*: restoration of glycogen biosynthesis by acquisition of a plasmid shuttle vector. *PLoS Pathog.* 7, e1002258.

Wehland, J., Henkart, M., Klausner, R., and Sandoval, I.V. (1983). Role of microtubules in the distribution of the Golgi apparatus: effect of taxol and microinjected anti-alpha-tubulin antibodies. *Proc. Natl. Acad. Sci. U. S. A.* *80*, 4286–4290.

Whipple, R.A., Vitolo, M.I., Boggs, A.E., Charpentier, M.S., Thompson, K., and Martin, S.S. (2013). Parthenolide and costunolide reduce microtentacles and tumor cell attachment by selectively targeting detyrosinated tubulin independent from NF- κ B inhibition. *Breast Cancer Res. BCR* *15*, R83.

Wilson, D.P., Timms, P., McElwain, D.L.S., and Bavoil, P.M. (2006). Type III secretion, contact-dependent model for the intracellular development of chlamydia. *Bull. Math. Biol.* *68*, 161–178.

Wolf, K., and Hackstadt, T. (2001). Sphingomyelin trafficking in *Chlamydia pneumoniae*-infected cells. *Cell. Microbiol.* *3*, 145–152.

Wylie, J.L., Hatch, G.M., and McClarty, G. (1997). Host cell phospholipids are trafficked to and then modified by *Chlamydia trachomatis*. *J. Bacteriol.* *179*, 7233–7242.

Yamaji, R., Adamik, R., Takeda, K., Togawa, A., Pacheco-Rodriguez, G., Ferrans, V.J., Moss, J., and Vaughan, M. (2000). Identification and localization of two brefeldin A-inhibited guanine nucleotide-exchange proteins for ADP-ribosylation factors in a macromolecular complex. *Proc. Natl. Acad. Sci. U. S. A.* *97*, 2567–2572.

Yang, Z., Tang, L., Sun, X., Chai, J., and Zhong, G. (2015). Characterization of CPAF during *Chlamydia* infection —CPAF critical residues and secretion revisited. *Infect. Immun.* *IAI.00275–15*.

Yeung, T., Terebiznik, M., Yu, L., Silvius, J., Abidi, W.M., Philips, M., Levine, T., Kapus, A., and Grinstein, S. (2006). Receptor Activation Alters Inner Surface Potential During Phagocytosis. *Science* *313*, 347–351.

Al-Younes, H.M., Brinkmann, V., and Meyer, T.F. (2004). Interaction of *Chlamydia trachomatis* serovar L2 with the host autophagic pathway. *Infect. Immun.* *72*, 4751–4762.

Yu, H., Schwarzer, K., Förster, M., Kniemeyer, O., Forsbach-Birk, V., Straube, E., and Rödel, J. (2010). Role of high-mobility group box 1 protein and poly(ADP-ribose) polymerase 1 degradation in *Chlamydia trachomatis*-induced cytopathicity. *Infect. Immun.* *78*, 3288–3297.

Al-Zeer, M.A., Al-Younes, H.M., Kerr, M., Abu-Lubad, M., Gonzalez, E., Brinkmann, V., and Meyer, T.F. (2014). *Chlamydia trachomatis* remodels stable microtubules to coordinate Golgi stack recruitment to the chlamydial inclusion surface. *Mol. Microbiol.*

Zhong, G. (2009). Killing me softly: chlamydial use of proteolysis for evading host defenses. *Trends Microbiol.* *17*, 467–474.

Zhong, G. (2011). Chlamydia trachomatis secretion of proteases for manipulating host signaling pathways. *Front. Microbiol.* 2, 14.

Zhong, G., Liu, L., Fan, T., Fan, P., and Ji, H. (2000). Degradation of transcription factor RFX5 during the inhibition of both constitutive and interferon gamma-inducible major histocompatibility complex class I expression in chlamydia-infected cells. *J. Exp. Med.* 191, 1525–1534.

Zhong, G., Fan, P., Ji, H., Dong, F., and Huang, Y. (2001). Identification of a chlamydial protease-like activity factor responsible for the degradation of host transcription factors. *J. Exp. Med.* 193, 935–942.

Biography

Marcela Kokes was born on September 18th, 1986 in Boulder, Colorado. She obtained a Bachelor of Arts degree in December of 2007 from Lewis and Clark College in Portland, Oregon. During her time there, she studied lysosome-related organelle biogenesis using a *Caenorhabditis elegans* model under Greg Hermann, PhD, and published the article entitled, “*glo-3*, a novel *Caenorhabditis elegans* gene, is required for lysosome-related organelle biogenesis” in *Genetics*.

In 2008 she began her PhD training at Duke University in the laboratory of Raphael Valdivia, PhD, the Vice Dean for Basic Science for Duke University School of Medicine and Associate Professor of Molecular Genetics and Microbiology. There, her research focused on using newly developed genetic tools to study how the obligate intracellular human pathogen *Chlamydia trachomatis* manipulates host cell biology, a process which is vital for its survival and disease pathogenesis. While at Duke, she published several articles including “Integrating chemical mutagenesis and whole genome sequencing as a platform for forward and reverse genetic analysis in *Chlamydia*” in *Cell Host and Microbe*, “Reassessing the role of the secreted protease CPAF in *Chlamydia trachomatis* infection through genetic approaches” in *Pathogens and Disease*, and a book chapter entitled “Cell biology of the *Chlamydia* inclusion” published in *Intracellular Pathogens I: Chlamydiales* by ASM Press. While at Duke, Marcela actively worked to expand career development opportunities for graduate students in the biomedical sciences and engaged in conversations about scientific training and education. In June 2015, she accepted a position to be an HHMI postdoctoral scholar at Stanford University in the laboratory of Kang Shen, PhD to study the cell biology of neuronal morphogenesis using *C. elegans*.

For her research accomplishments and potential, during her graduate training Marcela Kokes received a number of awards and honors including the Jo Rae Wright Fellowship for Outstanding Women in Science, an American Heart Association Predoctoral Fellowship, a Bass Instructional Fellowship, a Preparing Future Faculty Fellowship, and numerous travel and presentation awards for scientific conferences. She is a member of the American Society for Cell Biology.